CZECH TECHNICAL UNIVERSITY IN PRAGUE

Faculty of Civil Engineering

Department of Concrete and Masonry Structures

Mechanical response of concrete structures to effects of ionizing radiation

DOCTORAL THESIS

Ing. Michaela Herzfeldt

Doctoral study programme: Civil Engineering

Branch of study: Structural and Transportation Engineering

Doctoral thesis tutor: prof. Ing. Petr Štemberk, Ph.D., D.Eng.

Prague, 2024

CZECH TECHNICAL UNIVERSITY IN PRAGUE

Faculty of Civil Engineering

Thákurova 7, 166 29 Praha 6

DECLARATION

Ph.D. student's name: Michaela Herzfeldt

Title of the doctoral thesis: Mechanical response of concrete structures to effects of ionizing radiation

I hereby declare that this doctoral thesis is my own work and effort written under the guidance of the tutor prof. Ing. Petr Štemberk, Ph.D., D.Eng.

All sources and other materials used have been quoted in the list of references.

In Prague on   22.1.2024

....

                                        signature

Abstrakt

V současné době mnoho jaderných elektráren překračuje plánovanou životnost a proto vyvstává otázka v jakém stavu se nácházejí betonové konstrukce vystavené ionizujícímu záření. Vliv radiace na změnu mechanických vlastností betonu je velmi důležitý pro vyhodnocení spolehlivosti a bezpečnosti konstrukce. Zásadní se ukazuje vliv radiace na kamenivo obsažené v betonu. Efekt zvaný objemová expanze kameniva způsobená radiací je výrazně ovlivněn složením kameniva na úrovni minerálů.

Tato práce se představuje model ozářeného kameniva, který v závisloti na mineralogickém složení vyhodnocuje expanzi kameniva vlivem radiace. Data použitá pro vytvoření modelu jsou posbírána z různých zdrojů a zároveň jich je málo, proto obsahují rozptyl, který je možné eliminovat s použitím fuzzy logiky při vytvoření modelu.

Hlavním cílem této práce je využití dostupných dat na ozářených minerálech a kamenivu, aby bylo možné vyhodnotit celkový vliv objemové expanze kameniva způsobené radiací na betonovou konstukci po mnoha letech provozu jaderného zařízení. Vyhodnocení vlivu je zaměřené primárně na konstrukci biologického stínění, což je ochranná obálka přímo okolo jaderného reaktoru.

Abstract

The worldwide need of nuclear power plant (NPP) lifetime extension raises the question of the condition of concrete structures exposed to ionizing radiation. Therefore the impact of radiation on mechanical properties of concrete is crucial knowledge in process of assessment of soundness and safety of NPP structures. It has been discovered that radiation has degradation effect on aggregates that are contained in concrete material. The phenomenon is called radiation-induced volumetric expansion (RIVE) and is strongly dependent on minerals that form particular aggregate.

This thesis presents model of aggregate swelling due to radiation that captures the actual composition of minerals within aggregate. Since the data on irradiated minerals are limited and moreover exhibit scatter caused by different testing condition, the fuzzy logic is used in this model to interconnect data received by various expert groups.

The main goal of this work is to utilize available data on irradiated concrete components such as minerals and aggregates to estimate the RIVE which has impact on mechanical properties of concrete structures after years of nuclear reactor operation. The obtained data should serve for estimate of condition of biological shielding structure specifically. The volumetric change of irradiated aggregate is then used for modeling irradiated concrete in the actual NPP structure based on the composition of concrete, the average temperature on the surface of the biological shield structure and the neutron dose received by biological shield.

Acknowledgement

I wish to thank Dr. Thomas M. Rosseel, Dr. Yann Le Pape and Dr. Alain Giorla for their guidance and valuable discussions during my internship at Oak Ridge National Laboratory that supported this research.

Cervenka Consulting s.r.o. supports lot of students and their research worldwide. Finishing of this work is possible due to help and guidance I have been provided in last few years in this company. Therefore I want to thank all colleagues and mentors who are part of this family.

I am also very grateful to Prof. Petr Štemberk for his abiding support since my early years at the university.

Finally, the greatest thanks belong to my ever supportive family, namely loving parents Jana and Milan, and witty brother Petr. Matter of course is gratefulness to my beloved husband Sebastian for his continuous support and love, and my son Dominik who introduced me to unconditional love.

Contents

1 Introduction

Since the 1950's the nuclear industry has undergone an extensive development of technologies and equipment in nuclear facilities. However, one of the most important component has not changed much: the biological shielding and the structural material used for its construction. Even though concrete is an extremely variable material usually containing aggregates from local sources, in the civil engineering practice the concrete is handled as a homogeneous material. Since the biological shield has shielding as well as load-bearing function, the material condition and soundness are essential conditions for safe reactor operation. The worldwide need for nuclear facilities license renewals has raised the question of what are the effects of radiation on concrete. The community of researchers has attempt to find the answer since the very beginning of nuclear era in 1960's and 1970's as noted by [1]-[5]. The major conclusion of their research was that neutron fluences above 10^{19} n/cm^2, not specifying energy spectrum of neutrons, cause reduction of mechanical properties [3]. They also discovered that some aggregates are more susceptible to radiation effects and may increase in volume significantly [6]-[7]. Nowadays, calculations of neutron fluence received by biological shielding exceeds the threshold in 40 or more years of operation for 2-loop pressurized water reactor (PWR) [6]. Data summarized in [6] are based on extensive research of [8]-[19].

The assembly of irradiated concrete data shows large scatter which is given by different testing conditions and material compositions [1],[6]. Regarding the conditions, the greatest difference is the temperature during irradiation which can be low as 40°C or as high as 200°C. By the nature of concrete that contains a lot of water, the extensive cracking can be associated with elevated temperatures on its own. However the temperature effect might be particularly eliminated by control samples with same thermal treatment, it does not give the proper understanding of the main effect of irradiation on the concrete samples.

The other differences supporting the data scatter when irradiated concrete properties are evaluated are different shapes (prism, cylinder etc.) and size of specimens, different materials not just on the aggregate level but also cement paste that might contain common Portland cement or alumina cement.

Following figures show development of mechanical properties of concrete such as compressive strength or tensile strength, see Fig. 1-1 and Fig. 1-2.
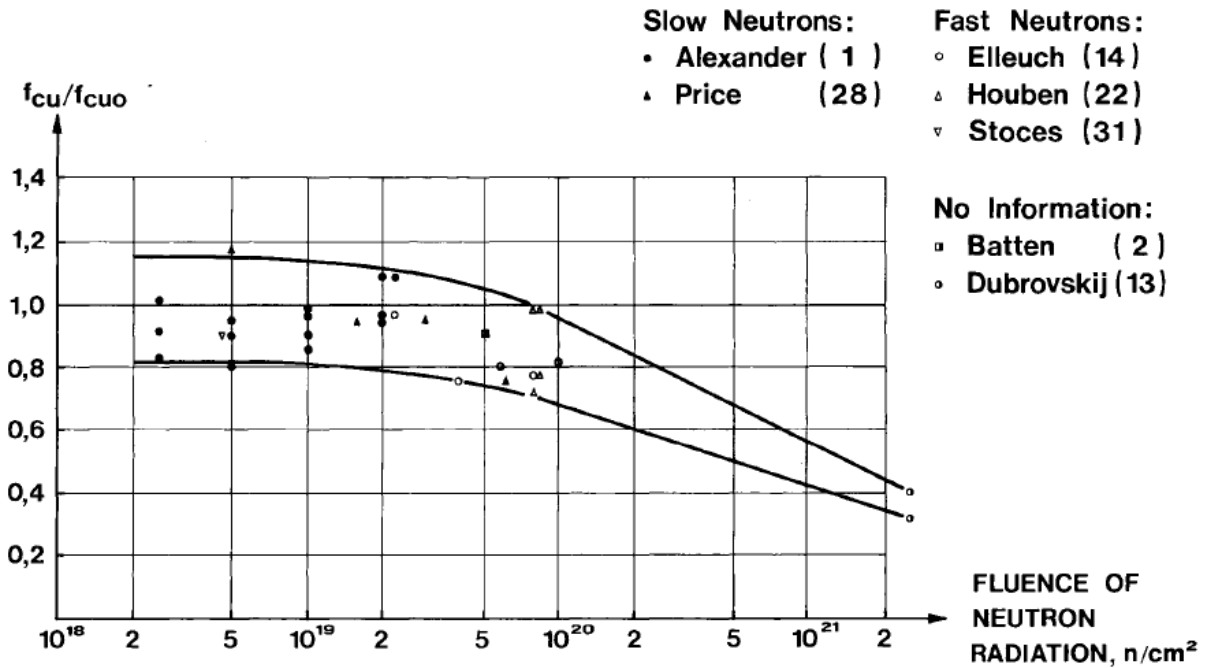
Fig. 1-1 Reduction of compressive strength of irradiated concrete samples [1]
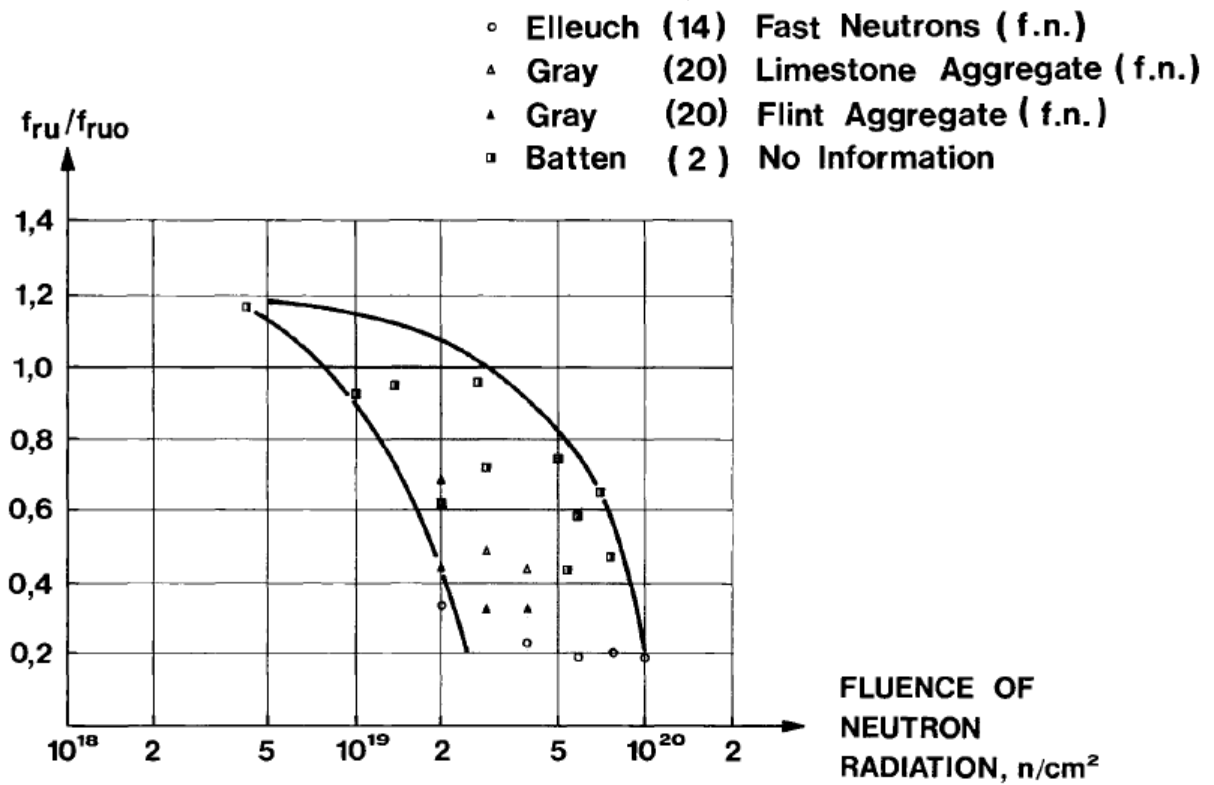

Fig. 1-2 Reduction of tensile strength of irradiated concrete samples [1]

Important effect of radiation on concrete and aggregate used in concrete that has been observed is swelling of both. Since the aggregate exhibit swelling it is the main cause of concrete expansion because about 80% of concrete volume is coved by aggregate. Irradiation caused swelling clearly depends on aggregate type, see Fig. 1-3. Filed et. al. named this phenomenon radiation-induced volumetric expansion (RIVE) in [6]. This effect is caused by neutron radiation.
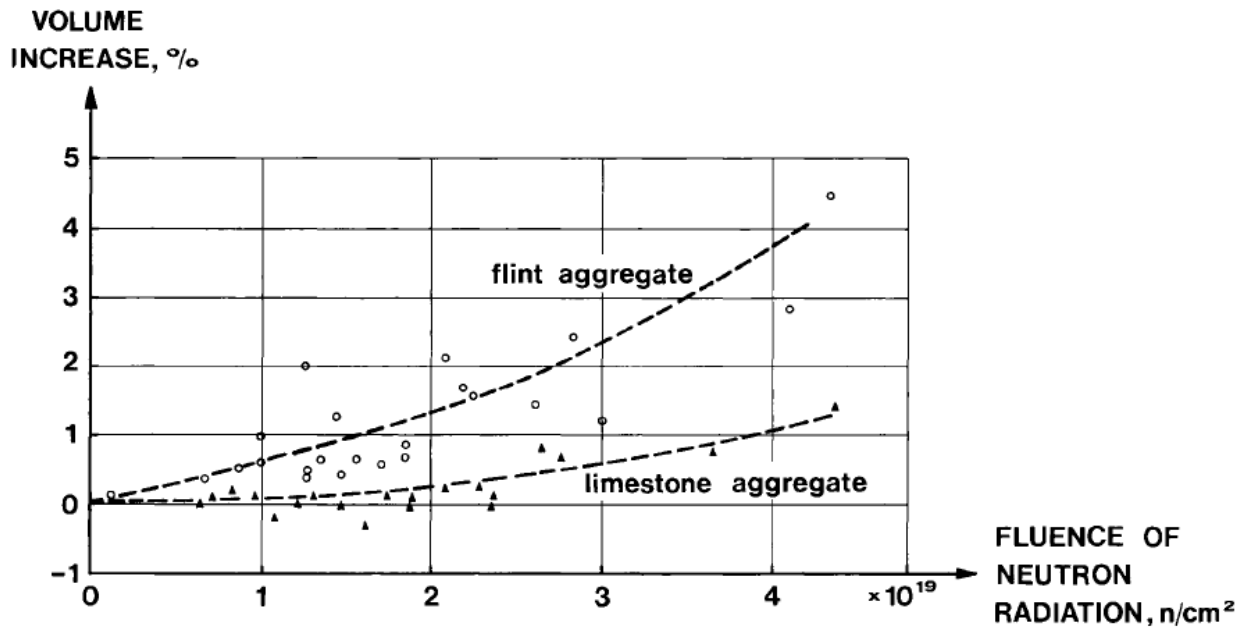

Fig. 1-3 Increase of volume of irradiated aggregates [1]

Beside aggregate the concrete contains cement paste, the matrix which glues aggregate together. What is observed in irradiation experiment is mostly shrinkage of paste that is caused by two reasons, see Fig. 1-4. The first one is related to elevated temperature above 100°C during irradiation which naturally leads to loss of water within cement paste. The result of the process is drying shrinkage of concrete. The second reason of water loss is connected to radiolysis of water in cement paste that leaves the structure in gas form and might not be limited to vapor only. This is caused by exposure to gamma radiation.
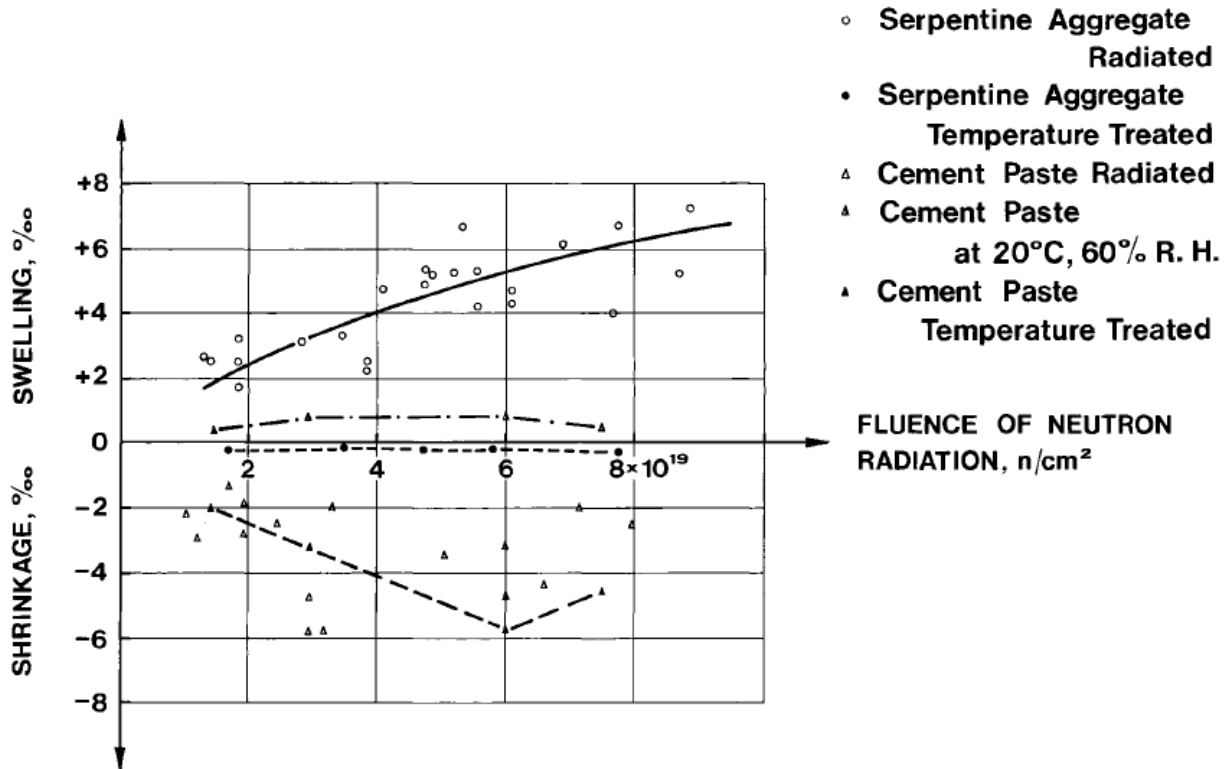
9

Fig. 1-4 Comparison of volumetric change on irradiated/temperature treated/testing samples of cement paste and aggregates [1]

Therefore, deeper understandings of testing condition effects as well as material composition effects on concrete properties are crucial issues for comprehensive assessment of a biological shielding structure condition. Not only is concrete a composite or multiphase material, but the aggregates used in concrete are composed of minerals that exhibit radiation-induced volumetric expansion. That is why the minerals deserve attention in order to understand the overall effects of radiation on concrete. The minerals determine the resulting behavior of irradiated aggregate, which in turn determine the behavior of the irradiated concrete. It seems that step-by-step upscaling of the material behavior leads the way to obtain concrete properties after years of irradiation, Fig. 1-5 and Fig. 1-6.

The following thesis describes an approach to utilize the current understanding of radiation-induced effects on minerals to obtain properties of irradiated aggregate.
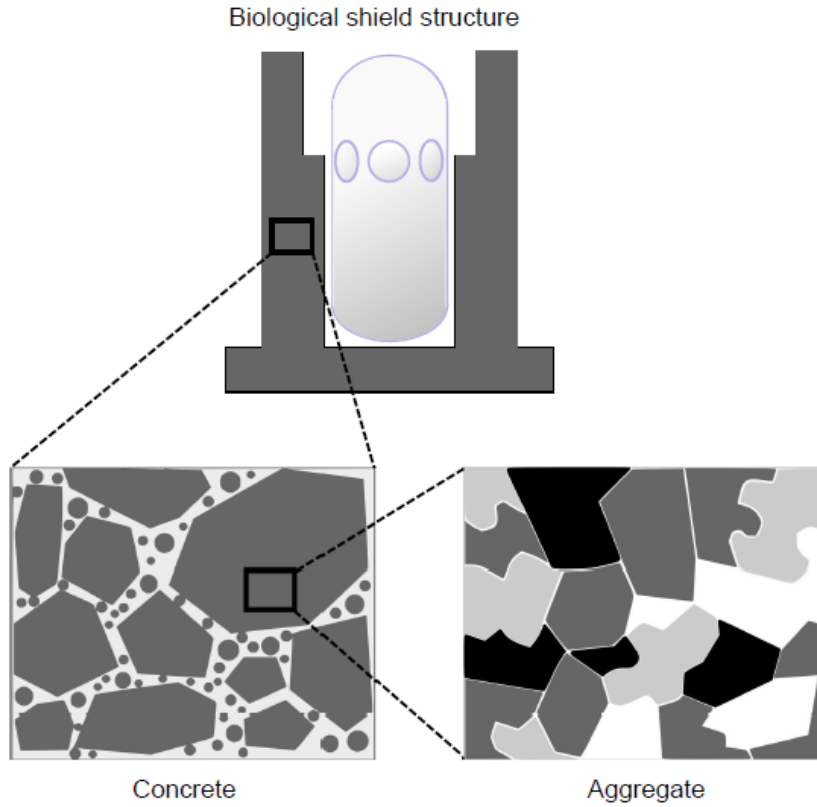
10

Fig. 1-5 Scaling of concrete structure (macro), concrete (meso) and mineral composition of aggregates (micro) [20]
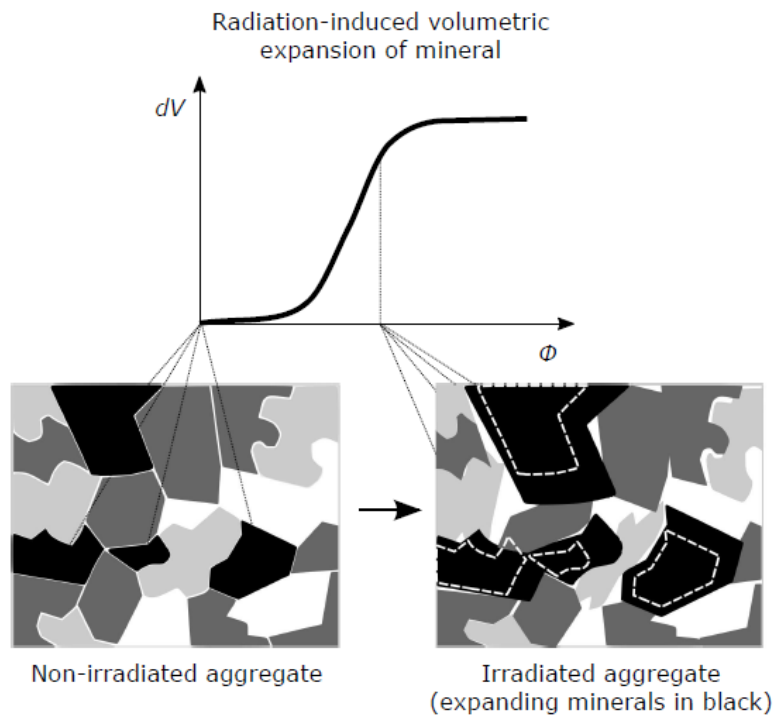

Fig. 1-6 Effect of radiation on concrete microstructure [20]

2   Interaction of radiation with matter

Nuclear fission is controlled reaction when heavy atom nuclei are bombarded by neutrons while high amount of energy is released together with other irradiation fields. The energy of neutrons produced during the reaction is different in thermal reactor and fast neutron reactor. While fast neutron reactor needs for maintaining the nuclear fission a highly enriched fissile materials, the thermal reactors need moderator for proper maintenance of fission process, [21].

Other irradiation field that is to be considered is high energy photons (γ) released during the fission or as a product of inelastic neutron interactions. Furthermore electron flux (β⁻) and flux of heavy ions (α) could be considered, however their lack of ability to penetrate the thick steel wall of nuclear reactor suggest very limited effect on the concrete biological shielding structure.

2.1   Gamma ray interaction with matter

The gamma rays are basically side product of the fission process within reactor. As the gamma rays are emitted during nuclear fission, three different types of interaction between matter (concrete) and gamma rays:

- Photoelectric effect
- Compton scattering
- Pair production.

When gamma ray hits an atom and only orbital electron is ejected, the collision is called Photoelectric effect. Whereas Compton scattering is considered when orbital electron is released while the original gamma ray looses energy and changes direction. Finally the high energy gamma rays produce pair of electron and positron in vicinity of atomic nucleus from neutral boson, such phenomenon is called Pair production, see Fig. 2-1 [22].

Based on the levels of gamma rays produced in nuclear reactor and atomic number of elements found in usual cement paste and aggregates, the main decay of gamma rays is Compton scattering. Primarily the water radiolysis takes place during concrete exposure to gamma rays due to low energy level of released electrons. Therefore the solid phase in concrete is not affected as much by gamma rays directly. Kontani [22] suggests three different effects of gamma rays on water phase

of cement paste. Beside the loss of water due to radiolysis, the hydrogen peroxide that is product of radiolysis may react with cement paste. And finally the water can be evaporated as a result of the gamma heating.
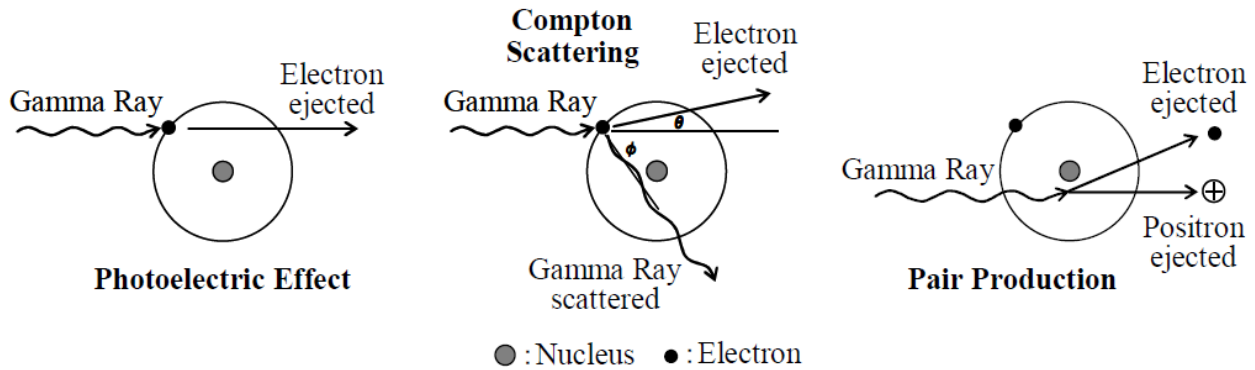

Fig. 2-1 Interaction of gamma rays with matter [22]

2.2 Neutron interaction with matter

Neutrons, based on their energy, can be divided into groups of:

- Fast neutrons, 10 keV – 1MeV
- Intermediate neutrons, 1 eV – 1 keV
- Thermal neutrons, 0.025 eV – 1 eV.

The energy of neutron defines the type of its interaction with matter. It can be either inelastic or elastic interaction, see Fig. 2-2. The neutrons interact with atomic nucleus only. When the elastic interaction occurs one neutron is produced and the nucleus travels in different direction, the kinetic energy of system is preserved. In case of inelastic interaction one neutron is released from atomic nucleus along with energy in form of gamma rays.

It is reported that inelastic collisions can cause the chemical changes mainly studied in case of alloys, however the radiation damage of materials is mainly related to the displacement of atoms caused by neutron irradiation, [21]. The actual displacement within crystalline lattice occurs when

13

the transfer energy of neutron exceeds the required critical energy for displacement in atom. Such limit for materials is called displacement energy and its typical value is of order 10-50 eV [23].

When material is exposed to radiation, in order to measure the extent of irradiation the term of irradiation dose is used. More specifically the dose can be viewed in two different time scales. First, the instantaneous measure of dosage is denoted as neutron flux whose unit is $n \cdot m^{-2} \cdot s^{-1}$. Second view on dosage is in its integral form that is called neutron fluence in $n \cdot m^{-2}$ that refers to the specific time interval. Since the damage of concrete structures is expected after decades of reactor operation which means dosage of neutrons over extent period of time, the neutron fluence is referred in connection with radiation damage of concrete. The effect of neutron radiation on concrete is more broadly explained in following text.
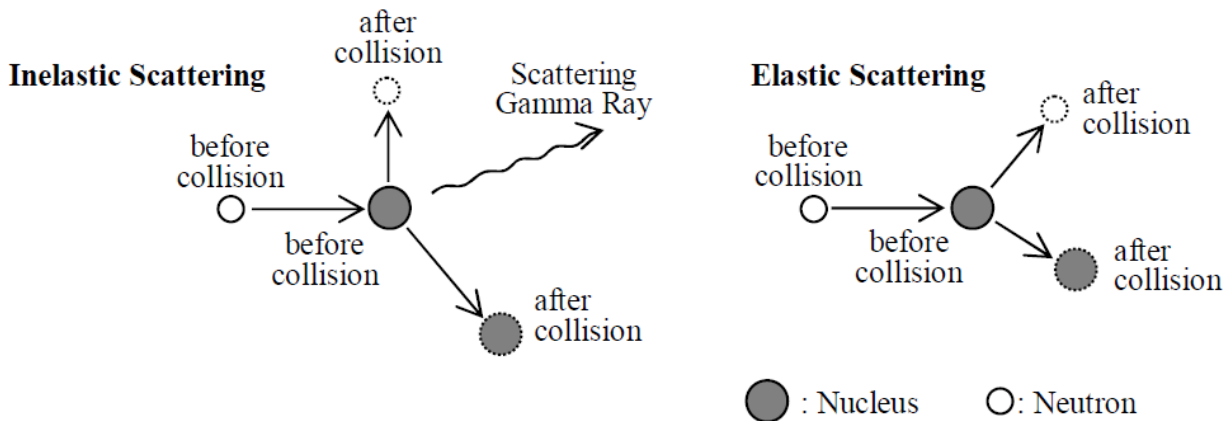

Fig. 2-2 Interaction of neutrons with matter [22]

14

3 Irradiated aggregates

The aggregate content in concrete is usually 60-80% by volume making it the main component of concrete and therefore the component that determines properties of concrete [24]. The aggregate itself consists of minerals suggesting that the aggregate could be viewed as a composite or multiphase material. Thus, as the aggregate properties affect concrete properties, aggregate properties are derived from minerals.

3.1 Minerals

The essential issue of understanding the effects of radiation damage in concrete is therefore the formation of radiation defects or damage in minerals. Neutrons interacting with atoms in a crystalline lattice cause displacement of atoms that results in vacancies, interstitial atoms or substitution of one atom with another. According to the experimental data, the neutrons causing the damage range in energy primarily from 0.01-1 MeV [25]. Furthermore, Remec's calculation in [26] identify the observed cut-off energy of neutrons causing the damage at the same level. The accumulation of defects leads to changes in the crystalline lattice parameters and elementary cell volume due to the effect of interstitial atoms. The main defects in well-crystalized materials (minerals) caused by irradiation are:

- Disruption of structure periodicity – amorphization
- Partial or complete transformation into other minerals
- Anisotropic changes in crystalline lattice
- Changes in physical properties.

The mineral properties studied by most researchers are changes in density, crystalline lattice parameters, dimension, coefficient of thermal expansion, and other optical properties that do not necessarily reflect the impact of radiation on mechanical properties. From the mechanical properties point of view, the most interesting effect is the dimensional change of minerals. The anisotropic nature of dimensional changes results in unequal expansion along different axes of crystals. Accordingly, shrinkage may take place in certain directions while in other directions the mineral expands.

Since the aggregate for neutron shielding may contain boron, which is found in minerals (ulexite, colemanite etc. in colemanite, borocalcite aggregates [27]), additional radiation effects take place when B^{10} is present in the mineral. The irradiated B^{10} emits α particles with high kinetic energy (2~8 MeV) that collide with atoms and create additional high temperature peaks in minerals during irradiation [25].

3.2 Classification of mineral

Minerals are divided into classes based on their chemical composition with the main groups of minerals being silicates, carbonates, oxides and sulfates. Beside the chemical composition, the microstructure of minerals determines the structural type of the mineral and those can be isle, chain or band, laminated (sheet), framework and coordination structure, [25]. The name of each structural type illustrates very well the spatial orientation of the main molecule of each mineral group. Further characteristics that are studied on minerals are also elementary cell, appearance or various physical properties.

Silicates

Mineral group of silicates contains a tetrahedron of silicon-oxygen (SiO_4^{4-}) whose connection determines the type of structure. Since the Earth's crust is formed from 95% out of silicates, this group of minerals makes most common one, [28]. Examples of minerals within different structural types is given in Tab. 3-1.

As has been mentioned above, the dimensional change of minerals has dominant effect that affects the change of overall mechanical properties of aggregates and consequently concrete. The most comprehensive assembly of tested data on minerals is given in [25]. There can be identified trends of volumetric change of minerals based on the neutron fluence and temperature during irradiation. All of the following data presenting quartz, potassium and plagioclase feldspars, and pyroxenes, Fig. 3-1-Fig. 3-4, are obtained with neutron's energy E>10 keV.

Tab. 3-1 Example of common silicates divided by their structural type

	Structural type	Minerals	Vol. change [%]
← Si content decreases and density and melting point increases	Framework	quartz, feldspars (*potassium feld.*: microcline, orthoclase, sanidine; *plagioclase feld.*: albite, oligoclase, andesine, labradorite, anorthite, bytownite)	Up to 18%
	Laminates	mica (muscovite, biotite), serpentine	Up to 16%
	Chain	pyroxenes (augite, diopside, enstatite)	Up to 2.7%
	Band	amphiboles	Up to 2.1%
	Isle	olivine, zircon	Up to 3.8%
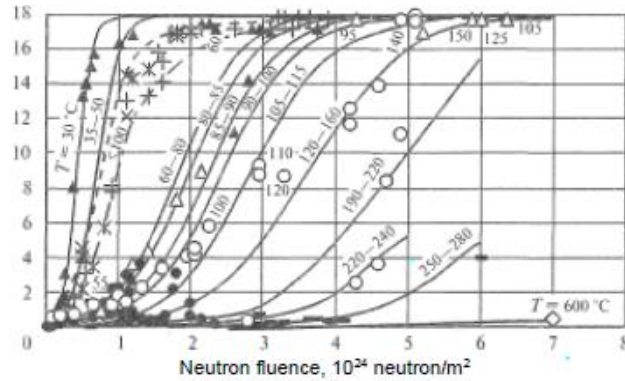
Fig. 3-1 Volumetric change of quartz caused by irradiation within temperatures 30-600°C [25]
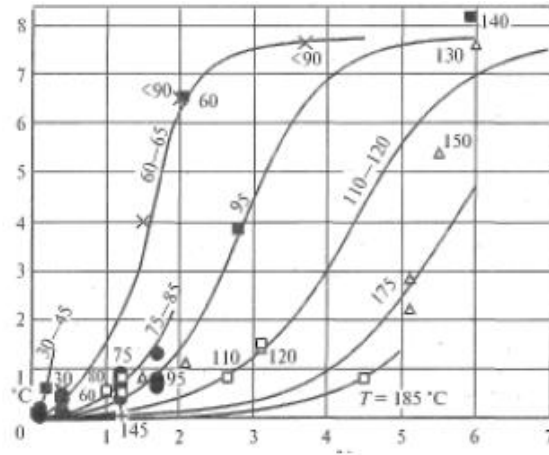
Neutron fluence, 10²⁴ neutron/m²

Fig. 3-2 Volumetric change of potassium feldspars caused by irradiation within temperatures 30-185°C [25]
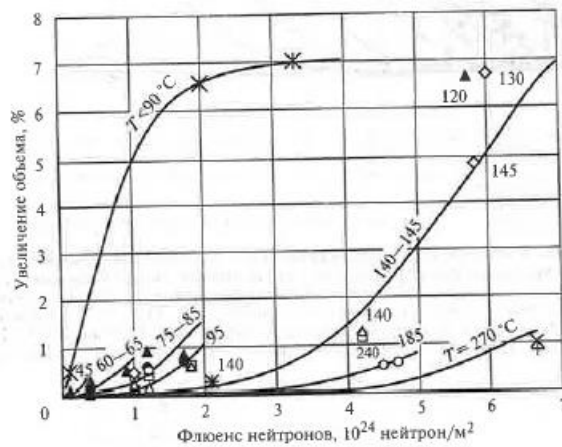
Fig. 3-3 Volumetric change of plagioclase feldspars caused by irradiation within temperatures 45-270°C [25]

Obtained laboratory testing proposes that some silicates are the most susceptible to radiation induced dimensional changes (quartz and muscovite expand up to 18% of their volume ([5] and [25]) not all silicates are that responsive (feldspars expand up to 8% of volume and pyroxenes up to 3%) suggesting that structure and bonding play as important role as chemical composition. Specifically, the covalent bound consisting of isotropic lattice structures is more resistant to neutron irradiation than the anisotropic structures, [5]. That explains the excessive volumetric changes in case of quartz and muscovite. Moreover, the change in mechanical properties is more significant

18

for polycrystalline minerals because of the development of the cracks in between the phases due to differential expansion along the axes.
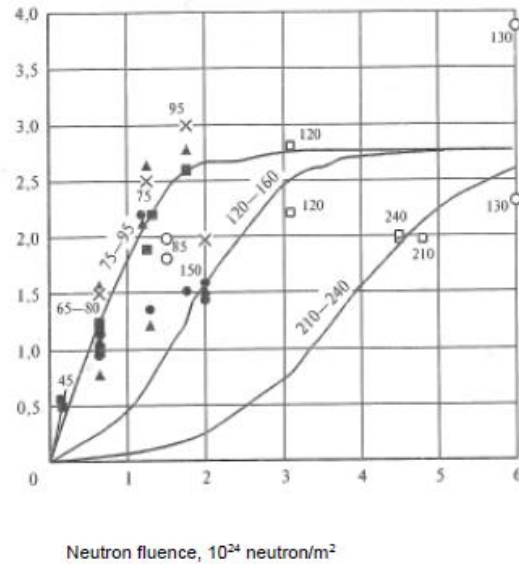

Neutron fluence, 10^{24} neutron/m^2

Fig. 3-4 Volumetric change of pyroxenes caused by irradiation within temperatures 45-240°C [25]

The available data [1],[6],[25] demonstrate that radiation expansion increases until it reaches saturation point or ultimate concentration of defects. For that reason, radiation-induced expansion of minerals (RIVE) is usually described by a sigmoid function. For silicates, the sigmoidal behavior of the expansion of aggregates as a function of the neutron fluence is significantly affected by the temperature of irradiation. The higher the temperature, the higher the neutron fluence needed to reach the maximum of the sigmoid function [25]. This phenomenon is due to the partial annealing of the material exposed to high temperatures and seems especially significant in silicates [25].

Carbonates

Minerals belonging to carbonate group contain carbonate ion CO_3^{2-}. Compared to silicates, the carbonates form only 2.5% of Earth's crust. Carbonates are unstable at elevated temperature compared to other groups of minerals. Especially siderite starts to decompose at 280°C releasing carbon dioxide (CO). Calcite resists up to 900°C. Tab. 3-2 shows main carbonate minerals.

19

Tab. 3-2 Example of common carbonates

Structural type	Minerals	Vol. change [%]
Isle	calcite dolomite magnesite siderite	Up to 3.3%

The volumetric change measurements on carbonates shows two phenomena occurring upon irradiation, firstly the swelling of minerals does not exceed 1% (Fig. 3-5) for most common carbonates (the exception is ankerite that swells up to 3.3% according to [25]) which suggest very low sensitivity to radiation, however the second phenomena is decomposition of up to 30% of sample in case of siderite and magnesite due to elevated temperatures while irradiated. However irradiation tests of carbonates presented in [5] declare that the volumetric change after irradiation is within the limits of measurement error range.
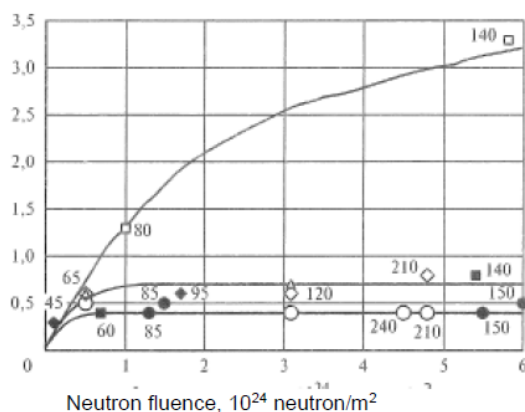
Fig. 3-5 Volumetric change of carbonates caused by irradiation within temperatures 45-240°C [25]

Oxides

Mineral group of oxides is created by compounds of oxygen ions surrounded by various cations. Even though the iron ores such as magnetite and hematite are sources of widely used iron, the

oxides in general comprises only 0.2% of Earth's crust, [28]. Moreover group of oxides has higher modulus of elasticity compared to other groups. Common oxides are presented in Tab. 3-3.

Tab. 3-3 Example of common oxides

Structural type	Minerals	Vol. change [%]
Laminates	corundum hematite	Up to 3.2%
Coordination	spinel chromite magnetite	Up to 0.9%
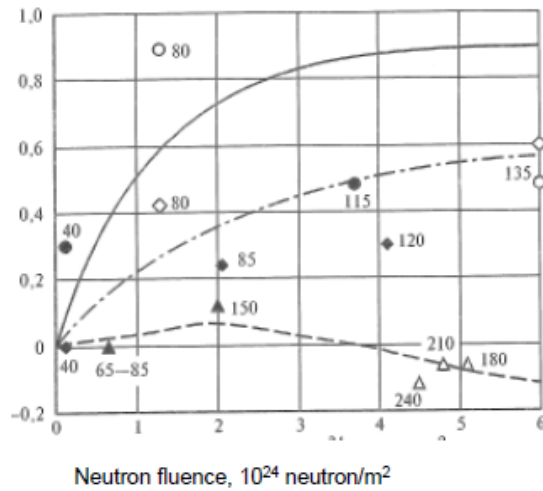
Fig. 3-6 Volumetric change of oxides caused by irradiation within temperatures 40-240°C [25]

Oxides irradiated data tend to show that this group is least sensitive to radiation swelling since most of the data are below 1.5% (Fig. 3-6).

3.3   Aggregates

Irradiated rocks exhibit similar changes as polycrystalline minerals because of the similarity of defects developed in between the phases and minerals due to their different volumetric expansion

eventually leading to cracking. The dimensional changes of irradiated rocks can be as large as 7% resulting in volumetric expansions up to 23%. The contribution of cracking in the volumetric changes can be greater than 67%. A significant portion of cracking causes a reduction in the mechanical properties of rocks. This effect is most strongly exhibited by the decrease in the modulus of elasticity with radiation-induced damage. Although, the compressive and tensile strength also exhibit decreases, the change is not as strong and in some cases an increase in the volumetric compression strength has been observed after irradiation [25].

It has been observed that rocks irradiated at temperatures up to 400°C are mainly affected by irradiation induced effects, while heating is the main degradation effect for rocks irradiated above 400°C. Serpentinized rocks and carbonate rocks, which are close to the dissociation temperature, however, tend to change their properties upon heating rather than irradiation [25].

Radiation induced effects in rocks depend on neutron fluence and spectrum, temperature, and the structure and bonding of its component atoms. The composition and structure of rocks affect the susceptibility to defect formation. Moreover, large grain and medium grain rocks undergo significantly more cracking than small grain rocks and may result even in self-destruction or crumbling. Denisov and his colleagues suggest that the glass content in rock reduces the impact of radiation. However, Boffy noted that glass may expand or shrink upon irradiation [29].

Since the minerals that exhibit the largest expansion are silicates, rocks with silicate minerals are the most susceptible rocks to radiation. Detailed information concerning volumetric expansion and changes in mechanical properties of silicate rocks is shown in Tab. 3-4.

As shown in Tab. 3-5, rocks with carbonate minerals and ores with oxide minerals do not exhibit changes as large as silicate rocks. The only exception is siderite, which expands more than other carbonate rocks because of the presence of quartz. The carbonate rock exhibiting the largest expansion is dolomite. Furthermore fine grain ores exhibit 1.5-3 times less expansion than the medium to large grain ores [5]. Detailed information concerning radiation induced changes in carbonate rocks and ores are shown in Tab. 3-5.

Tab. 3-4 Example of common siliceous rocks

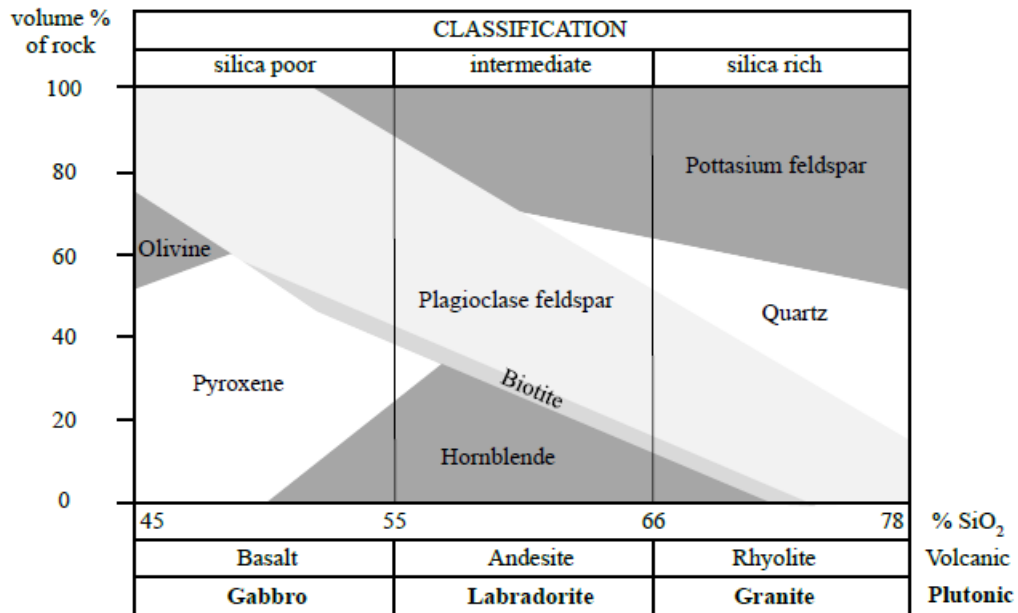| Rock	Main minerals	Dimensional/Volumetric change [%]	Mechanical properties decrease [%]
granite, granodiorite, diorite, quarzitic syenite, sandstone, aleurolite	quartz, feldspar	7 / 23	90-100
gabbro, basalt, diabase, pyroxenite	pyroxene, hornblende	2.5 / 7.7	14
olivinite, dunite, serpentine	olivine, serpentine, silica ceramic containing glass	1 / 3	no significant changes

Fig. 3-7 Classification of siliceous aggregate based on mineral composition [20]

Tab. 3-5 Volumetric change of carbonate rocks and ores

Rock	Main minerals	Volumetric change [%]
dolomite rock	dolomite	up to 3
dolomitized limestone, magnesite rock	calcite, dolomite, magnesite	1.5
calcitic limestone	calcite	0.6
siderite rock	siderite	8.4
hematite ore	hematite	4.8
magnetite ore	magnetite	0.9
chromite ore	chromite	0

<u>Analytical expression of defect accumulation</u>

In 1966 Zubov and Ivanov [30] presented analytical expression that captured irradiation induced changes in quartz structures. Based on available experimental data which showed expansion or change in density of quartz the trends of S-shaped curves have been observed. These trends are also visible on experimental data presented on mineral above in this chapter. Moreover, Zubov and Ivanov explained that S-shaped curve captures the physical phenomenon which is occurring in irradiated minerals meaning accumulation of changes in crystalline structure going amorphous. The kickoff the change is showing slowly on the outer level until certain level of change is attained, then the increase in change is almost linear until the limit of accumulation of defects is approached. The S-shaped curve expression is as follows (*Eq. 3-1*):

$$dV = \frac{a\,dV_{max}[exp(b\varphi)-1]}{dV_{max}+a\,exp(b\varphi)}, \qquad\qquad Eq.\ 3\text{-}1$$

Where dV is relative expansion, dV_{max} is maximum relative expansion, a and b are empirical parameters to approximate experimental data as well as possible and φ is dose of neutrons. In general, the S-shaped curve in other word sigmoid curve is shown in following Fig. 3-8.
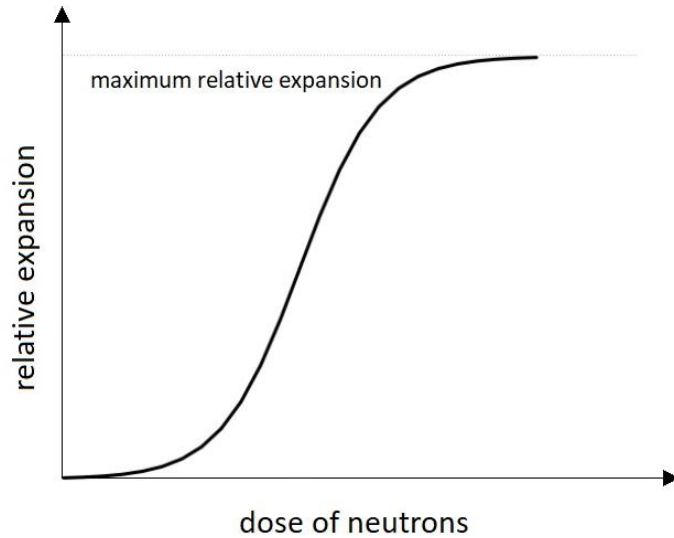
Fig. 3-8 Sigmoid curve used for approximation of relative expansion

3.4 Irradiated aggregate properties trends

An extensive compilation of experimental data on the dependence of aggregate properties on radiation induced volumetric expansion can be found in [25]. However the concise version of trends that are expressed by various aggregates are summarized in following text to understand the overall phenomena exhibited by aggregates depending on aggregate structure. In this context, the aggregate structure is meant the connection between individual grains of minerals and their size. Thus, the cemented and granular aggregates are distinguished. While cemented aggregates are formed by rather smaller grains and have more homogenous structure, the granular aggregates contain rather larger grains of minerals, and the structure tends to be non-homogeneous.

The main reason for reduction of mechanical properties of aggregate is the significant portion of cracking during aggregate expansion. Generally the portion of cracking volume is about 2/3 of the whole aggregate swelling. Therefore the drop-off of mechanical properties can be detrimental. It is quite relevant to know volumetric expansion of aggregate including the mechanical properties change because both of these effects have crucial impact on the properties of concrete containing such aggregate. The change of mechanical properties of aggregate is then added to the cracking of cement paste within concrete caused by aggregate swelling.

The mechanical behavior of aggregates during irradiation/RIVE strongly depends upon the type of aggregates including composition, structure and whether it is a cemented aggregate or not. The cemented aggregate can maintain mechanical properties on the initial level even with small amount of RIVE while compact aggregate exhibit the reduction of mechanical properties right away with initiation of the RIVE. The difference between the two is the matrix of cemented aggregate which can absorb part of the initial RIVE. It can be also given by lower elasticity of the matrix which does not cause high stresses like the high elastic modulus of minerals joined within the compact aggregate lacking the matrix. The stresses in the connection between the minerals of compact aggregate are significantly higher than in cemented aggregate which leads to immediate reduction of modulus, strength of aggregate etc. Another reason might be porous structure of cemented aggregate which is expected to be much higher compared to compacted aggregate. The pores create extra space where the RIVE can develop without significant affection of mechanical properties of aggregate. To illustrate the difference between cemented and compact aggregate the typical representative of cemented aggregate is sandstone and compact aggregate is assumed as granite in this context, see Fig. 3-9.
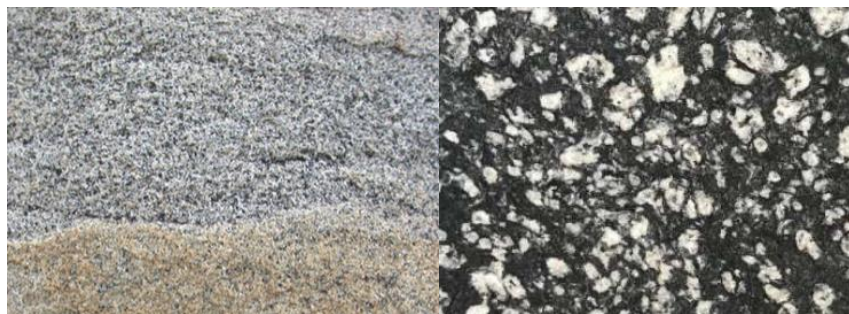
Fig. 3-9 Aggregate structure, cemented (sandstone) and compact (granite)

As it has been mentioned before, the cracking volume of aggregate is very important attribute when referring to mechanical properties of irradiated aggregate. Therefore the portion of cracking volume needs to be investigated for different aggregate structures. The experimental data, see Fig. 3-10, are limited but when it comes to cracking volume increase depending on total volume increase there might visible trend for magmatic aggregate (gabbro, granite, basalt, andesite) with little steeper slope than in case of sedimentary aggregates (sandstone).
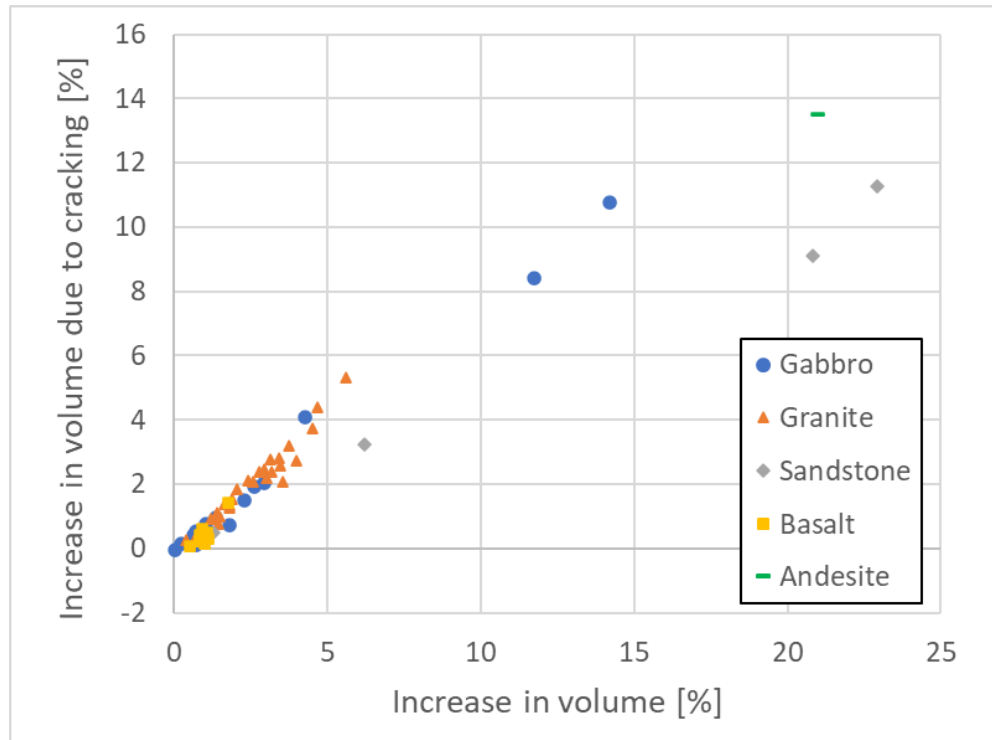
Fig. 3-10 Dependence of cracking volume on total increase of aggregate volume

Two mechanical properties of aggregate are documented in literature with regard to the volume of cracks, elastic modulus and compressive strength. While in case of elastic modulus the data are more comprehensive than in case of compressive strength. Elastic modulus data can be divided into three groups of aggregate depending on their structure: plutonic (gabbro, granite), volcanic (basalt) and sedimentary (sandstone), Fig. 3-11. All three groups show slightly different trend in elastic modulus drop-off with increasing cracking volume. The plutonic aggregate with larger grain structure shows the fastest reduction of elastic modulus. While volcanic aggregate exhibits intermediate response and sedimentary group shows the slowest reduction compared to other groups.
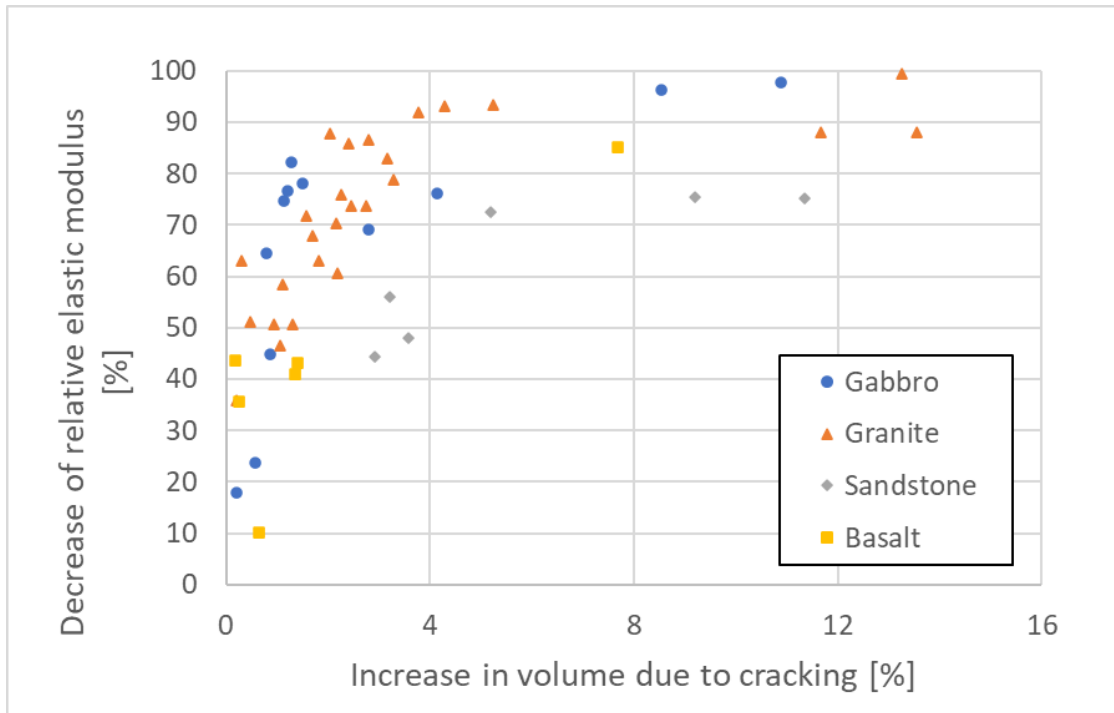
Fig. 3-11 Dependence of elastic modulus reduction on cracking volume of aggregate

Finally the compressive strength trends of reduction depending on the extent of cracking volume can be divided into two groups, Fig. 3-12. The first group represents magmatic rock (plutonic and volcanic) regardless of grain size. The second group represents cemented aggregate as a sedimentary aggregate. Magmatic aggregate loose compressive strength very rapidly at the beginning of the cracking volume development, it can very quickly drop to 50% or 80% of reduction of original strength. Then the reduction progress slows down, but the extent is already almost at its maximum. While sedimentary aggregates initially gain some extra strength which might be related to pore filling RIVE and internal stress state seemingly increasing strength but then the drop-off progresses to near limit of about 90%. It is about at the same volume of cracking when the nearly complete reduction is attained for both aggregate groups, magmatic and sedimentary.
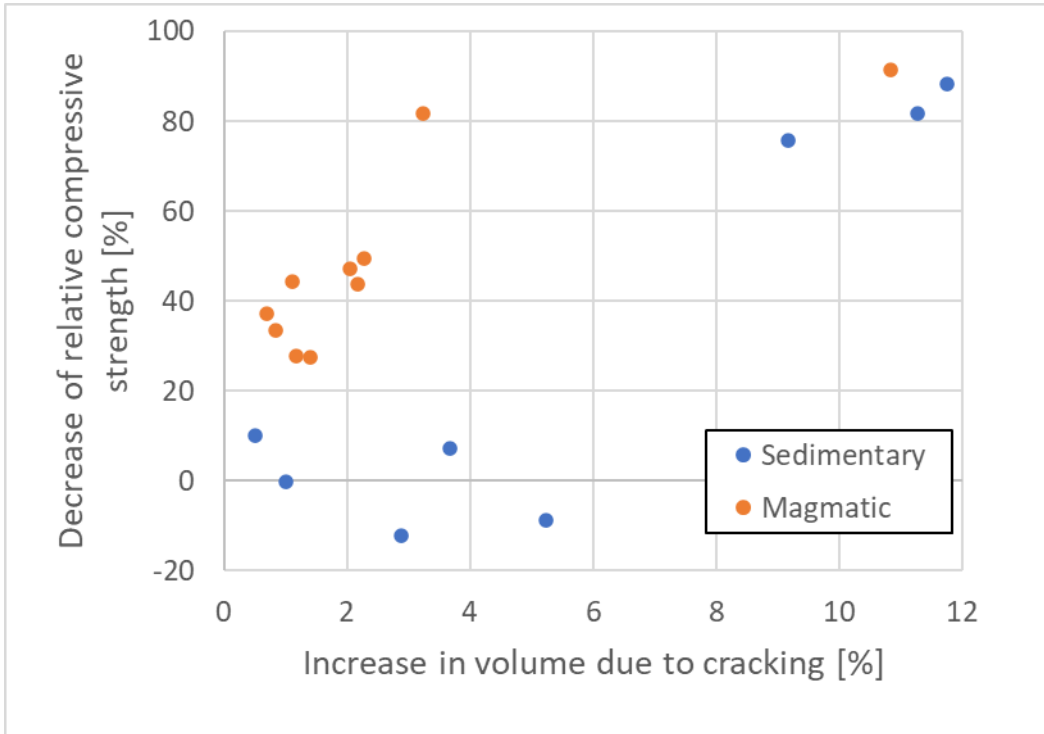
Fig. 3-12 Dependence of compressive strength reduction on cracking volume of aggregate

4 Irradiated cement paste

The binder in concrete has different structure compared to the main admixture - aggregate. Unlike dense, stiff and hard aggregate the cement paste created from three typical components which are sand, water and cement, is rather porous therefore open for transport phenomena and the mechanical properties are usually lower than aggregate ones. One of the main factors ruling the density and pore distribution within cement paste is water-cement ratio.

The content of water in cement paste showed to be highly important aspect while irradiated. As it has been mentioned before the interaction of matter with gamma rays result in water radiolysis therefore more water means greater impact on the cement paste. Also as the cement paste contains sand with grains usually smaller than 4 mm which react to neutron irradiation as other aggregate with RIVE. That results in two counteractive phenomena appearing at the same instant. Another process that may appear along is shrinkage of cement paste due to drying when exposed to elevated temperatures which is highly possible in conditions during irradiation, [3].

However to properly study the combination of effects of irradiation on cement paste various experiments have been performed ([2],[3],[4]). In order to separate the phenomena at least partially, beside irradiated specimen, the so called hot and cold control specimen have been studied as well. Since the short time irradiation during experiments often result into elevated temperatures reaching 200°C, the hot specimens are heated-up similarly in the oven with the same temperature treatment as in case of irradiated samples to compare the results on the heated samples with and without radiation. The cold specimen are usually stores in controlled environment with stable temperature and ambient humidity and are the control samples with properties without any defect caused by irradiation or heating. Such studies showed interesting trends regarding the dimensional change, the irradiated samples shrunk in same order as hot control specimens. Similar results have been found in case of Young's modulus, bending or compressive strength test results that irradiated samples and samples subjected to same thermal cycles are of the same order. Kelly performed irradiation experiments keeping the temperature at the level of 40°C which does not have comparable thermal effect as temperatures above 100°C. The results of these experiment confirmed the previous assumption that the damage within cement paste causing the drop of mechanical properties is mainly caused by elevated temperatures because the Young's modulus and strength of cement paste exposed to irradiation without elevated temperatures do not show any considerable

change, Fig. 4-1. Only dimensional change is observed on samples that shrunk which is related to gas release upon water radiolysis.
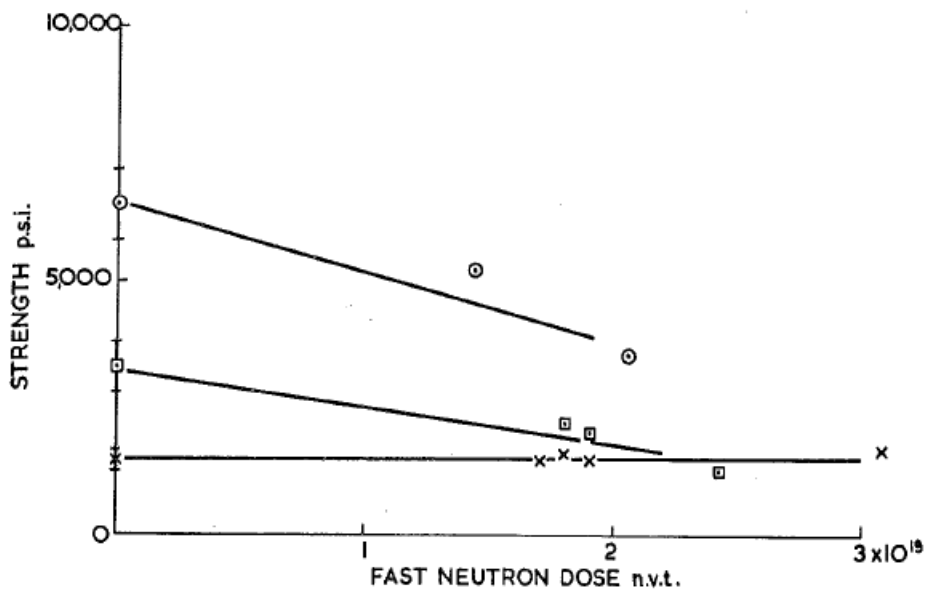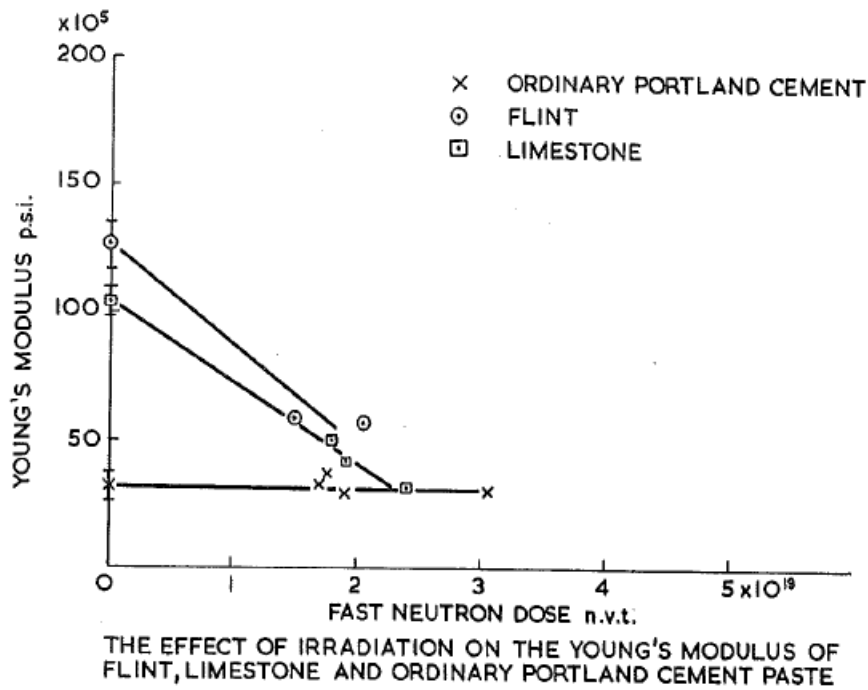

THE EFFECT OF IRRADIATION ON THE YOUNG'S MODULUS OF
FLINT, LIMESTONE AND ORDINARY PORTLAND CEMENT PASTE

Fig. 4-1 Effect of radiation on cement paste elastic modulus and compressive strength [2]

5 Goals

The knowledge on the irradiated minerals and aggregates shows the trends of behavior but is limited in amount of data. Also the composition of minerals in the aggregate has impact on the overall behavior of RIVE. Based on the knowledge of behavior of irradiated minerals, the model for irradiated aggregates considering the mineral composition is proposed. The fuzzy logic as a tool for simulation with knowledge but limited data is utilized.

For the assessment of actual NPP structures such as biological shield, the concrete behavior must be studied. The mesoscale model incorporating aggregates that exhibit RIVE within the brittle matrix is studied using finite element method of modeling the structure. The model needs to be validated on experimental data to secure its potential.

Finally the real biological shielding structure is modelled to observe the damage that can be expected on the existing structures exposed radiation for decades. Ideas how to avoid potential damage in the new designs of NPP structures is proposed.

6 Model of irradiated aggregate

Effect of irradiation on minerals including the brief introduction of effect on aggregates are presented in previous chapter. It is based on experimental data collected by various research groups worldwide [6]. From the knowledge that is presented above can be concluded crucial effect of mineral type and content within aggregate, dose of neutrons accumulated in sample and its temperature while irradiated. Various minerals exhibit different amount of swelling and its possible limit while dose of neutrons combined with temperature during irradiation rule the speed of maximum swelling attainment. Profound swelling is discovered primarily within silicate aggregate therefore the focus of this work is going to be on the most susceptible silica aggregates. Best example is the most studied mineral quartz which is prone to RIVE and available data show the temperature effect very clearly, see Fig. 6-1. The effect of temperature on quartz and other silicate minerals changes the slope of sigmoid curve showing the expansion dependent on neutron dose. While lower temperatures exhibit steep slope the higher the temperature the lower the slope. Specifically, temperatures above 200°C show slower RIVE and temperatures above 600°C nearly stop the RIVE completely. It is given by annealing effect of silicate minerals at elevated temperatures. Even though the annealing effect improves quartz resistance to radiation exposure it is not always the case that elevated temperatures enhance radiation resistance of mineral or aggregates, for example the carbonates rather release carbon dioxide and decompose, or iron ores melt.
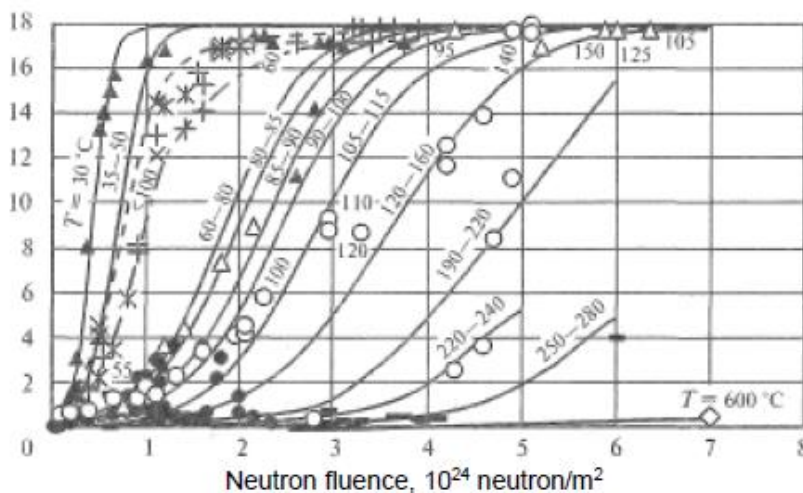
Fig. 6-1 Volumetric expansion of quartz dependent on neutron dose [25]

The problem of RIVE of aggregates is rather complex with many influencers and the experimental data for such a complex problem are still very limited. The lack of data for all possible combinations of mineral types, their content, exposure temperature and dose of neutrons of service life in facilities, calls for joint effort of expert knowledge on geology combined with experimental data on tested samples in nuclear facilities. It is the goal of this section to create a model covering the gaps in experimental data. For this purpose the fuzzy logic method is chosen as an instrument to interconnect knowledge on irradiated minerals from experiments and determine the behavior of aggregates exposed to irradiation. The crucial parameters chosen to be ruling the model are composition of aggregate (content of silicate minerals), temperature while irradiated and integral dose of neutrons.

6.1 Fuzzy logic

Fuzzy logic has been shown to be a flexible and robust instrument for controlling processes since its introduction in 1960's, [31]-[33]. For example, fuzzy logic demonstrated its versatility in material modeling of early age concrete or corium-concrete interaction during a severe nuclear accident [34]-[36]. Fuzzy logic works with fuzzy numbers. The difference between classical logic crisp numbers and fuzzy numbers is given by the degree of membership in the set. In the case of classical logic, the number either belongs to the set or not which gives degree of membership of 1 or 0 respectively. For the fuzzy number, the degree of membership is an interval of values from 0 to 1, see example in Fig. 6-2.
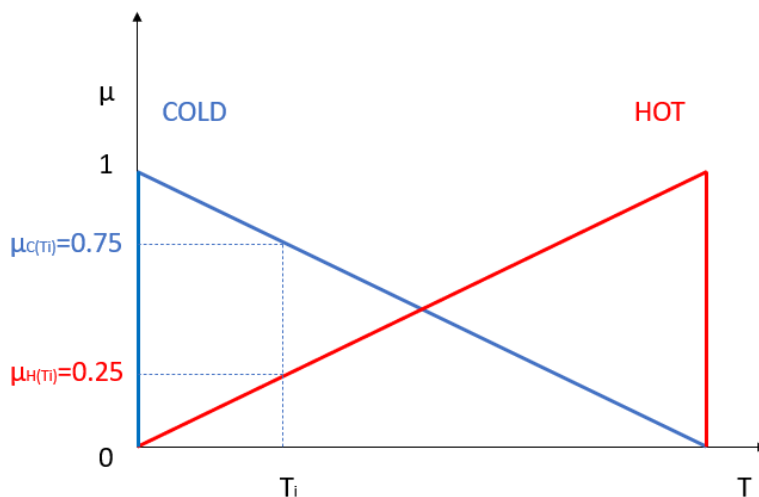
Fig. 6-2 Example of membership functions describing a fuzzy number

Accordingly, the fuzzy set is the set of fuzzy numbers. The basis of the fuzzy logic is represented by the logic relationship:

$$if\ X\ then\ Y, \hspace{4cm} Eq.\ 6\text{-}1$$

where *X* represents the input fuzzy sets and *Y* represents the output fuzzy sets determined by fuzzy logic processing. The fuzzy logic model can substitute an analytical model when experimental data are limited. The uncertainty of the experimental data is reflected in the fuzzy sets. The result of the fuzzy logic processing can be either a crisp value that represents a mean value or the fuzzy number that represents an interval of possible results with a distribution of values.

Even though the amount of irradiated concrete experimental data appears to be extensive, the utilization of the data is very limited due to its scatter, which is primarily caused by the external testing conditions, variations in experimental conditions (dose rate and temperature) and concrete (aggregate) composition. For these reasons, fuzzy logic is expected to be a useful tool to evaluate the assembled data. This is expected to be especially valuable since the acquisition of radiation-induced property changes is difficult and time-consuming to obtain.

6.2   Fuzzy logic model structure

The first fuzzy logic models have been mainly developed as verbal models working with expert's opinions describing the problem's input/output and reasoning in between [37]. The process of fuzzy model development consists of fuzzification of inputs, inference that contains rule base and inference mechanism resulting in membership function of model output, and defuzzification which turns membership function into crisp value. The membership functions in input/output fuzzy sets can be linear or nonlinear depending on the type of the problem and relation between variables. The fuzzification is process of making the fuzzy numbers from crisp values. Following inference is decision making what happens for each set of input values combination. Most common inference used in fuzzy modelling is Mamdani [38], which is also used in following model. The standard rule in Mamdani model can be expressed as:

$$if\ (X{=}A)\ then\ (Y{=}B). \hspace{3cm} Eq.\ 6\text{-}2$$

In the defuzzification process, more method can be applied such as middle of maxima method, center of gravity method, mean-max membership method etc. In the following model weighted average method of defuzzification is used.

Example of fuzzy model with two inputs/one output is showed on the chart with the steps of fuzzification, inference and defuzzification leading to get crisp value as an output, see Fig. 6-3.
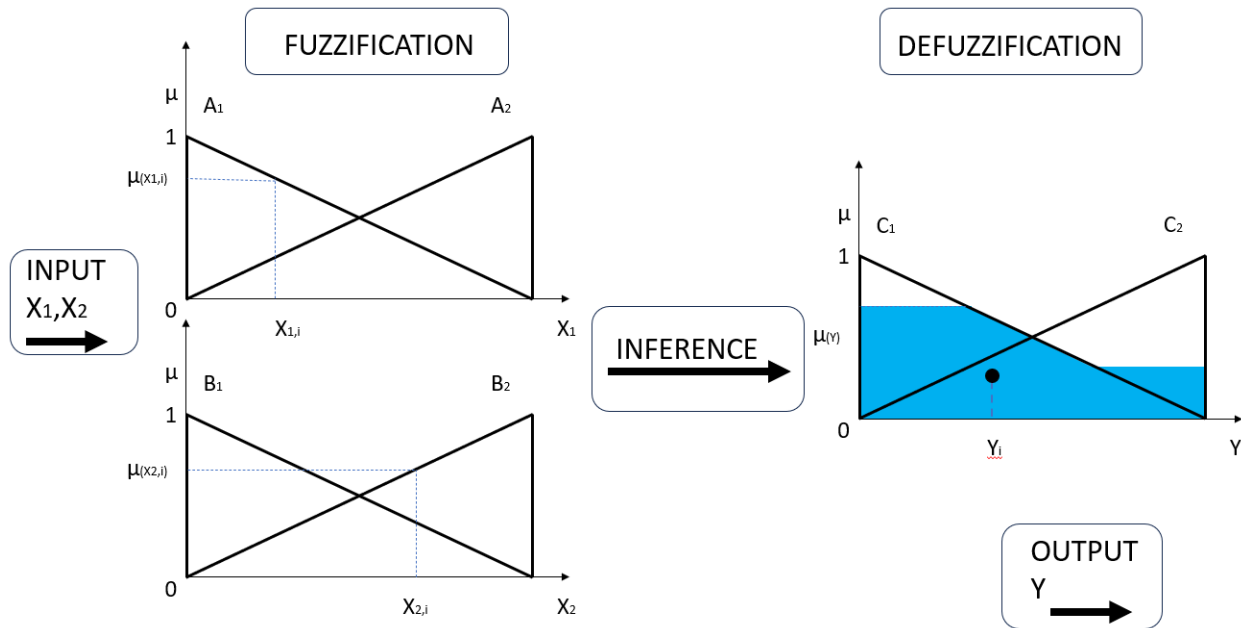
Fig. 6-3 Fuzzy model flowchart

6.3 Dimensional changes description

Since the change of mechanical properties of aggregate is bound to dimensional changes, an estimate of dimensional changes of aggregates induced by radiation is the crucial step to determine the resulting mechanical properties. The driving parameters for aggregate expansion consist of the types of minerals in aggregate, their content, and the aggregate structure. Therefore, the main input to an aggregate expansion model is the expansion of the component minerals. Since the minerals expand differently under various temperatures, the expansion of minerals has to be controlled also by temperature. Also, the mineral expansion is limited by a saturation point mentioned above in the section 3.2. In order to use mineral expansion data, the membership function of sigmoid curves for different temperature ranges are fitted to the data points based on the coefficient of determination (R^2), Fig. 6-4.
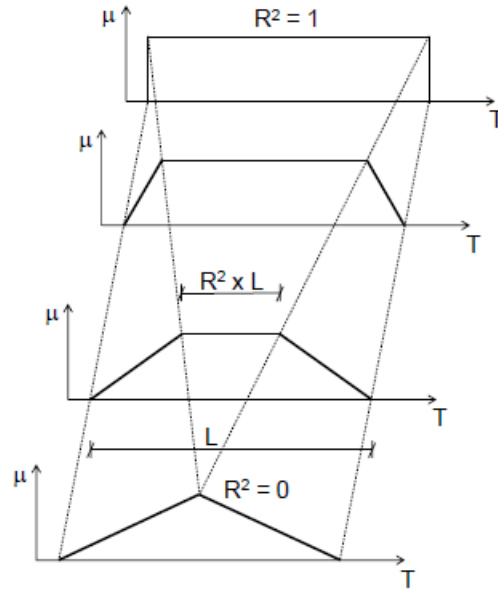
Fig. 6-4 Membership function dependent on coefficient of determination of sigmoid curves fitted on experimental data [20]

Sigmoid curve for quartz data have been already used by Zubov in 1966, [30]. The general formula of sigmoid curve is

$$dV_{(\Phi)}=dV_{max}/(1+e^{-p(\Phi-q)}) - r, \qquad\qquad Eq.\ 6\text{-}3$$

where dV is the volumetric expansion, dV_{max}-r is maximum expansion of the mineral, Φ is neutron fluence, and $p,\ q$ and r are parameters prescribing the shape of sigmoid curve specifically the slope and its position in coordinate system. Figure 4 shows the effect of parameters dV, p and q on the shape of sigmoid function. The parameter r shifts the function vertically that it goes through the origin, Fig. 6-5.

Fig. 6-6 depicts the volumetric expansion of quartz, which is mineral with the most data and therefore should have the best reliability. The curves for different temperatures show the effect of annealing on the material upon irradiation. Specifically, the higher the temperature the less effect of the radiation dose. Furthermore, the change of the curve slope with temperature has decreasing trend that can be utilized in aggregate expansion model.
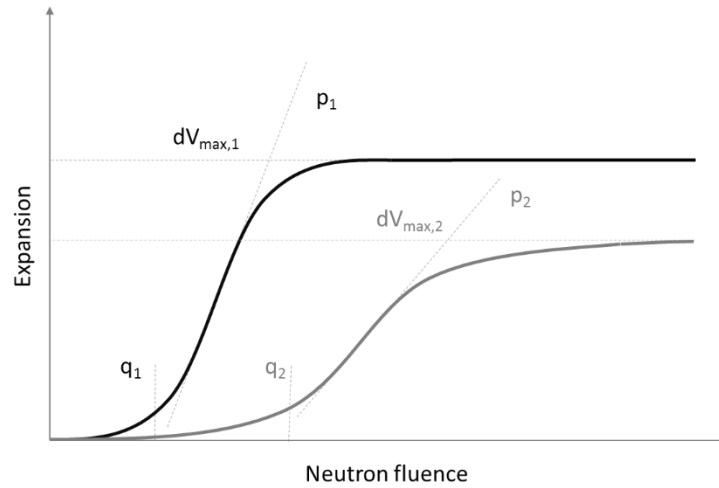
Fig. 6-5 Parameters influence function shape

Then, the Fig. 6-7 depicts volumetric expansion of acidic plutonic magmatic rocks like granite, diorite, granodiorite etc. The curves of volumetric expansion for these rocks are given at temperature ranges 90-110°C and 115-160°C, while the expansion development for the lower temperatures is unknown. Therefore the trends in mineral behavior at lower temperatures can be extrapolated to obtain the volumetric expansion of aggregate at lower temperatures as well.
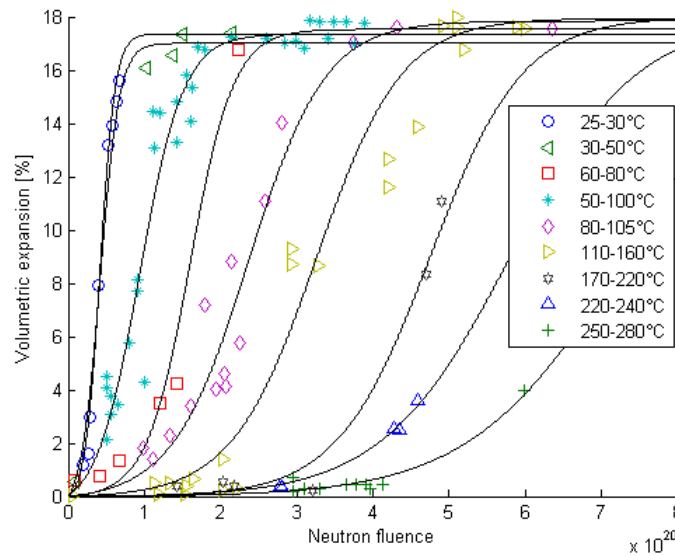
Fig. 6-6 Model of volumetric expansion of quartz [20]
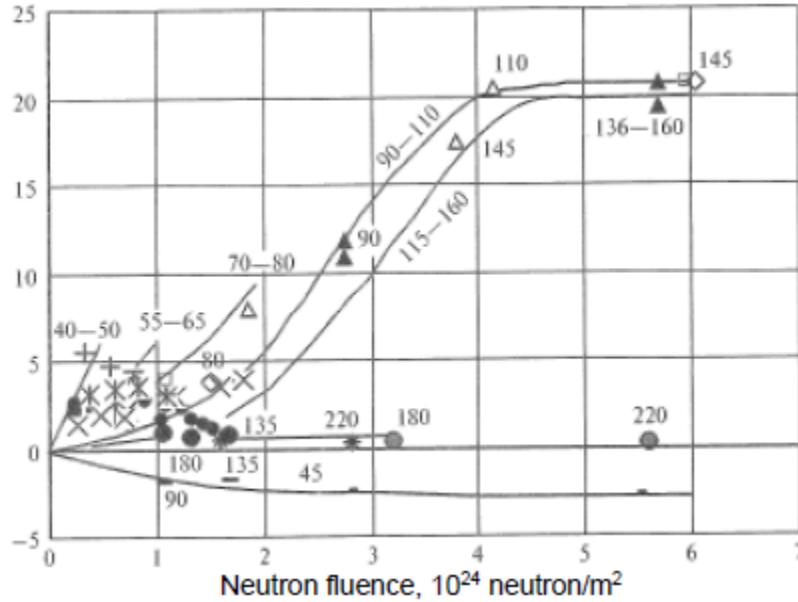
Fig. 6-7 Volumetric expansion of acidic plutonic rocks dependent on neutron dose [25]

6.4 Method of mixing of minerals

The volumetric expansion of irradiated aggregate at high dose levels can either reach the saturation point or cause the destruction of the sample. Since the significant part of radiation-induced volumetric expansion of aggregate consists of cracks, the material integrity may be affected. The loss of material integrity, which was observed by Seeberger [5] in the case of granite containing mica, led to the collapse of the sample. Although, the actual content of cracks in irradiated aggregate has not yet been measured, the model should take it into account.

Each aggregate has a specific mineral composition. For the aggregate behavior prediction, the content of minerals is the determining parameter. Beside the mineral content, the parameters influencing aggregate expansion in proposed model are temperature and neutron fluence. Since the curves for mineral expansion are given within the temperature range, the temperature as an input parameter in the model is fuzzified using triangular membership functions. Also parameters dV_{max}, p and q describing the mineral radiation-induced expansion in specific temperature range are fuzzified because the temperature itself is fuzzy number with upper and lower limit of triangular membership function, see Fig. 6-8.
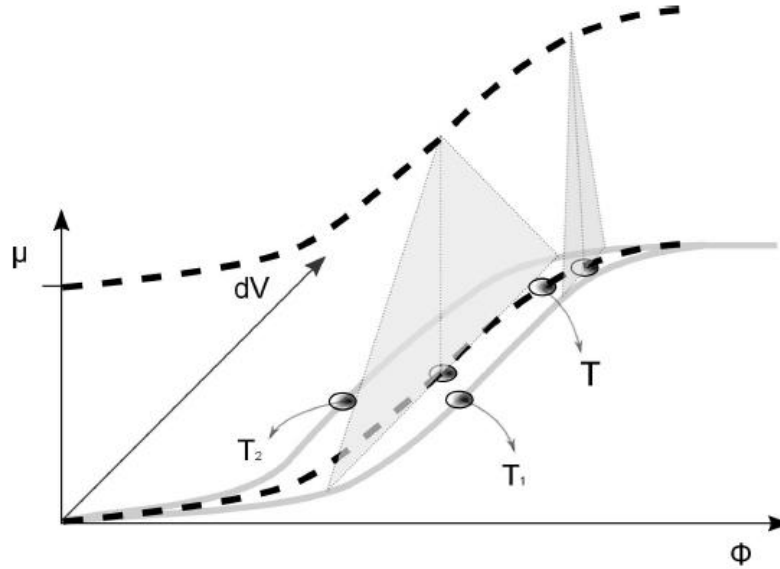
Fig. 6-8 Triangular membership function for temperature with lower and upper limit [20]

The shape of aggregate expansion curve is identical to the function used for radiation-induced expansion of minerals (2) in order to utilize the parameters of the mineral curves to obtain parameters of aggregate expansion curves. This model intends to apply the trends of mineral behavior described by parameters dV_{max}, p and q to obtain aggregate expansion. Therefore the parameters dV_{max}, p and q are calculated as linear interpolations of parameters for the minerals in aggregates based on fuzzy sets for temperature and volume fraction of minerals. Then the parameter dV_{max} is corrected according to the maximum radiation-induced expansion observed for the specific aggregate that includes effect of cracking in the overall expansion. Since the experimental data of rocks show the peak of the radiation-induced expansion within a few temperature ranges, the estimate of the volumetric fraction of cracks in the total expansion can be determined. Moreover, the estimate of crack volume is used in the calculation for the same aggregate but within the temperature range where the peak expansion has not yet been measured. The volumetric fraction of cracks in a particular rock is designated as dV_{cr}. The algorithm of the model considering various content of fractions of minerals determining the total volumetric expansion is shown in Fig. 6-9.

The values used for mineral expansion curves are listed in Tab. 6-1, the mineral composition of aggregates are listed in Tab. 6-2 and the example of resulting parameters for aggregates are listed in Tab. 6-3.

```
Define: irradiation temperature T, maximum aggregate expansion $dV_{max_a}$, frac-
tion of each mineral $f_{m_i}$ and neutron fluence $\phi$.
for i do
   if $f_{m_i}$>0 then
      Evaluate one input (T) — three output fuzzy logic model
      Store output data ($p_{m_i}$, $q_{m_i}$ and $dV_{m_i}$)
   else
      Continue
   end if
end for
Determine $dV_{cr}$
Determine $p_a(f_{m_i})$, $q_a(f_{m_i})$ and $dV_a(f_{m_i})$
Determine $dV(\phi)$ {Eq. (1)}
```

Fig. 6-9 Algorithm of mineral mixing [20]

Tab. 6-1 Parameters of sigmoid curves for silica minerals

Silica minerals	dV$_{max}$	p	q
quartz	17.6-18	1-10x10^{-20}	0.42-7.3x10^{20}
pottasium feldspars	7.4-8.2	1.19-10x10^{-20}	0.7-4.45x10^{20}
plagioclase feldspars	7-7.2	1.3-2.9x10^{-20}	1.2-5.3x10^{20}
pyroxenes	2.35-3.1	2-7.2x10^{-20}	0.3-1.68x10^{20}
biotite	1.64	0.99x10^{-20}	0.99x10^{20}
hornblende	1.2-2.2	1.7-7 x10^{-20}	0.57-2 x10^{20}

Tab. 6-2 Content of respective minerals in aggregate samples

Silica minerals	Aggregate samples			
	Gabbro	Granite	Labradorite	Sandstone
quartz	0.02	0.25	0	0.8
pottasium feldspars	0.03	0.35	0	0.1
plagioclase feldspars	0.5	0.2	0.85	0.1
pyroxenes	0.3	0.05	0.15	0
biotite	0.08	0.05	0	0
hornblende	0.07	0.1	0	0

Tab. 6-3 Example of resulting parameters of aggregate RIVE from fuzzy model

Aggregate	T[°C]	dV_{cr}	dV_{max}	p	q
gabbro	70	0.63	13.70	3.98×10^{-20}	1.32×10^{20}
granite	90	0.56	20.35	2.55×10^{-20}	2.33×10^{20}
labradorite	80	0.55	14.00	2.46×10^{-20}	2.23×10^{20}
sandstone	80	0.31	22.76	2.72×10^{-20}	2.03×10^{20}

6.5 Model evaluation by Mean error method

Fig. 6-10 show the results for granites in different temperature ranges. For each temperature range two boundary curves of radiation-induced expansion of aggregate are determined to provide an estimate of the possible results within the temperature range. The experimental data plot in the same figure as model curves provides a visual comparison between the model and experimental data available for the given temperature range.
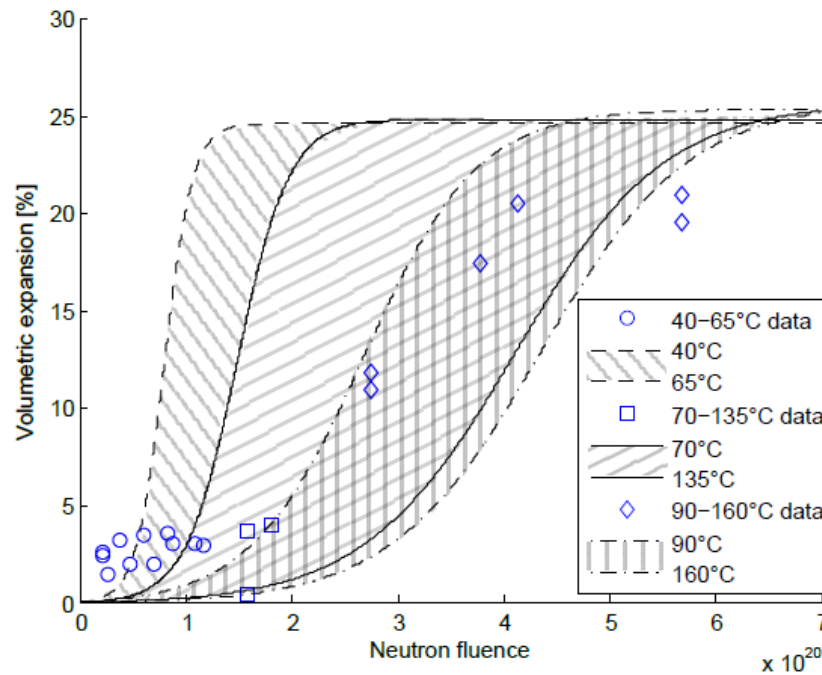
Fig. 6-10 Example of results of modeling of granite in different temperature [20]

In order to evaluate the model accuracy compared to experimental data, a method to evaluate such a model is developed. Since the fuzzy logic model of radiation-induced expansion of aggregates gives the boundary curves of each temperature range, the data between the curves are assumed to be results with no errors. However, the data outside the boundary curves do contain errors. Each data point error is evaluated twice to get errors for both boundary curves. The minimum error is then used in the calculation of the mean model error *ME* using equation (*Eq. 6-4*):

$$ME = 1 - \frac{\sum_{i=1}^{n}\left|\frac{f_i - y_i}{y_i}\right|}{n},$$

Eq. 6-4

where *n* is the number of data points, f_i is the output of the aggregate radiation-induced expansion model function (corresponding to the curve nearest the data point), and y_i is the experimentally obtained radiation-induced expansion of aggregate. The mean error evaluation of the proposed model gives a sense as to how the model is able to capture experimental data and also provides the ability to compare how the model works for different types of rocks. Following figures show ME for developed models, see Fig. 6-11 - Fig. 6-13.
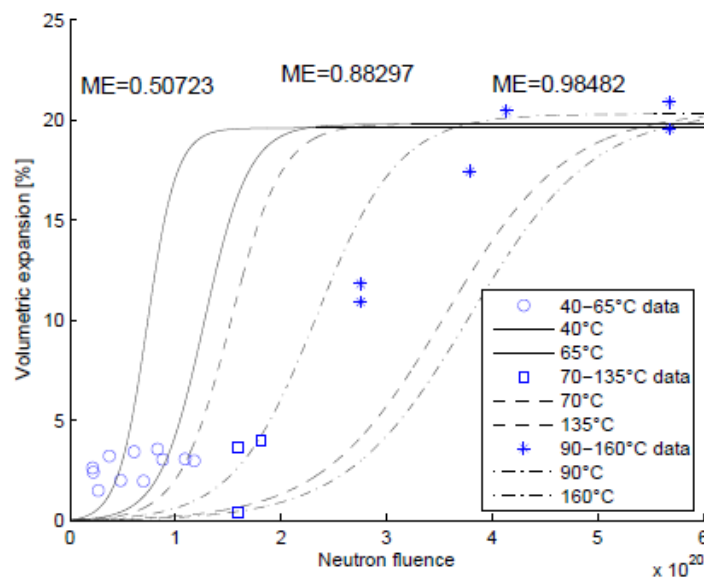
Fig. 6-11 Radiation-induced expansion of granite
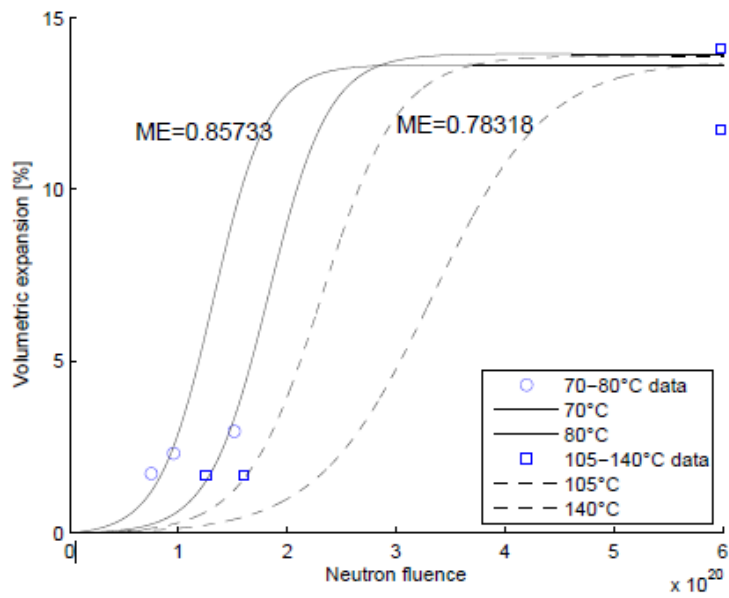
Fig. 6-12 Radiation-induced expansion of gabbro
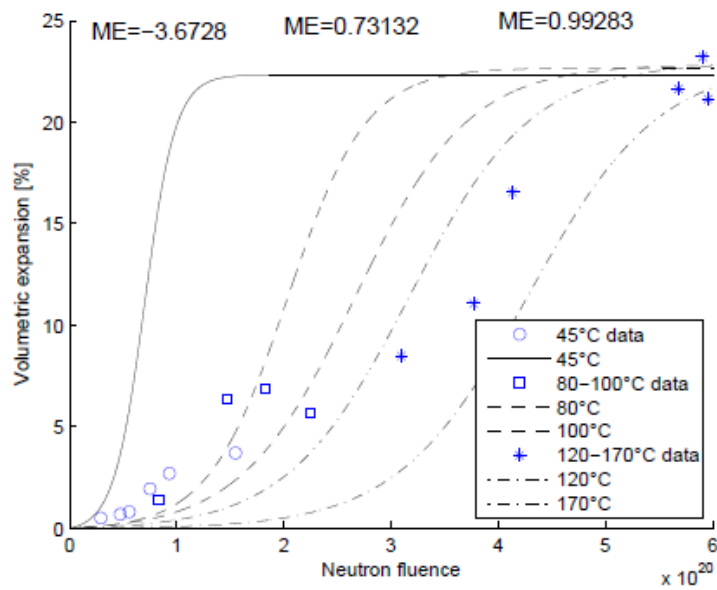
Fig. 6-13 Radiation-induced expansion of sandstone

6.6   Discussion of aggregate expansion model

All of the tested aggregates consist of silicate minerals. In some cases, for example labradorite aggregate, the correlation of the experimental data and the model is very good. For other cases, the correlation with regard to the ME is poor or the experimental data are limited resulting in an unacceptably low ME. This can be seen in the case of sandstone at 45°C where the model completely misses the experimental data then the ME becomes a negative number.

Firstly, the model is based on individual mineral expansion so the lower R^2 of the mineral expansion curve affects the ME of the resulting aggregate expansion curve. The low R^2 is due to the limited data for that particular mineral or the specific temperature range of mineral expansion. This is especially apparent in the case of pyroxenes and potassium feldspars at 45°C. The R^2 is low which results in a low ME for aggregates containing these minerals. Secondly, the aggregate structure that is given by the aggregate origin (how it is formed in nature) affects defect formation. For example, sandstone, a sedimentary rock (cementitious), contains more pores than granite or other plutonic magmatic rocks (compaction). Therefore, the interconnection between the minerals contained in the rock should be incorporated into the model in order to obtain more realistic data. For this reason, the model clearly works better for compacted and well-crystallized aggregates than for cementitious aggregates. For cementitious rocks the kinetics of RIVE of minerals with respect to the neutron fluence should be assumed.

Additionally, Fig. 6-14 depicts the gap between the model with the corrected maximum expansion and without. The actual expansion of aggregate clearly does not depend only on the expansion of minerals comprising the aggregate but also on the volume of cracks developed during the differential expansion of the minerals.

Described model has been published by author in [20].
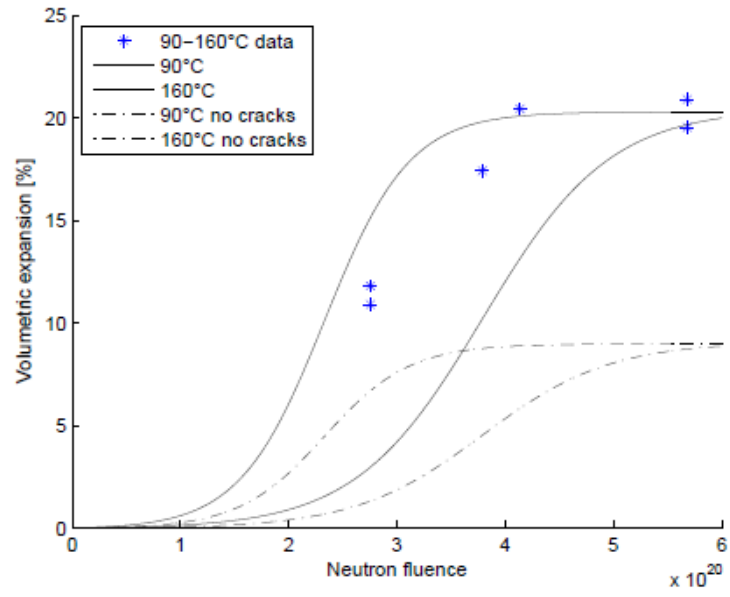
Fig. 6-14 Radiation-induced expansion of granite with and without cracking

7 Mesoscale model of concrete

While in previous chapters the studied changes of material properties have been done on microscopical level and focused on behavior of minerals, the mesoscale and macroscale must be included when assessment of real structures is assumed. For this purpose the ATENA software is used to study impact of RIVE on concrete material properties. ATENA is advanced software for numerical modelling of brittle materials especially reinforced concrete structures using finite element method (FEM). The non-linear material is modeled with fracture-plastic material model that assumes plastic behavior of concrete in compression and orthotropic smeared crack model in tension. This material model is called Cementitious2 and it was developed by Cervenka and Papanikolaou [39] and it is suitable for concrete and rocks.

In the following part the main focus is on aggregate swelling while irradiated and impact of such behavior on the rest of the concrete sample. Mesoscale samples of concrete are developed in ATENA Preprocessor GiD which serves for preparation of model topology, material model properties and boundary conditions of the model that is then executed in ATENA software.

ATENA as an advanced software specialized on concrete material contains various material parameters within results of the simulation that allow to study material development under irradiation into detail. Such material parameters are softening based on equivalent plastic strain ε_{eq}^{p} and reduction of initial compressive strength fc (*Eq. 7-1*), current tensile strength which is in the direction of the first crack (principal directions) related to decrease of compressive strength and others like displacement, strain or crack development.

$$\frac{fc(\varepsilon_{eq}^{p})}{fc}$$

Eq. 7-1

Material deterioration is studied on the mesoscale samples with aggregate which is expected to be most problematic in nuclear application - siliceous aggregate. Silicate minerals and rocks exhibit substantial volumetric change therefore they present the worst-case scenario with the volumetric swelling up to 23%.

ATENA software has been used to study damage of concrete structures in various nuclear facilities such as containment accident analysis, pushover analysis of NPP's buildings, radioactive waste containers, [40]-[43].

7.1 Fracture-plastic material model

Material model for concrete combines two constitutive models for compressive and tensile behavior separately. Classical orthotropic smeared crack model with crack band is employed in tension (fracture), the Rankine criterion is assumed for the failure (when the maximal principal stresses are reached, the failure occurs) with exponential softening. As the crack is developing the model can capture either fixed crack which is opening in the direction of the initial principal tensile stress that initiated the crack or the rotated crack that develops in the direction of current principal tensile stress. The fracture model is defined by fracture energy which is integration of tensile stress inducing the crack and by tensile strength of material, the softening of material as a function of crack opening has been introduced by Hordijk [44]. The crack band in ATENA is assumed as length of finite element in the direction of crack opening, see Fig. 7-1, which is described in [45].

CRACK BAND METHOD

crack opening law

crack band

fracture energy G_f

crack opening-strain transformation

$$w = \varepsilon \, L_t$$
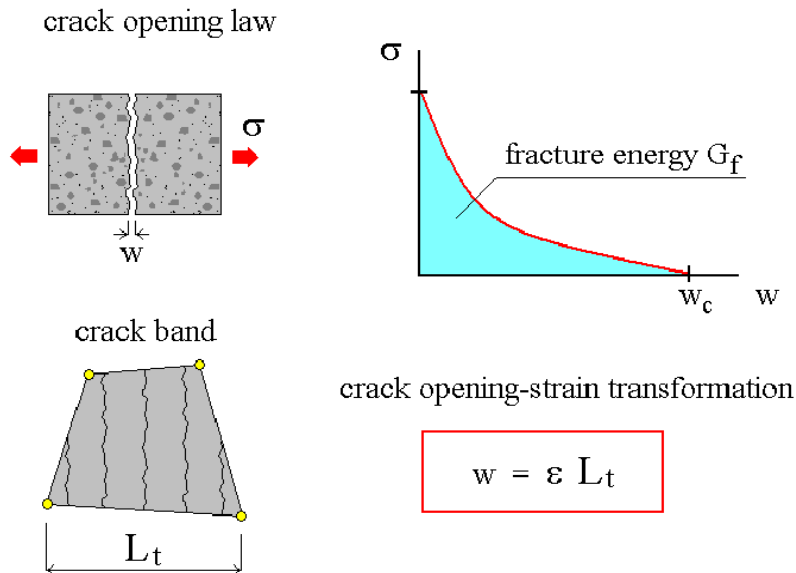
Fig. 7-1 Crack band method – crack width calculation [49]

Constitutive model in compression is based on Menétrey-Williams failure surface [46] with hardening/softening parameter and non-associated flow rule based on nonlinear plastic potential function. The failure surface is depicted in Fig. 7-2. The softening/hardening parameter control the position and size of the failure surface and potential function surface in stress space, Fig. 7-3. The

non-associated flow is adopted in a way that plastic flow direction depends on the location of the failure surface but not the direction of loading.
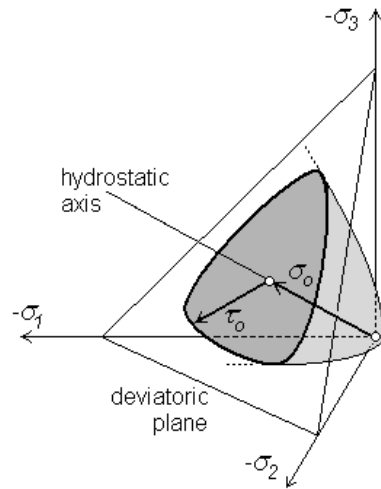
Fig. 7-2 Menétrey-Williams failure surface [49]
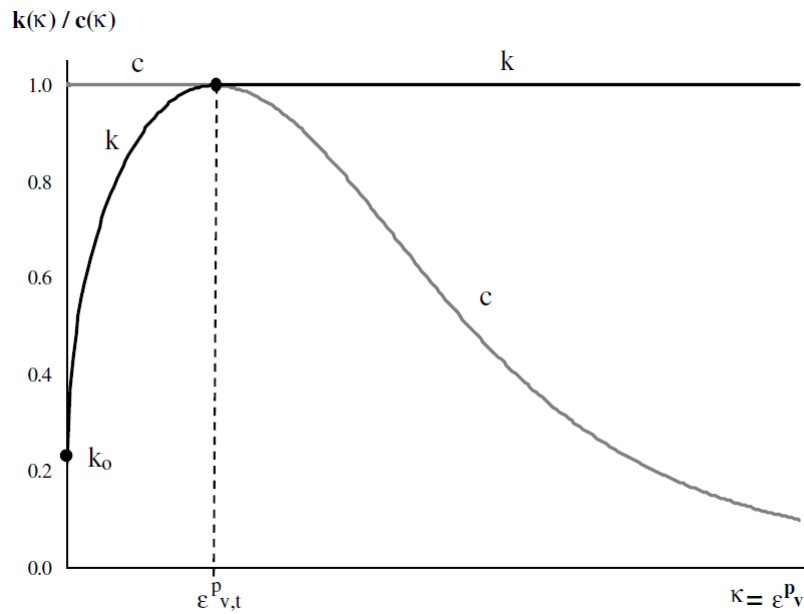
Fig. 7-3 Hardening/softening parameter controlling failure surface [49]

The hardening part of the material definition is related to plastic strains while the softening branch is associated with displacement which should ensure the mesh size independency, [47]. The

characteristic length size also called crush band is analogical solution as crack band which takes the size of element in the direction of the minimal principal stress, Fig. 7-4.
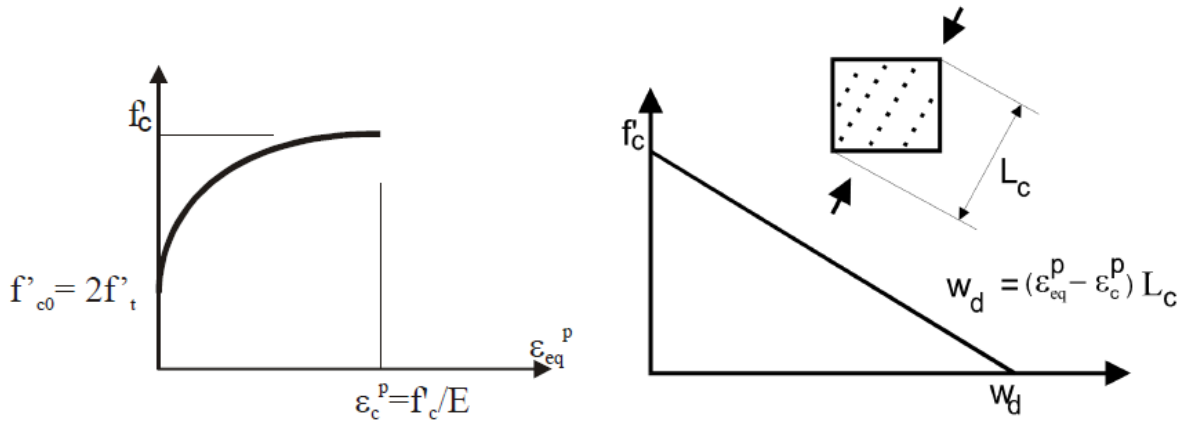
Fig. 7-4 Hardening related to plastic strains and softening related to displacement in crushed band [49]
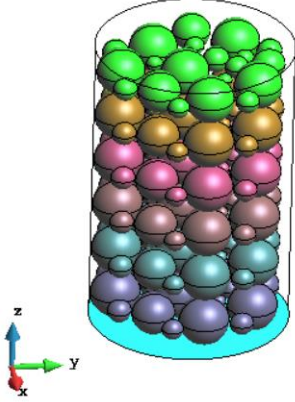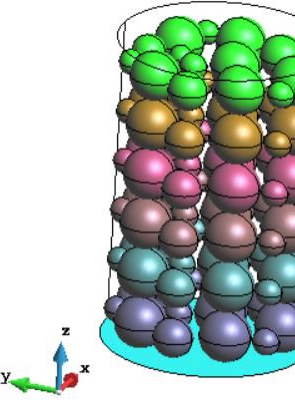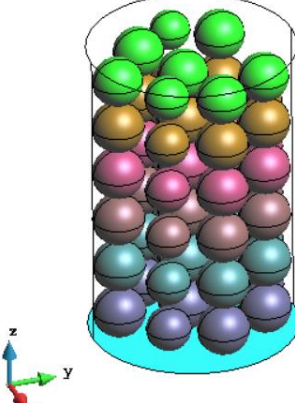
The combination of the model is robust solution to capture physical changes in material such as closure of cracks. More detailed description of the model and using ATENA software can be found in [48]-[53].

7.2   Study of model of mesoscale sample of concrete

The first part of the ATENA model is dedicated to mesoscale modelling of concrete test sample in shape of cylinder with size 40 mm in diameter and 60 mm in height. This size is recommended for irradiated test samples that are actually inserted in test reactors since the standard larger size of specimen would not fit to the reactor restrained environment.

Because the sample size is limiting for the aggregate size, the aggregate grains representing the coarse aggregate in the mesoscale model are ranging from 2 mm to 10 mm in diameter and they are represented by spheres. The sample with maximum coarse aggregate content reaches about 35% of volumetric fraction of coarse aggregate which is reasonable amount considering size effect of test specimen even though standard concrete contains about 60 to 80% of coarse aggregate fraction.

Tab. 7-1 Overview of aggregate size and content in simulated samples

Aggregate size	Aggregate content in vol.%
2-10 mm	35%
4-10 mm	33%
6-10 mm	30%

The matrix of the sample creates cement paste. In order to evaluate the influence of aggregate size and amount in the sample, three different samples with various contents of aggregates are tested as well to see the aggregate content effect, see the samples in Tab. 7-1.

Boundary conditions and load

The specimen is supported in Z direction on the bottom surface and in X and Y direction at one peripheral point on the bottom surface too, Fig. 7-5. With these boundary conditions, the specimen can expand in all directions due to RIVE of aggregate without any extra loading caused by restraining beside the internal strain caused by aggregate expansion. The actual loading in ATENA model is represented by initial strain that is assigned just to aggregates and the strain is incrementally increasing in number of steps to achieve the total load which is 0.07 (initial strain in direction X,Y and Z) in the test example (corresponds to volumetric expansion of 23% which is basically maximal expansion observed on silicate aggregate), Fig. 7-6.
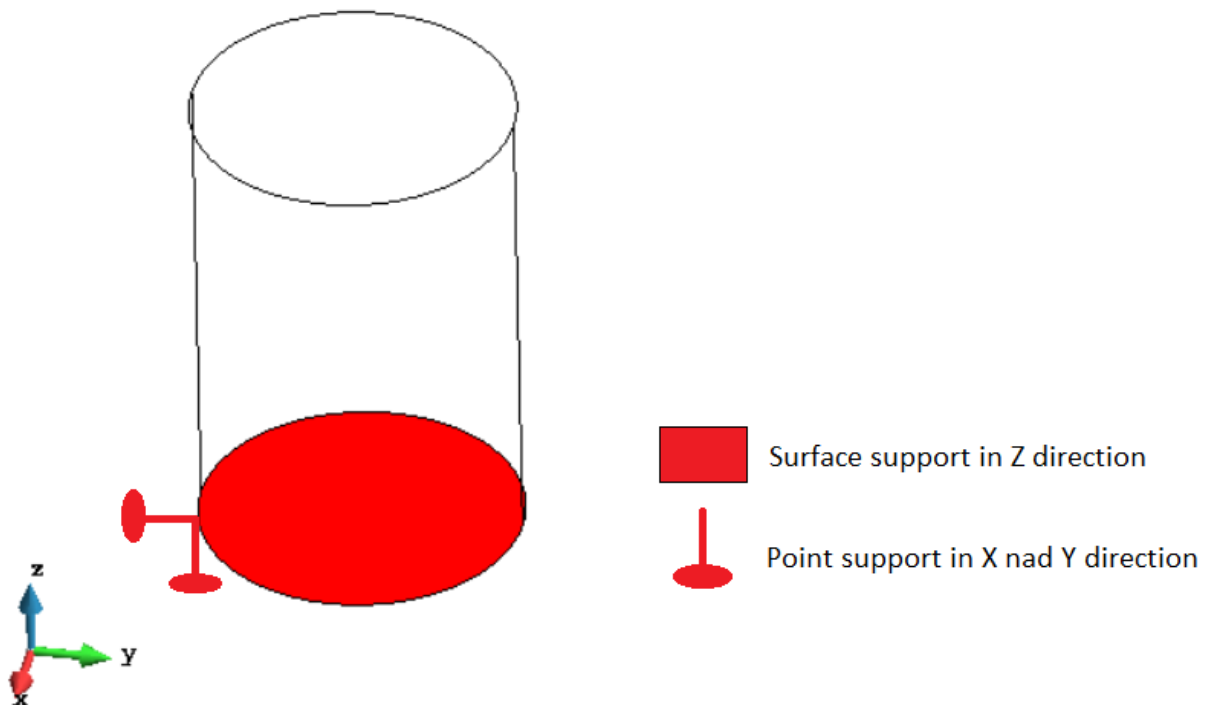
Fig. 7-5 Supports of the sample – in Z direction at the bottom surface and X and Y direction in peripheral point
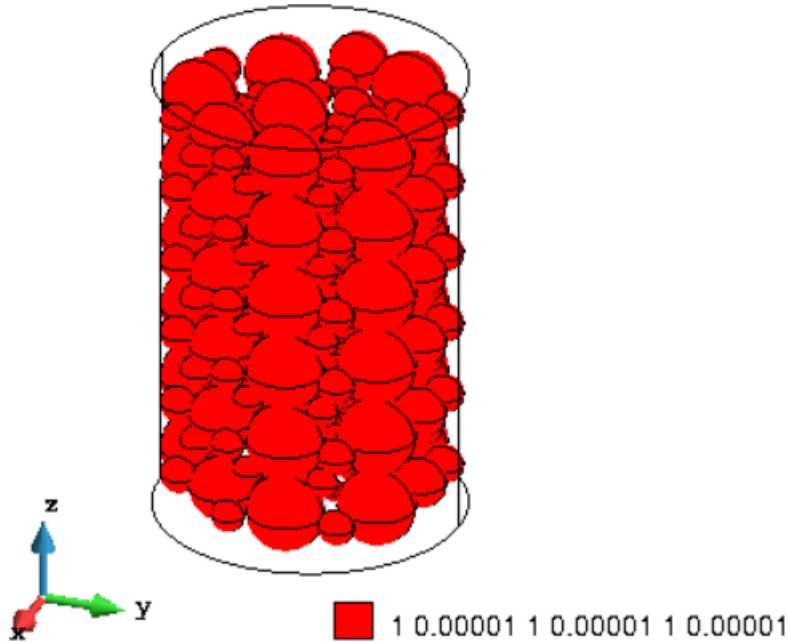
Fig. 7-6 Sample load – aggregate volumetric strain defined in X,Y and Z direction separately

Material parameters

The cylinder sample consists of two materials in this example, aggregates that are represented by spheres which are embedded in matrix that represents cement paste. Both components are made of Cementitious2 material which is fracture-plastic model described above. The material parameters for both components are specified in Tab. 7-2 respectively.

Fracture response of material is characterized by tensile strength f_t, fracture energy G_f and fixed crack while compressive strength f_c, plastic strain ε_{cp} and critical compressive displacement w_d define the plastic response.

Fracture energy represented by surface bellow tension function (softening) with tensile strength and crack opening is shown in Fig. 7-7.

Tab. 7-2 Material parameters of cement paste and granite aggregate

Cement paste	Mean values acc. Model Code 2010 [54]
Modulus of elasticity E [GPa]	35
Poisson's ratio v [-]	0.2
Compressive strength f_c [MPa]	-45
Tensile strength f_t [MPa]	3.3
Fracture energy G_f [N/m]	145
Plastic strain ε_{cp} [-]	-0.00123
Critical com. displacement w_d [-]	-0.0005
Fixed crack [-]	1
Maximum aggregate size [mm]	10
Eccentricity [-]	0.52
Granite aggregate	**Literature values [55]**
Modulus of elasticity E [GPa]	56
Poisson's ratio v [-]	0.22
Compressive strength f_c [MPa]	-163
Tensile strength f_t [MPa]	19
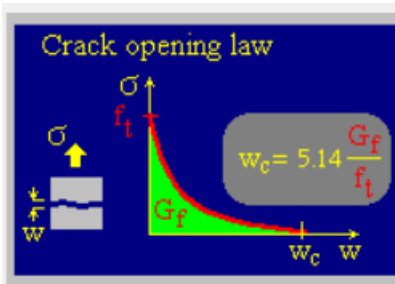
Fig. 7-7 Crack opening law based on G_f and f_t [51]

The plastic response is divided into hardening part where is defined onset of crushing f_{c0}, plastic strain that corresponds to total strain at the peak of compressive strength with deduction of elastic component. The softening part of plastic response is defined by critical compressive displacement, see Fig. 7-8.
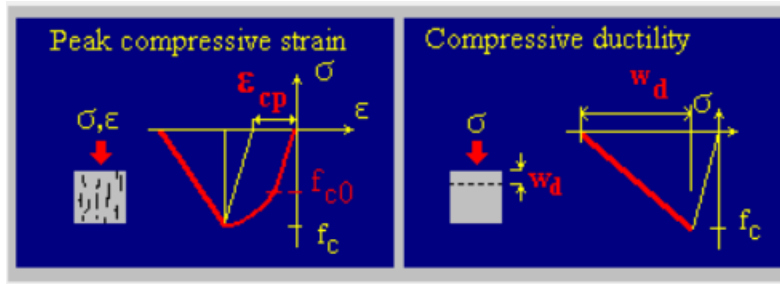
Fig. 7-8 Plastic strain at the peak ε_{cp} and critical compressive displacement w_d [51]

Parameters of cement paste are generated based on Model Code [54] with the mean compressive strength value 45 MPa. The aggregate is represented by granite which parameters are based on the literature values from [55]. with compressive strength 163 MPa and tensile strength 19 MPa.

Sensitivity study

The mesh sensitivity is crucial part of any FEM study since the mesh refinement influences results of the study substantially. Therefore, the six different mesh sizes are studied to determine the proper mesh size for the example in sense of results and computation performance. The sizes of mesh vary from 2.8 mm to 8 mm with resulting number of elements between 47000 and 4000 respectively, Tab. 7-3.

Tab. 7-3 Mesh size with corresponding number of elements

Mesh size [m]	Number of element
0.0080	4000
0.0050	17000
0.0045	20000
0.0042	**25000**
0.0034	27000
0.0028	47000

The mesh sensitivity is compared with regard to maximal principal strain within the sample developed during the inceremntal loading of the sample within 100 steps. Almost identical results of the simulation have been obtained with size mesh 2.8 mm and 4.5 mm. From the computational

effort point of view the mesh of size 4.2 mm is chosen for the rest of the study on the cylinder mesoscale samples, Fig. 7-9.
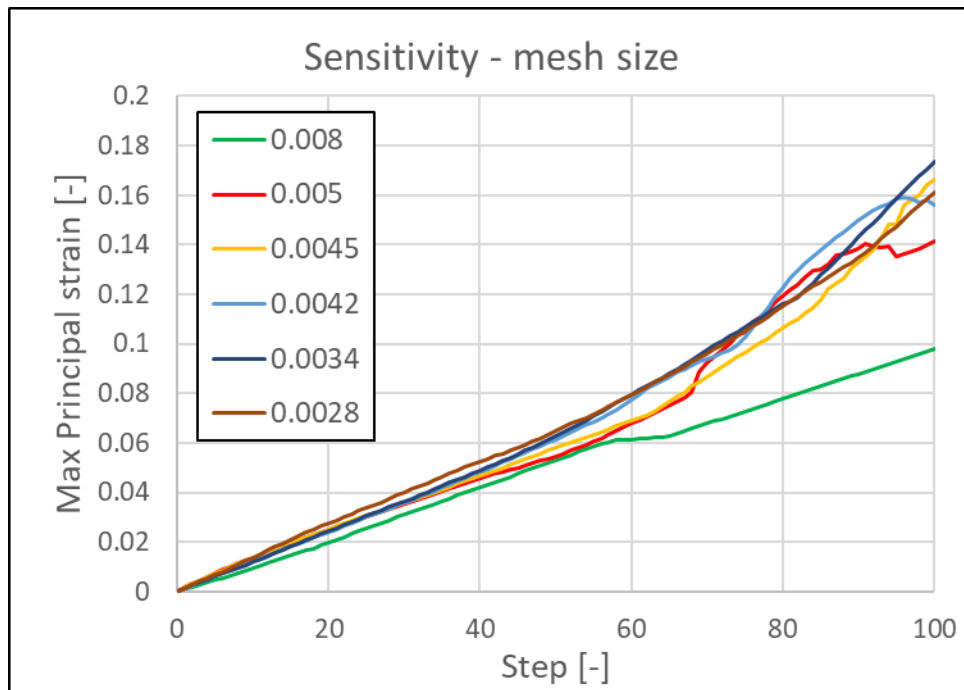
Fig. 7-9 Results of sensitivity study

Results of the mesh sensitivity study is also shown on the displacement in vertical direction of the sample, meaning the height of cylinder, see Fig. 7-10 - Fig. 7-12, and on the maximal principal strains within the sample, see Fig. 7-13 - Fig. 7-15. The three samples shown on figures are for the mesh size 8, 4.2 and 2.8 mm.
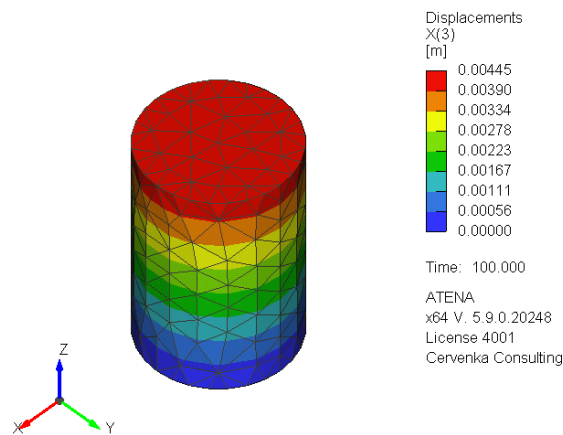
Fig. 7-10 Displacement in Z direction – mesh size 8 mm
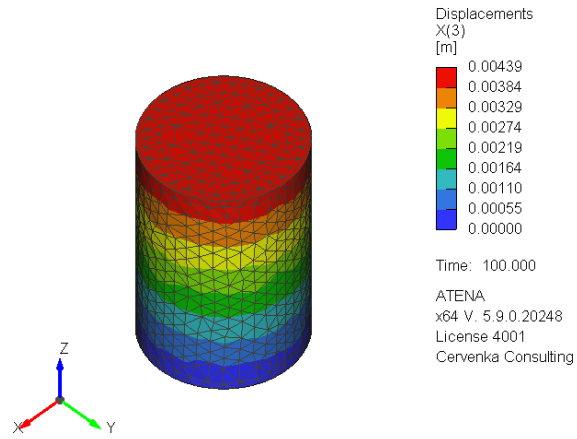
Fig. 7-11 Displacement in Z direction – mesh size 4.2 mm
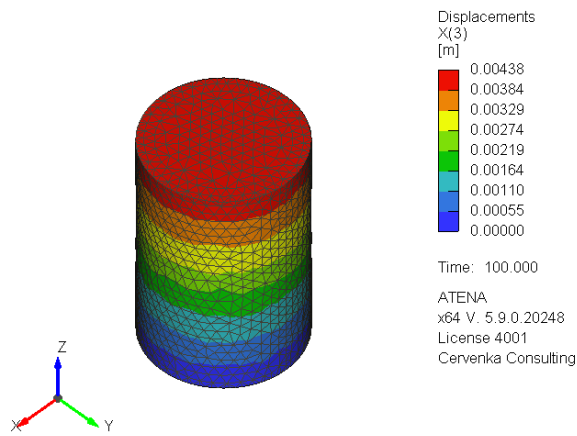
Fig. 7-12 Displacement in Z direction – mesh size 2.8 mm
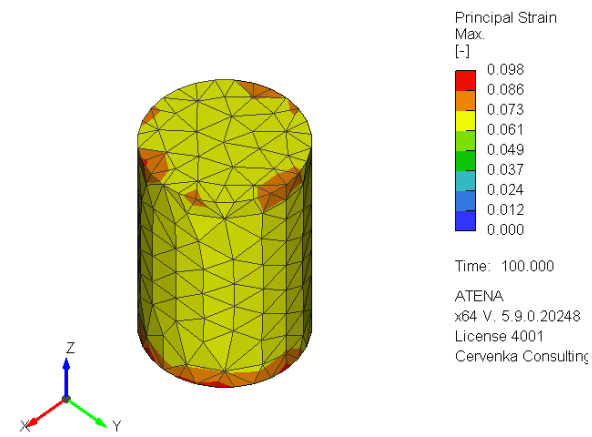
Fig. 7-13 Maximal principal strain – mesh size 8 mm
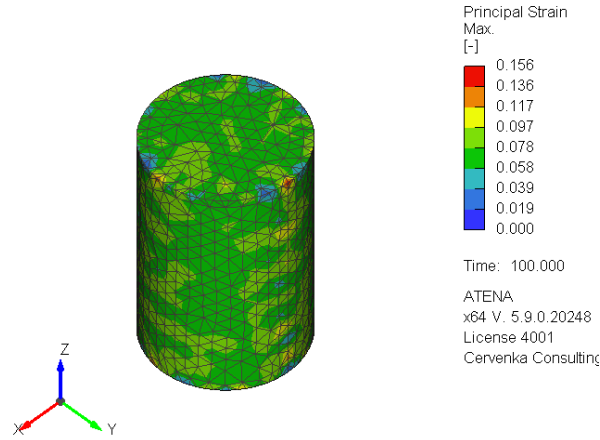
Fig. 7-14 Maximal principal strain – mesh size 4.2 mm
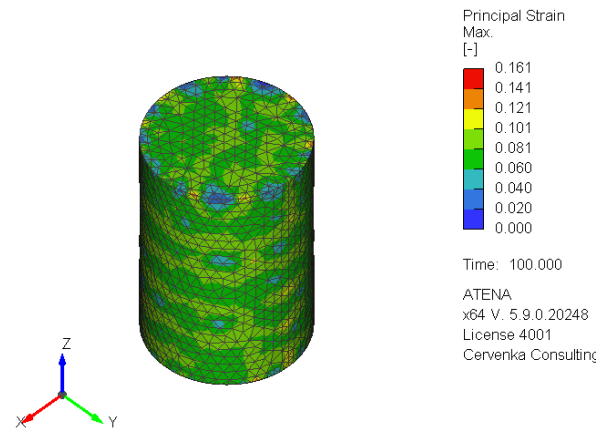
Fig. 7-15 Maximal principal strain – mesh size 2.8 mm

Part of sensitivity study is also the content of aggregate within the sample with various size of grain. The results of the different samples specified above in Tab. 7-1 are shown on average maximal principal strain (tensile). The final value of strain attained at the end of simulation is very similar in all three cases: 0.074, 0.076 and 0.076 respectively for aggregate content of 35%, 33% and 30%, see Fig. 7-16. Therefore the 33% of aggregate content is chosen for the following simulations.
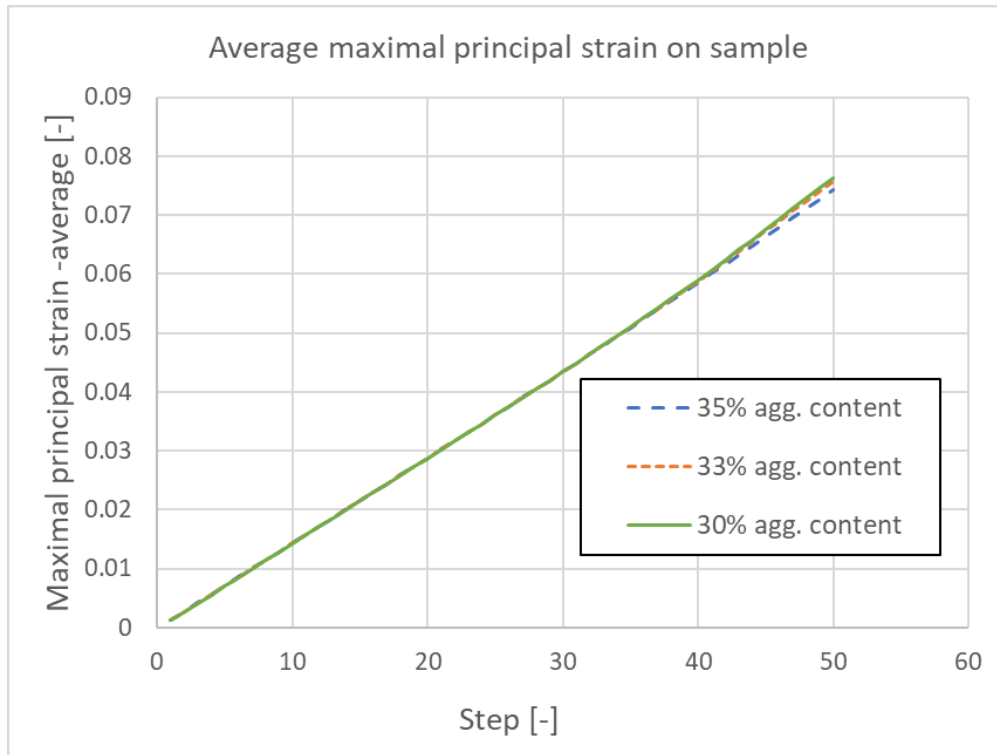
Fig. 7-16 Sensitivity of results based on aggregate content

<u>Results of mesoscale test example</u>

Beside the dimensional changes, the change of tensile strength which drops due to the cracking is possible to study on the presented model. Since the model is made of two fracture-plastic materials whose tensile strength can be reduced, the postprocessor of ATENA software can distinguish both materials and the residual strength of each of them is possible to show, see Fig. 7-17 - Fig. 7-21. It is also possible to get the result of average residual strength in total or of both components separately. It is expected from the results and usual practice to use good-quality strong aggregate that the weaker part is mostly the cement paste matrix which has normally lower initial tensile strength and the cracking that is distributed in it is enhancing the gap between higher tensile strength of aggregate and lower strength of cement paste.

59
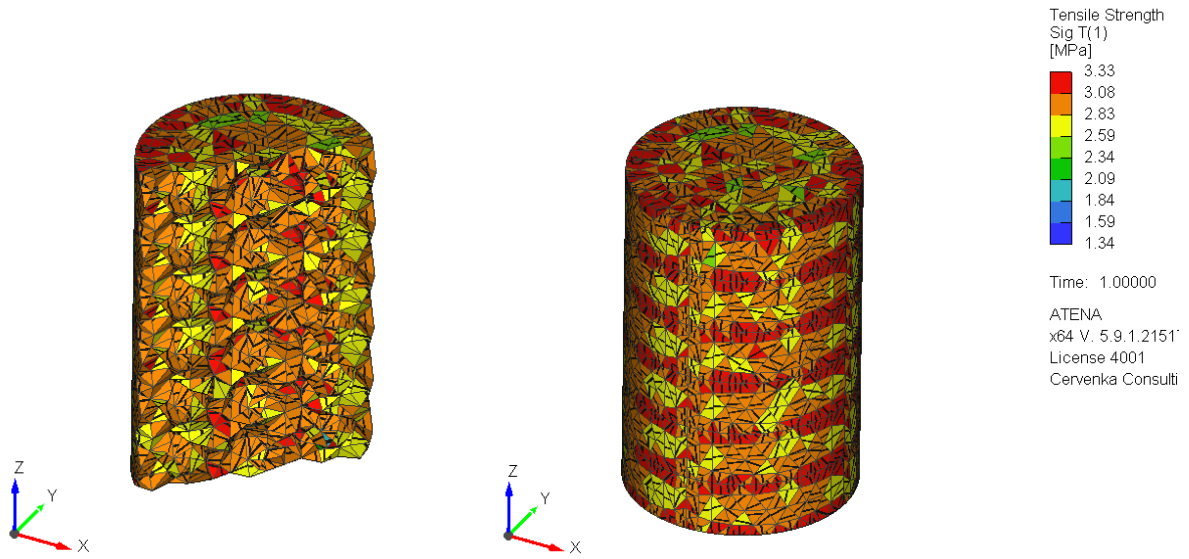
Fig. 7-17 Tensile strength of matrix after the first step of calculation, with cracks
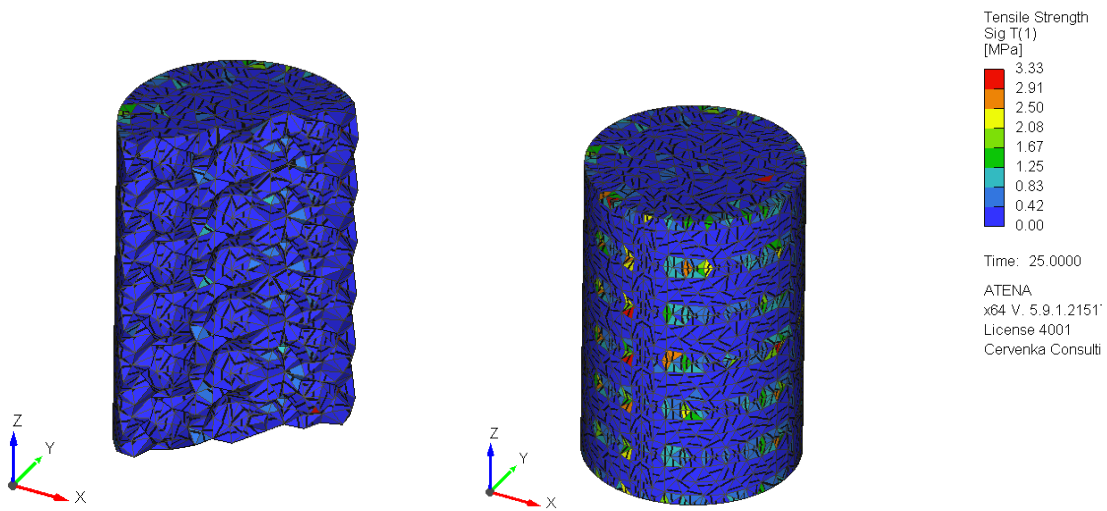
Fig. 7-18 Tensile strength of matrix at middle of calculation, with cracks
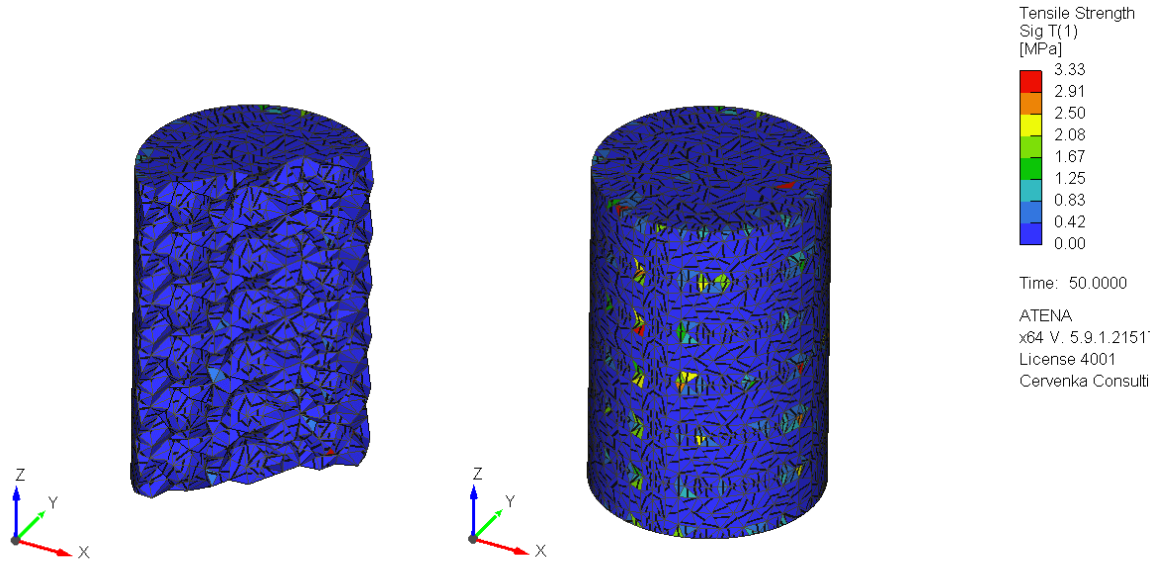
Fig. 7-19 Tensile strength of matrix at the end of calculation, with cracks
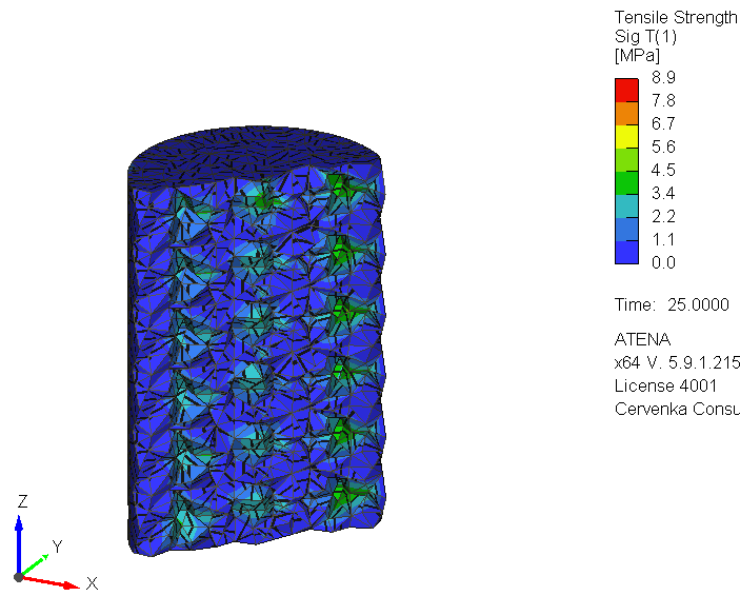
Fig. 7-20 Tensile strength of both components together at the middle of calculation, with cracks
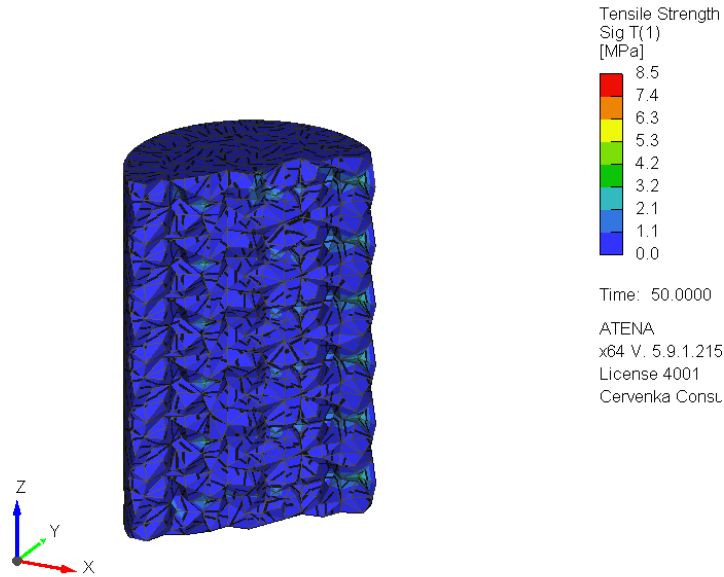
Fig. 7-21 Tensile strength of both components together at the end of calculation, with cracks

7.3 Validation - FEM modelling of experiment

Previous initial study of mesoscale concrete sample showed applicability of ATENA software in the field of irradiated concrete. In order to validate the applicability of such model on the concrete structure, the experiment conducted on concrete and cement paste samples are simulated in ATENA in the same manner as in previous example where aggregate spheres are embedded in cement paste matrix and the samples are loaded by initial strain which values depend on the dose of radiation. Previous studies of mesoscale modelling of irradiated concrete or homogenized irradiated concrete have been performed on similar experiments in [56] and [57] with similar results.

<u>Kelly et.al. 1969</u>

In this study, [2], the samples have been irradiated by neutron radiation while the temperature has been kept very low at 40°C. The temperature of samples while irradiated very often exceeds 100°C therefore this experiment where temperature is kept low is chosen for ATENA model validation, no thermal damage needs to be assumed in this scenario. Both irradiated and non-irradiated/control samples have been tested for their weight loss, dimensional change, change of Young's modulus and strength. Experimental study has been conducted on three types of samples: aggregate, cement

62

paste and concrete. Therefore, the input parameters for ATENA study such as properties of aggregate and cement paste are well known.

The main sample to be simulated is made of ordinary Portland cement and limestone aggregate which is generally assumed as not as detrimental thanks its lack of silica content. From the result collection, the dimensional change of concrete and tensile strength of concrete are chosen for validation of simulation results of the experiment.

Initially three simulations of the experiment have been executed with different dimensional change of aggregate corresponding to three levels of radiation dose. First simulation represents the aggregate dimensional change 0.3% that is related to irradiation dose of $2x10^{19}$ n.v.t. (time-integrated flux, $n \cdot cm^{-2}$). Second simulation assumes dimensional change of aggregate 1% corresponding to radiation dose of neutrons $2.5x10^{19}$ n.v.t. Third simulation represents the aggregate swelling of 2% at the radiation dose $4.5x10^{19}$ n.v.t., see Tab. 7-4. Fig. 7-22 shows aggregate dimensional change which occurred during experiment with marked levels approximated by simulations.

All simulations have same boundary condition as the example in previous chapter, the material models of both components are fracture-plastic models, and the load is mentioned beforehand. Material parameters used for the model are taken from experimental data summarized in the referenced paper.

Tab. 7-4 Radiation dose of fast neutrons related to dimensional change of limestone

Radiation dose – fast neutrons [$x10^{19}$ n.v.t.]	Dimensional change in aggregate [%]
2.0	0.3
2.5	1.0
4.5	2.0

Brittle aggregate

Portland cement paste used in material model is based on compressive strength 24 MPa that is experimental values [2] Table I. Material parameters such as tensile strength and elastic modulus

63

are generated from mean compressive strength value 24 MPa measured on cylindric samples. Material parameters in the model are specified in Tab. 7-5.
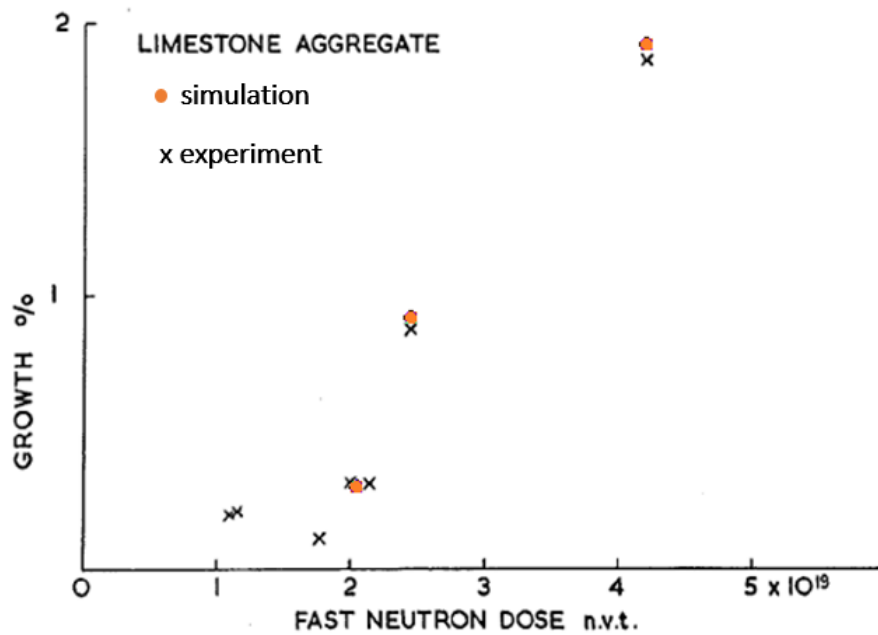
Fig. 7-22 Levels of dimensional change of limestone simulated by FEM

Tab. 7-5 Material parameters of cement paste and brittle aggregates

Cement paste cylindric mean 24 MPa	Mean values acc. Model Code 2010 [54]
Modulus of elasticity E [GPa]	28
Poisson's ratio v [-]	0.2
Compressive strength f_c [MPa]	-24
Tensile strength f_t [MPa]	1.9
Limestone aggregate - brittle	Experimental values [2] Table II.
Modulus of elasticity E [GPa]	72
Compressive strength f_c [MPa]	-23
Tensile strength f_t [MPa]	2.3

Results of simulation described above have been compared to experimental results, namely dimensional change of concrete samples and tensile strength of concrete samples. While the dimensional change of samples in simulation have been much higher than measured results, the results of tensile strength from simulation are well comparable to actual experiment. Since the results of tensile strength are directly in psi in the reference, the simulation results have been converted accordingly. The missing data of experimental test of tensile strength at the dose level 4.5×10^{19} n.v.t. is not explained in the paper, however from other experimental results of other studies it is quite possible the samples have been damaged too much to be tested, [5].

However, the excessive cracking of cement paste and aggregate show high overestimate in dimensional change of the whole sample compared to experiment, therefore another approach is tested as well.

Elastic aggregate

In the following approach the aggregate is assumed to be elastic instead of brittle because that eliminates part of excessive cracking of aggregates occurring in the simulation. With elastic aggregate the cracking is solely manifested within cement paste. The actual process occurring within aggregate and the extent of cracking in it is not easy to capture since the aggregate undergoes the amorphization process that changes the crystalline structure which influences the physical properties while the physical properties of aggregate in simulation are constant.

Regarding the material properties of the model with elastic aggregates, the fracture-plastic model is applied on cement paste. In order to simulate the sample with physical properties of concrete of compressive strength represented in the paper, the concrete properties are assigned to cement paste in this scenario. The elastic aggregate is defined only by its modulus of elasticity and Poisson's ratio, see Tab. 7-6.

Results of the second approach with elastic aggregate correlates to experiments much better especially the dimensional change. The tensile strength reduction is a little higher however it is on the safe side from the structural assessment point of view.

Tab. 7-6 Material parameters of cement paste and elastic aggregates

Cement paste cylindric mean 70 MPa	Mean values acc. Model Code 2010 [54]
Modulus of elasticity E [GPa]	41
Poisson's ratio v [-]	0.2
Compressive strength f_c [MPa]	-70
Tensile strength f_t [MPa]	5.7
Limestone aggregate - elastic	Literature values [2]
Modulus of elasticity E [GPa]	72
Poisson's ratio v [-]	0.2

Brittle aggregate with reduction of mechanical properties

The third and last approach is to assume brittle behavior of both components while the mechanical properties of the aggregate get reduced according to the literature data presented in chapter 3.4 Irradiated aggregate properties trends. The following flowchart, Fig. 7-23, shows the reduction of aggregate mechanical properties based on the RIVE of limestone aggregate (sedimentary). The RIVE of aggregate type gives the cracking volume of aggregate which is about 2/3 of the whole RIVE. The relation between the cracking volume and aggregate mechanical properties reduction is shown on diagrams within the flowchart. Reduction of aggregate properties is assumed at all three levels of irradiation which is 0.3, 1 and 2% of dimensional change that is 0.9, 3 and 7% RIVE (volumetric) respectively. As is shown in the trends of reduction of aggregate elastic modulus and compressive strength in flowchart, the reduction of compressive strength of sedimentary aggregate starts at the higher level of cracking volume than the one reached in the Kelly's experiment, therefore only elastic modulus is reduced in the last simulations, see Tab. 7-7.

Tab. 7-7 Reduced elastic modulus of aggregates at different levels of irradiation

Radiation dose – fast neutrons [x10^{19} n.v.t.]	Dimensional change in aggregate / RIVE [%]	Elastic modulus [GPa]
2.0	0.3 / 0.9	72
2.5	1.0 / 3	40
4.5	2.0 / 7	35
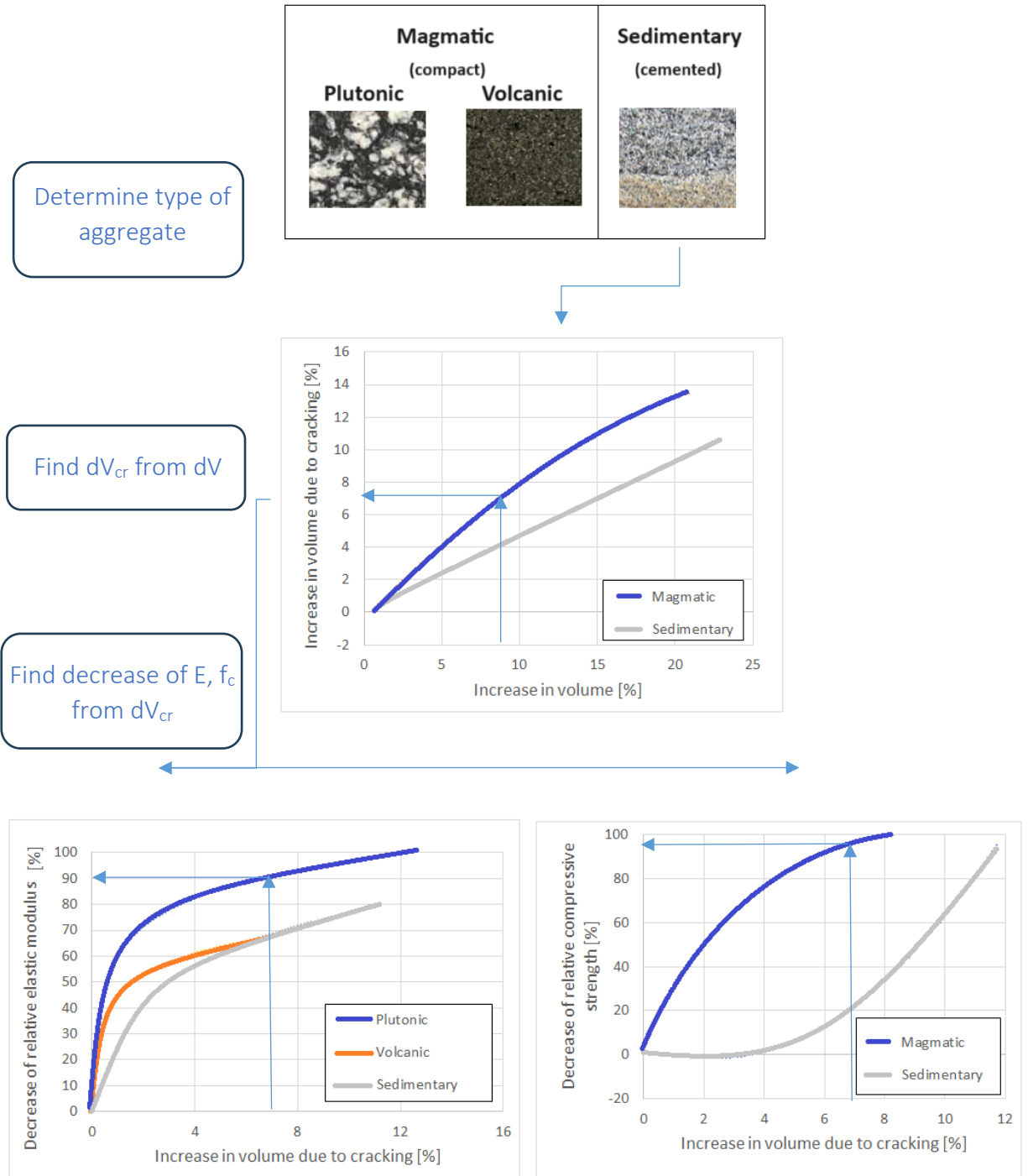
Fig. 7-23 Reduction of elastic modulus of aggregate based on level of irradiation related to RIVE and aggregate cracking volume

7.4 Results of modeling of experiment

Three different approaches how to simulate irradiated concrete samples in FEM software have been proposed. The results of simulation and actual experiment are compared on dimensional change of the samples and reduction of tensile strength (both characteristics are relative values). The first figure (Fig. 7-24) shows the results of dimensional change at three different levels of irradiation dose showing the three different approaches (model with brittle aggregate, elastic aggregate and brittle aggregate including mechanical properties reduction). Regarding the dimensional change both approaches with brittle aggregates tend to overestimate the overall growth of the sample while elastic aggregate approach gives very good correlation with experimental results.
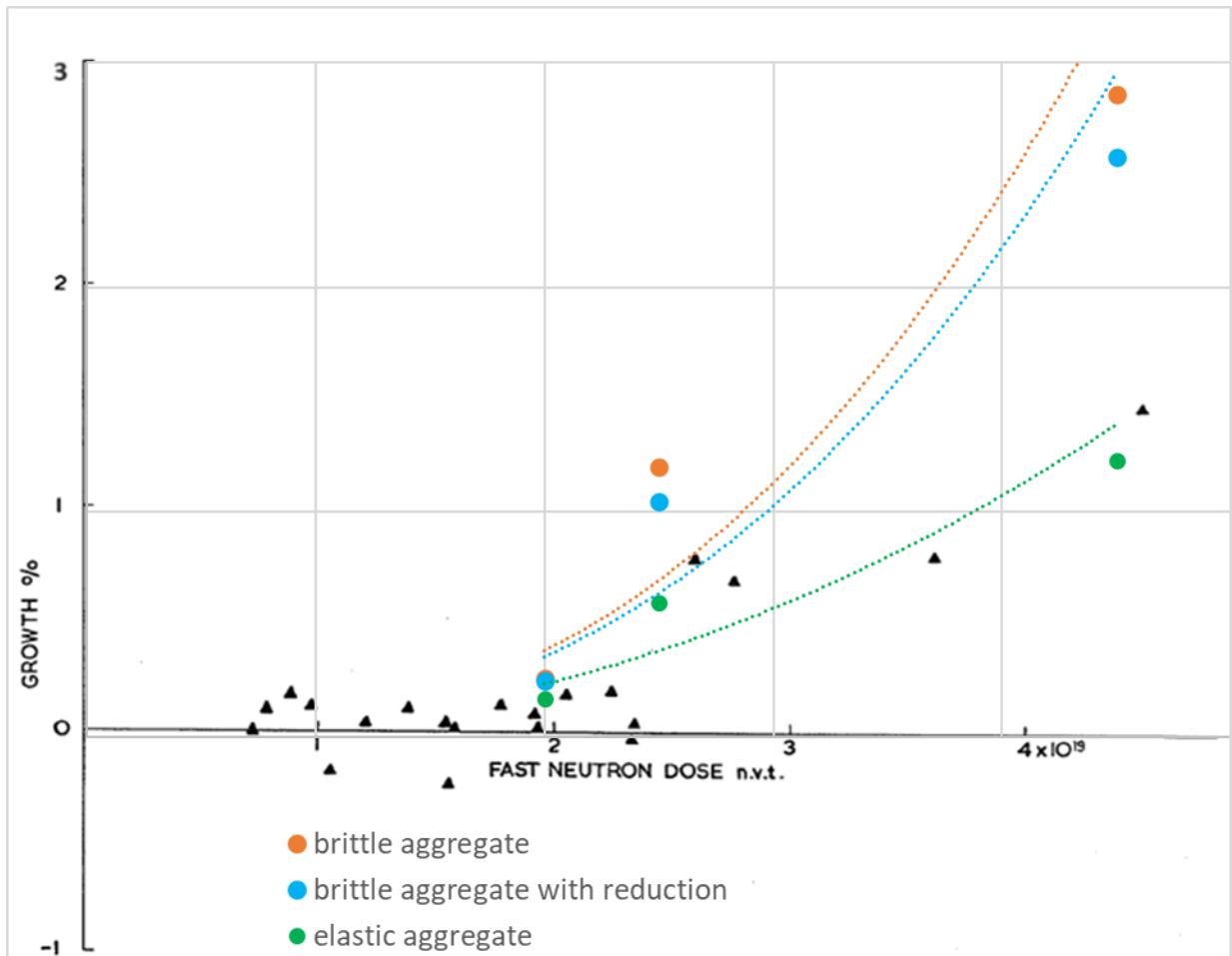
Fig. 7-24 Dimensional change of aggregate depending on fast neutron dose during experiment compared to simulation results

The overestimate of results with brittle aggregate is attributed to the development of cracks withing aggregate which increases the aggregate expansion. For the elastic aggregate the expansion is prescribed by its RIVE that has been observed during the experiment without any extra cracking.

The second figure (Fig. 7-25) with experimental results shows reduction of tensile strength of irradiated samples. In order to compare the experimental results with simulation, the tensile strength reduction from simulation is converted into relative value and transformed into experimental value. While the approaches with brittle aggregates seem to give more appropriate results than the approach with elastic aggregate. However, the results of Brazilian test (indirect tensile splitting test) tend to overestimate the actual tensile strength of specimen therefore the tensile strength from simulations should be lower than experimental results. The standards recommend α value between 0.67 to 0.95 when transforming tensile strength from splitting test ($f_{ctm,split}$) to mean tensile strength of concrete (f_{ctm}), ($f_{ctm} = \alpha \, f_{ctm,split}$,[54]).

Regarding the results from simulations and experimental ones, the elastic aggregate approach shows the best correlation with experimental data in both studied characteristics.
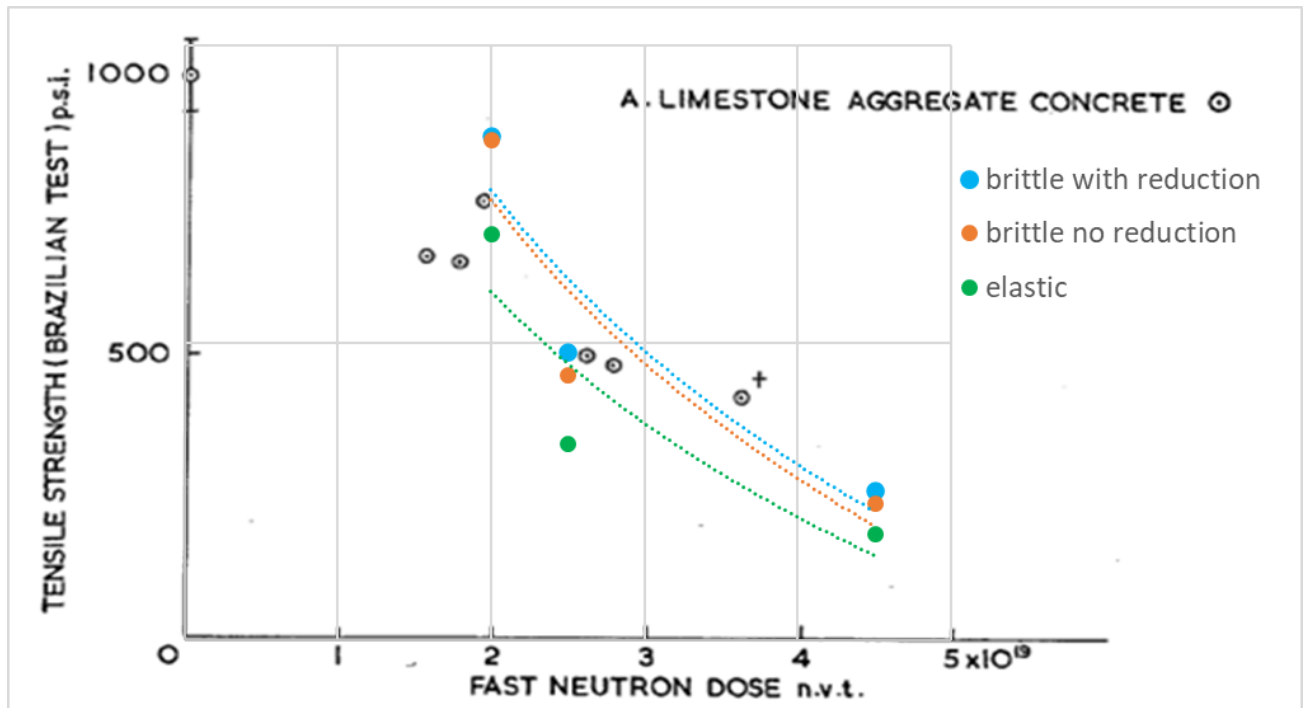
Fig. 7-25 Tensile strength of concrete depending on fast neutron dose during experiment compared to simulation results

Example of results of simulation considering brittle aggregate is shown in following figures. The Fig. 7-26 depicts the vertical displacement showing the growth of the sample in Z direction. The crack width within the sample that is cut in the middle is shown in Fig. 7-27 where the size of cracks is mostly in tens of microns. Last two Fig. 7-28 and Fig. 7-29 show the tensile strength of the sample at the beginning and at the end of simulation.
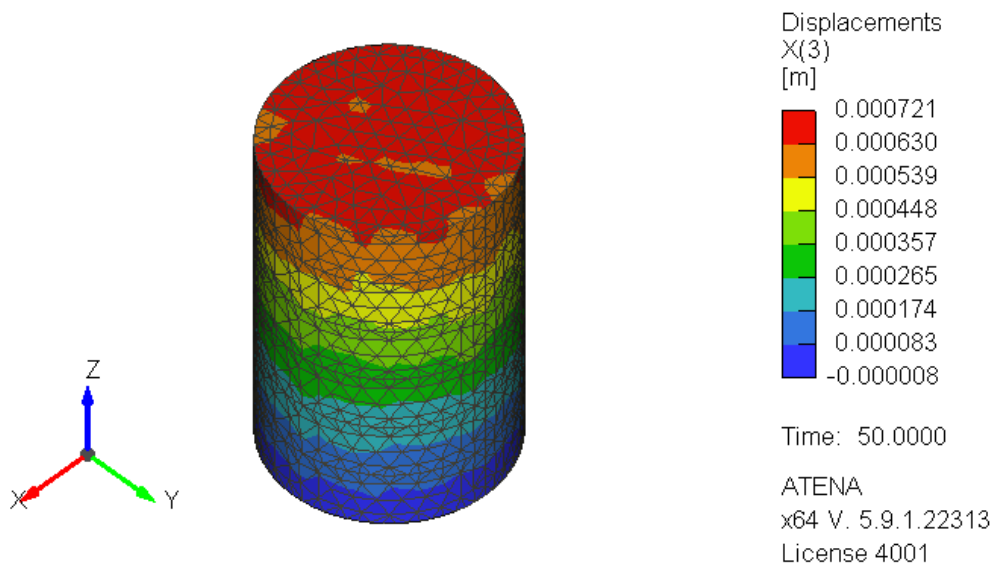
Fig. 7-26 Displacement in direction Z shows expansion of whole sample
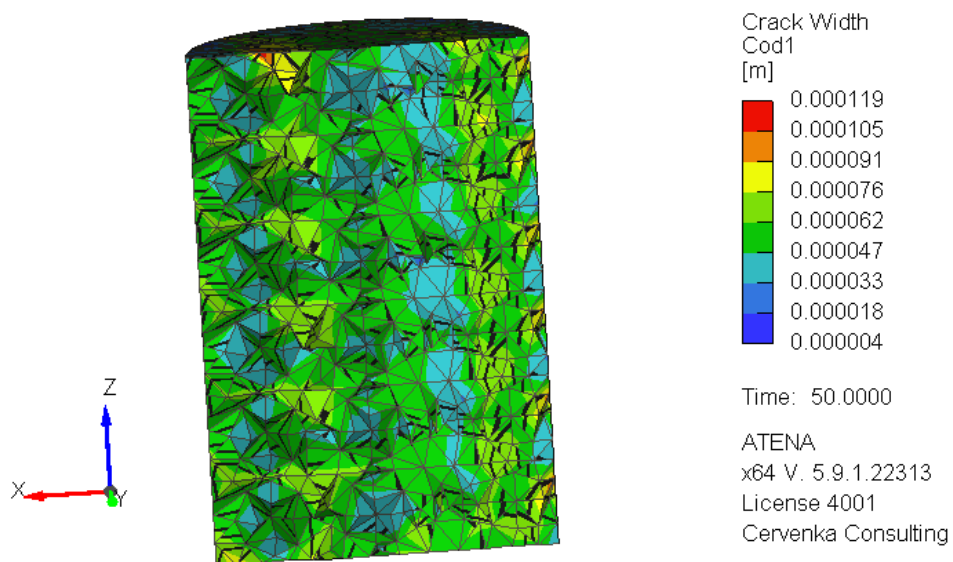
Fig. 7-27 Crack width in the sample cut in half, with cracking
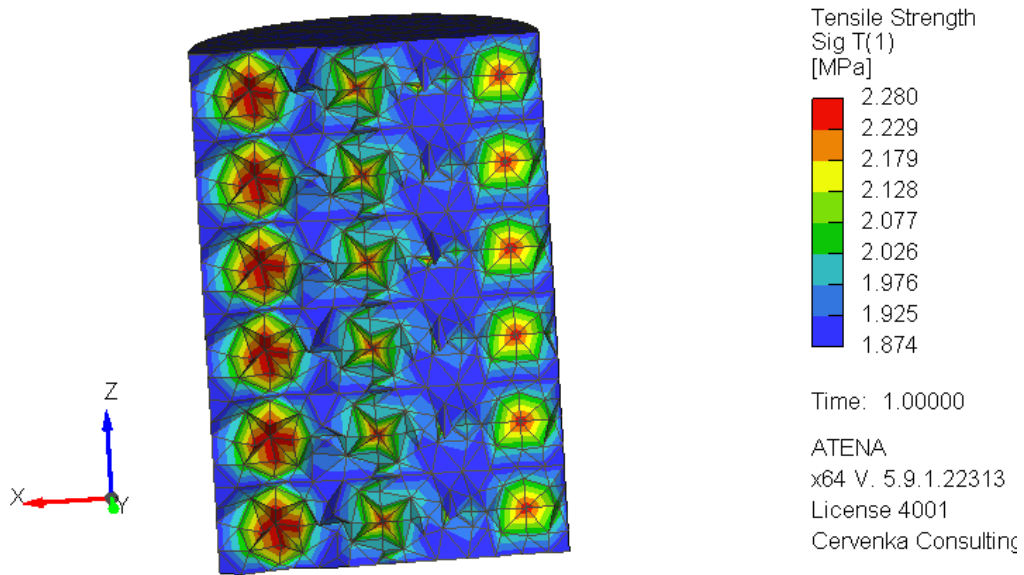
Fig. 7-28 Tensile strength of sample at the beginning of simulation, with cracking
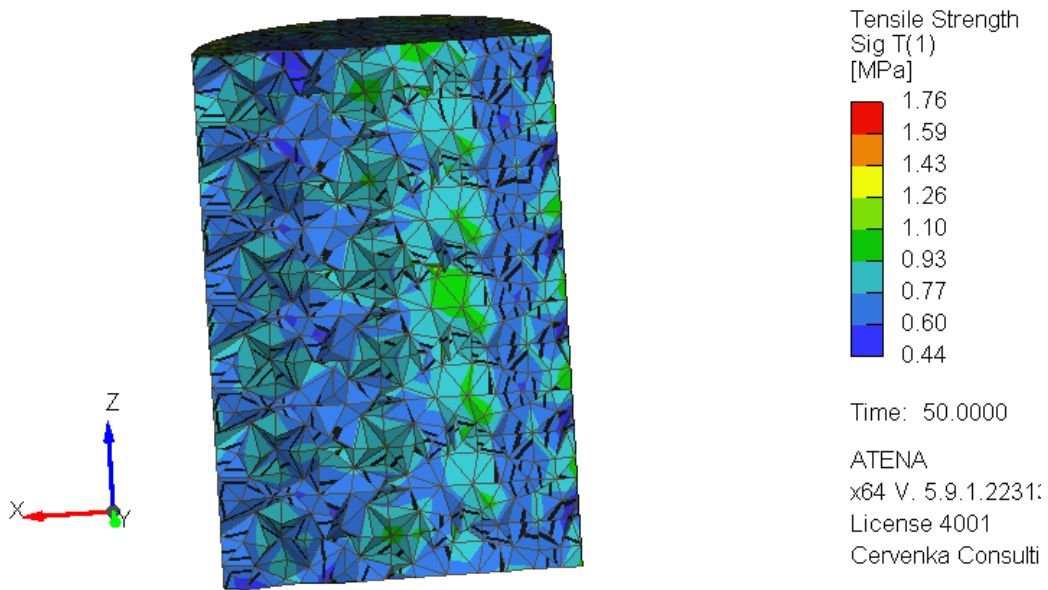
Fig. 7-29 Tensile strength of the sample at the end of simulation, with cracking

8 Marcroscale model of the structure

Last part of this work is dedicated to study of actual concrete structure exposed to irradiation. The biological shielding is protective structure around nuclear reactor in nuclear power plant. It can be assumed as one of the structures exposed to highest amounts of radiation dose. Its function is to protect every life form from radiation effects outside the shielding and in some cases also loadbearing supporting the pressure vessel such as VVER 1000 used in Czech nuclear power plant Temelín, see Fig. 8-1. Therefore soundness of the structure is essential for the safety operation of nuclear power plant.
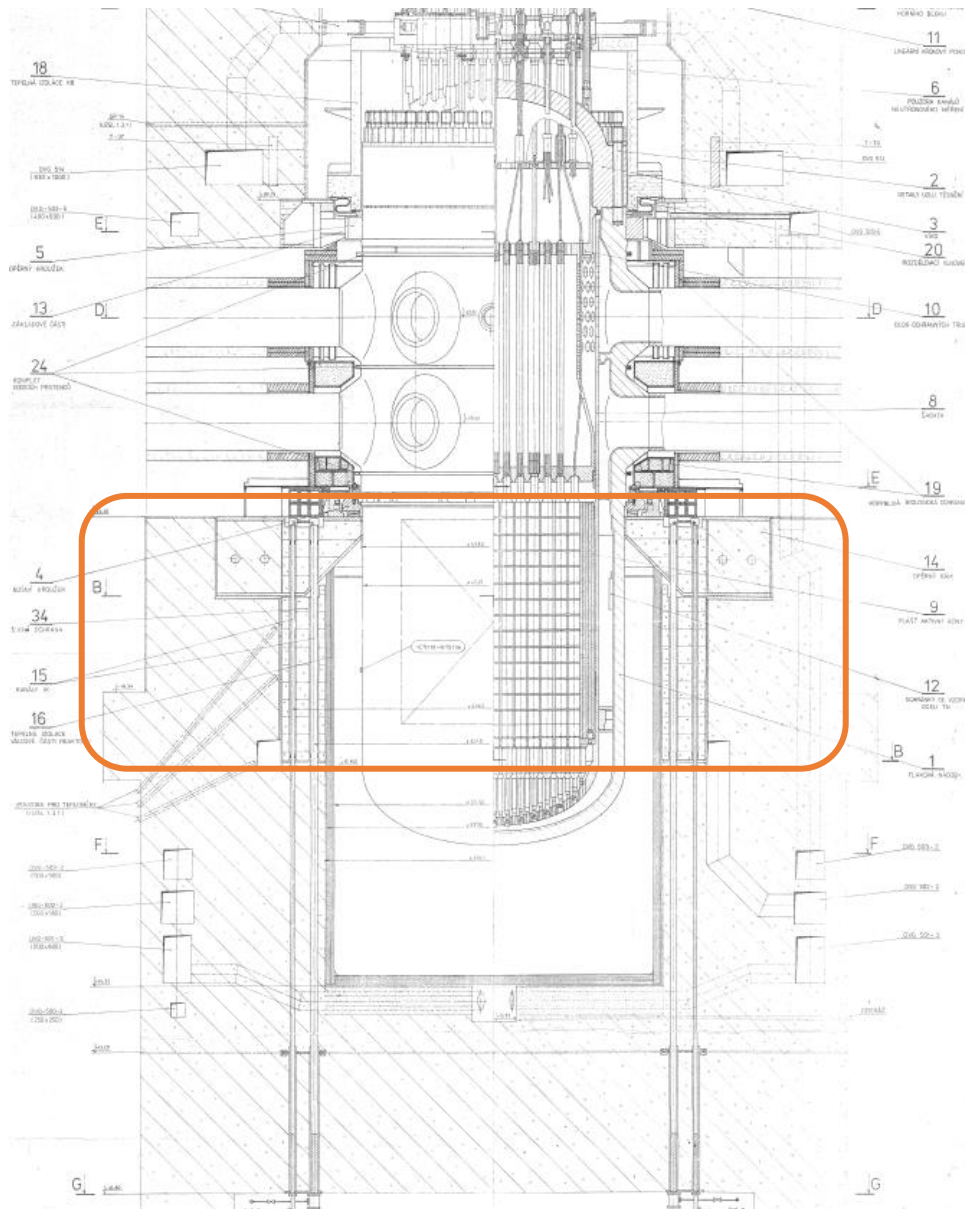
Fig. 8-1 Reactor shaft drawing – type VVER 1000 in Temelín, CZ

In order to investigate the potential damage of the structure exposed to radiation, the following chapter presents FEM model of irradiated biological shielding. The investigated part of the structure is the concrete ring around the active zone that is exposed to highest flux of neutrons.

8.1 Model of biological shielding inputs

<u>Geometry</u>

Modelled part of the structure is quarter of the ring with symmetry conditions to make the model concise and efficient. According to the VVER 1000 biological shielding, the height of active zone of reactor is about 4.3 m with the inner radius of the ring 2.885 m, thickness of the concrete shielding ring of 2.9 m resulting in outer radius 5.785 m, see Fig. 8-2.
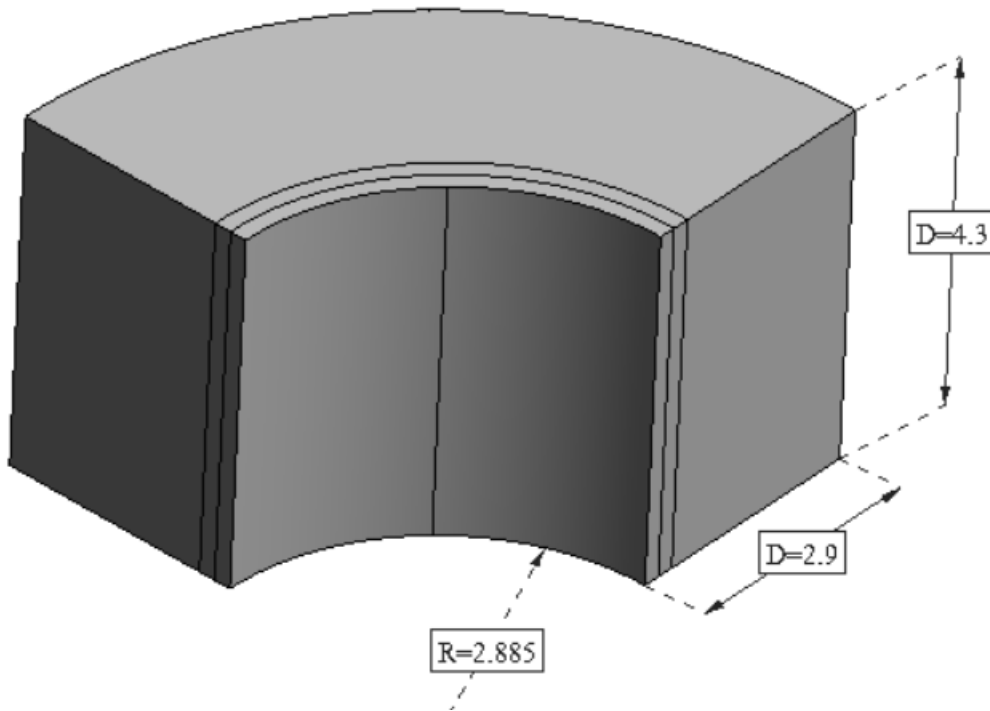
Fig. 8-2 Geometry of the quarter of the ring around the active zone in biological shielding

<u>Boundary conditions and Load</u>

The quarter of the ring is supported on the side faces in X and Y direction to create symmetry conditions in order to capture behavior of the whole ring. The ring is also supported at the bottom

in Z direction, see Fig. 8-3. Therefore structure can deform in radial direction and in direction of positive Z axis.
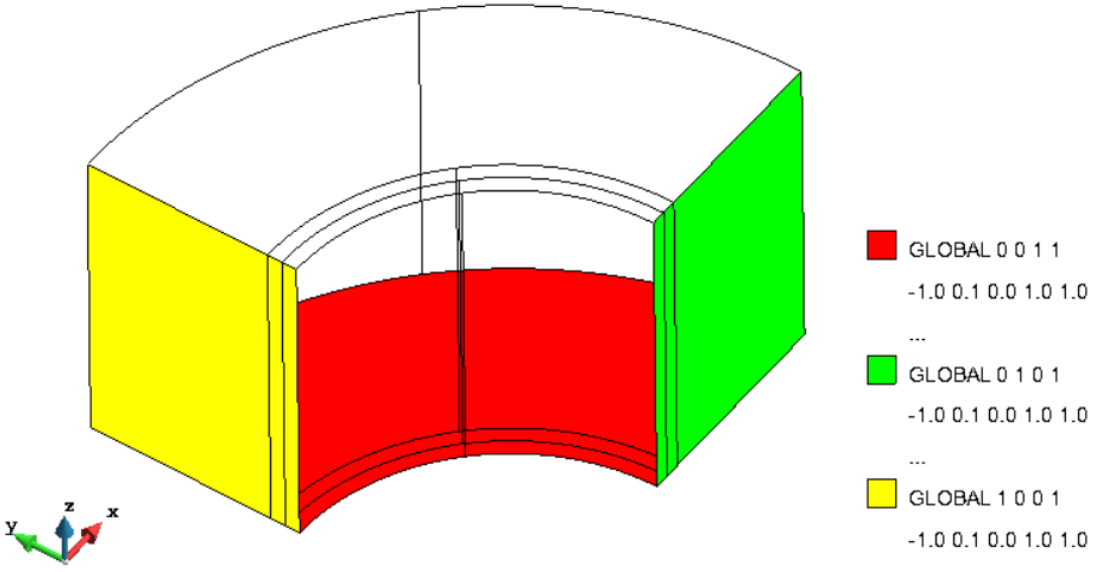
Fig. 8-3 Vertical support at the bottom of the structure and symmetry supports on the side faces

Then the structure is loaded by three different loads. The first load is the self-weight of the structure assuming 2300 kg/m^3 (Fig. 8-4), the second load is the weight of the reactor pressure vessel which is about 800 t (Fig. 8-5) and is applied as pressure on the top surface of the ring.
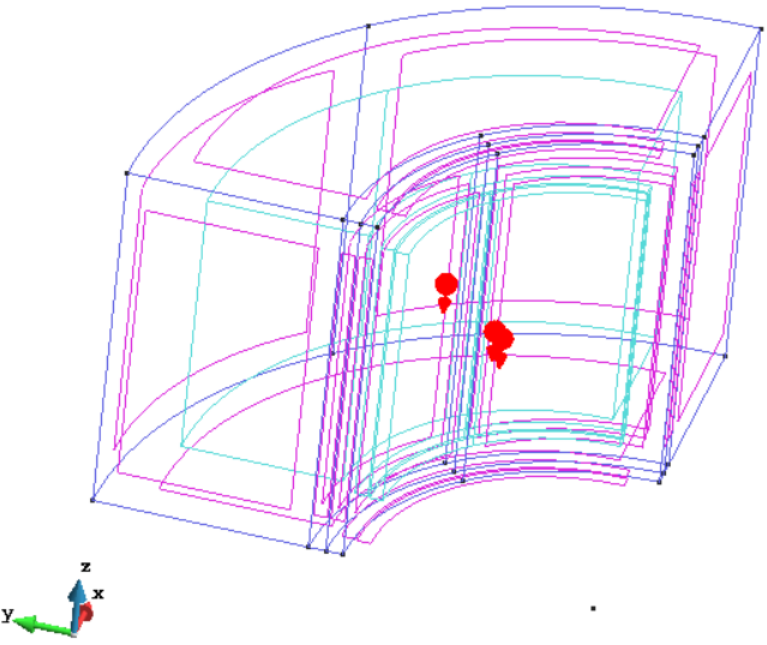
Fig. 8-4 Self weight of the structure

74
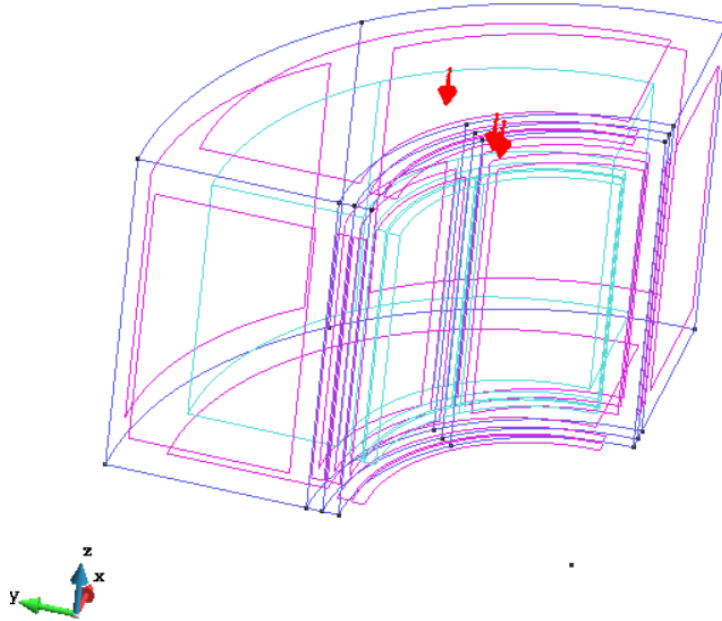
Fig. 8-5 Pressure on the top of the structure representing the weight of reactor

The third and last load is volumetric strain simulating the irradiation of the inner part of the ring structure. The depth of the structure that is affected by RIVE can be estimated from calculation of the neutron radiation flux prepared by Igor Remec in [58], see Fig. 8-6, for three-loop pressurized water reactor (PWR) while the VVER 1000 is four-loop PWR the estimate should be sufficient.
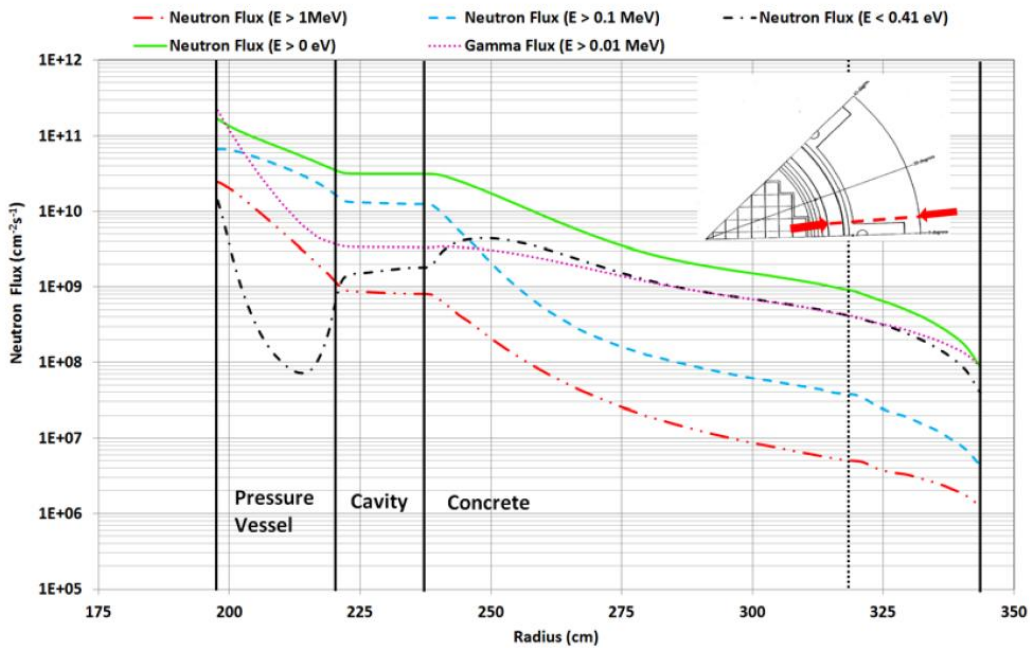
Fig. 8-6 Neutron flux in radial direction from the core of three-loop PWR [58]

The flux of intermediate and fast neutrons is represented by blue dashed line. While the neutron flux of 1E+8 n·cm^{-2}·s^{-1} results in neutron fluence of order 1E+17 n·cm^{-2} in 50 or 100 years of operation of reactor, the flux of 1E+10 n·cm^{-2}·s^{-1} in 50 or 100 years gives the fluence of order 1E+19 n·cm^{-2}. The actual RIVE and reduction of concrete mechanical properties starts between neutron fluence of order from 1E+18 to 1E+19 n·cm^{-2}. Therefore any RIVE is expected within the concrete layer of about 40 cm at maximum, Fig. 8-7. The maximal initial strain is 5% in all directions resulting in volumetric change of 16% that is expected maximum of volumetric swelling of concrete reported in the literature [6].
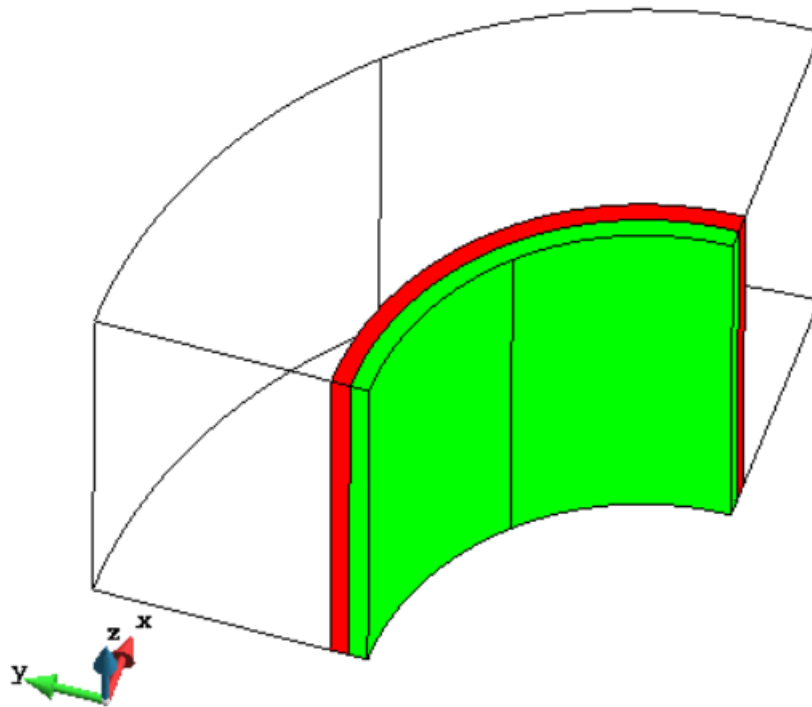
Fig. 8-7 Initial strain applied on volume within layer of 40 cm from the inner surface of the ring

Materials

There are two concrete materials used in this study of biological shielding structure because of the lack of data on structural concrete of biological shielding. First concrete is used as a structural concrete that is actually in the pit of the reactor shaft with compressive strength 20 MPa, [59]. Second concrete material that is used in this study has compressive strength 70 MPa to see the difference of structural damage with superior material. Finally, the reinforcement is added in the third model similarly as in study preformed in [60], where the reinforcing mesh is on the inner and outer surface of the structure. All materials are summarized in Tab. 8-1 - Tab. 8-3, stress-strain

diagram of reinforcement is in Fig. 8-8 and its layout is shown in Fig. 8-9. The mesh size of bars is 200 mm and the concrete cover is 150 mm.

Tab. 8-1 Material parameters of concrete with compressive strength 20 MPa

Material parameter	Value of parameter
Modulus of elasticity E [GPa]	32
Poisson's ratio v [-]	0.2
Compressive strength f_c [MPa]	-20
Tensile strength f_t [MPa]	1.33
Fracture energy G_f [N/m]	33.3
Plastic strain ε_{cp} [-]	-0.00154
Critical com. displacement w_d [-]	-0.0005
Fixed crack [-]	1
Maximum aggregate size [mm]	20
Eccentricity [-]	0.52

Tab. 8-2 Material parameters of concrete with compressive strength 70 MPa

Material parameter	Value of parameter
Modulus of elasticity E [GPa]	39
Poisson's ratio v [-]	0.2
Compressive strength f_c [MPa]	-68
Tensile strength f_t [MPa]	4.4
Fracture energy G_f [N/m]	110
Plastic strain ε_{cp} [-]	-0.00084
Critical com. displacement w_d [-]	-0.0005
Fixed crack [-]	1
Maximum aggregate size [mm]	20
Eccentricity [-]	0.52
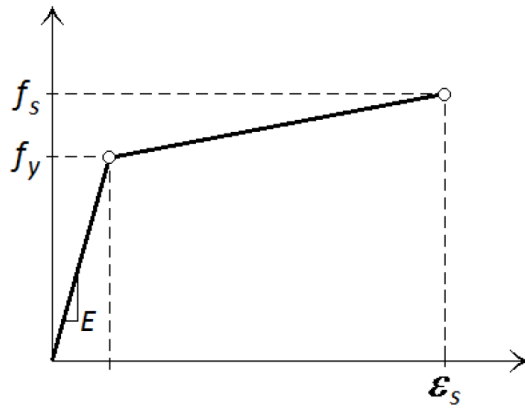
Fig. 8-8 Stress-strain diagram of reinforcing steel [49]

Tab. 8-3 Material parameters of rebars with diameter 16 mm

Material parameter	Value of parameter
Modulus of elasticity E [GPa]	200
Yield strength f_y [MPa]	550
Ultimate tensile strength f_s [MPa]	577.5
Ultimate strain ε_s [-]	0.025
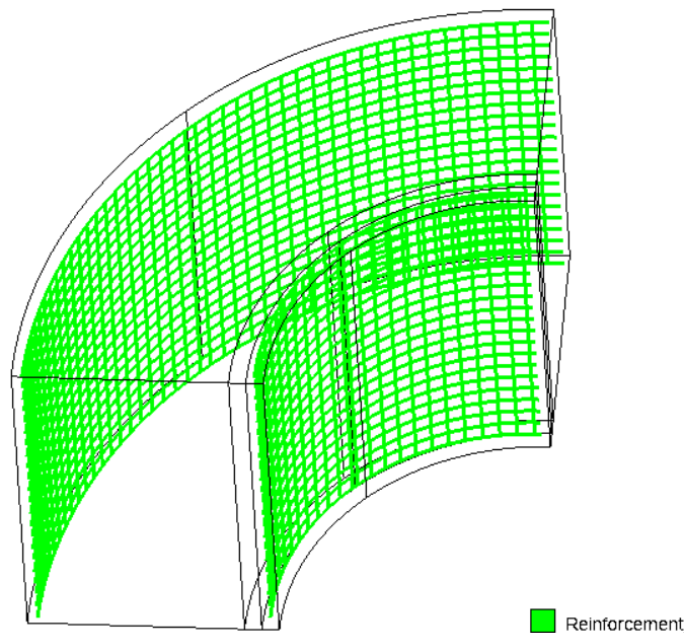
Fig. 8-9 Reinforcement layout

Finite element mesh used in this study has size 200 mm which is resulting from sensitivity study, Fig. 8-10.
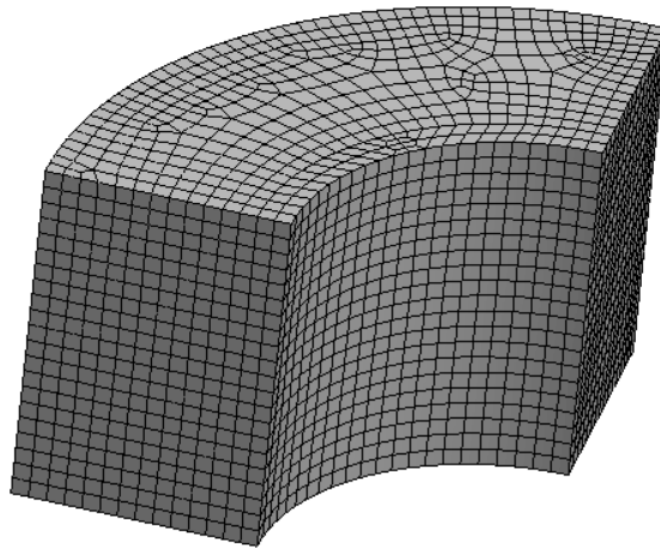
Fig. 8-10 Mesh size used for simulation

8.2 Results of modelling

Results of three simulations show the same type of failure where radial cracks through the shielding structure develop. This type of failure is most serious for the considered type of the structure because it shielding properties are compromised by radial cracks. When the same level of the load is reached (RIVE load) the maximal width of radial cracks is compared, Tab. 8-4, the maximal crack width is reached during the simulation with concrete of lower strength 13.7 mm, see Fig. 8-11 and Fig. 8-12. Then the crack width during the simulation with higher strength concrete shows very similar crack width regardless the reinforcement in the structure, 10.4 mm without and 11.5 mm with reinforcement. The larger crack width in the structure with reinforcement is caused by more localized cracking, see Fig. 8-13 through Fig. 8-16.

Tab. 8-4 Maximal crack width at the same level of load

Material	Concrete 20 MPa	Concrete 70 MPa	Concrete 70 MPa with reinforcement
Max crack width [mm]	13.7	10.4	11.5
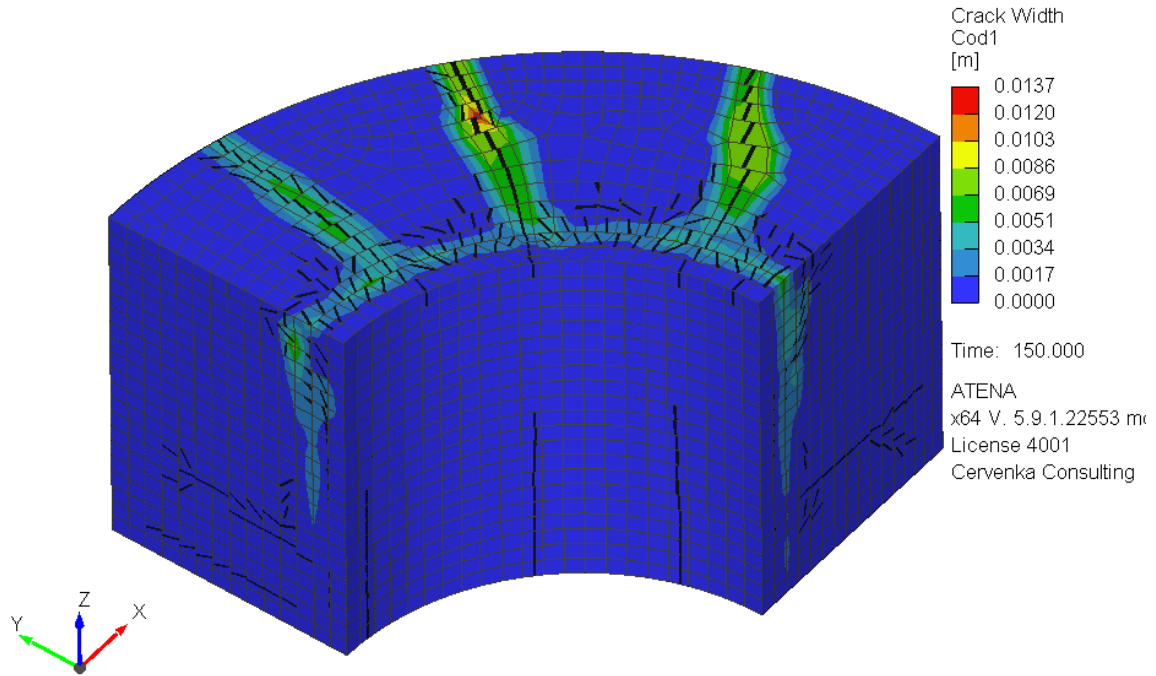
Fig. 8-11 Crack width in structure, concrete compressive strength 20 MPa without reinforcement
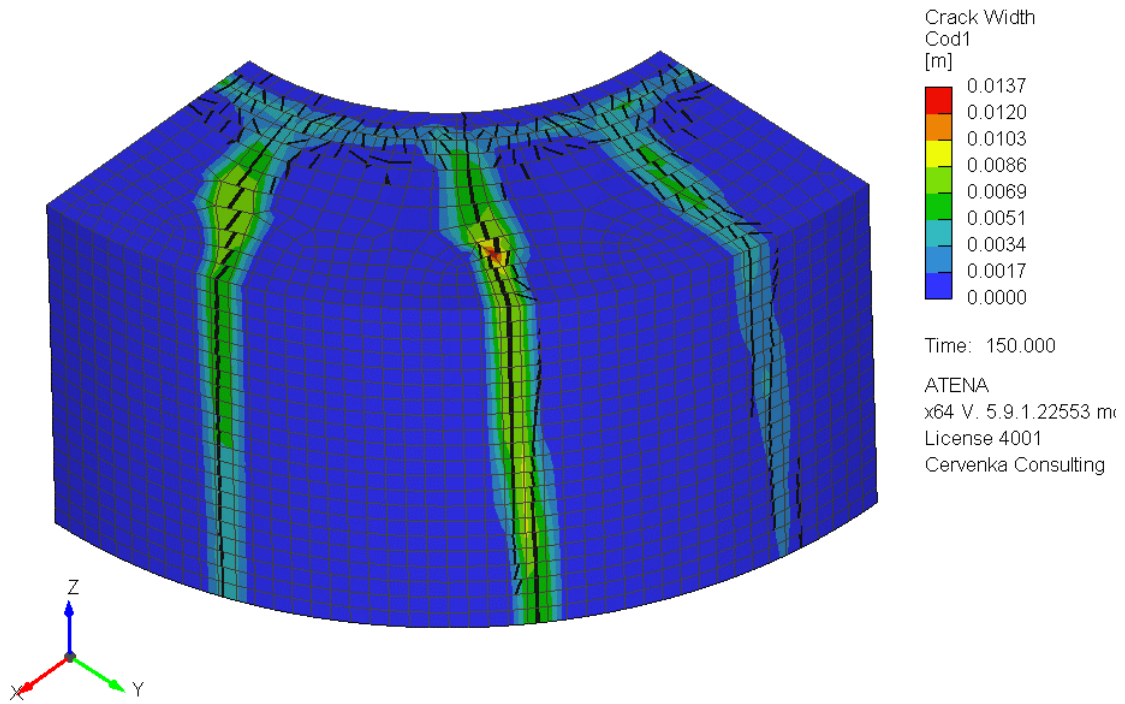
Fig. 8-12 Crack width in structure, concrete compressive strength 20 MPa without reinforcement
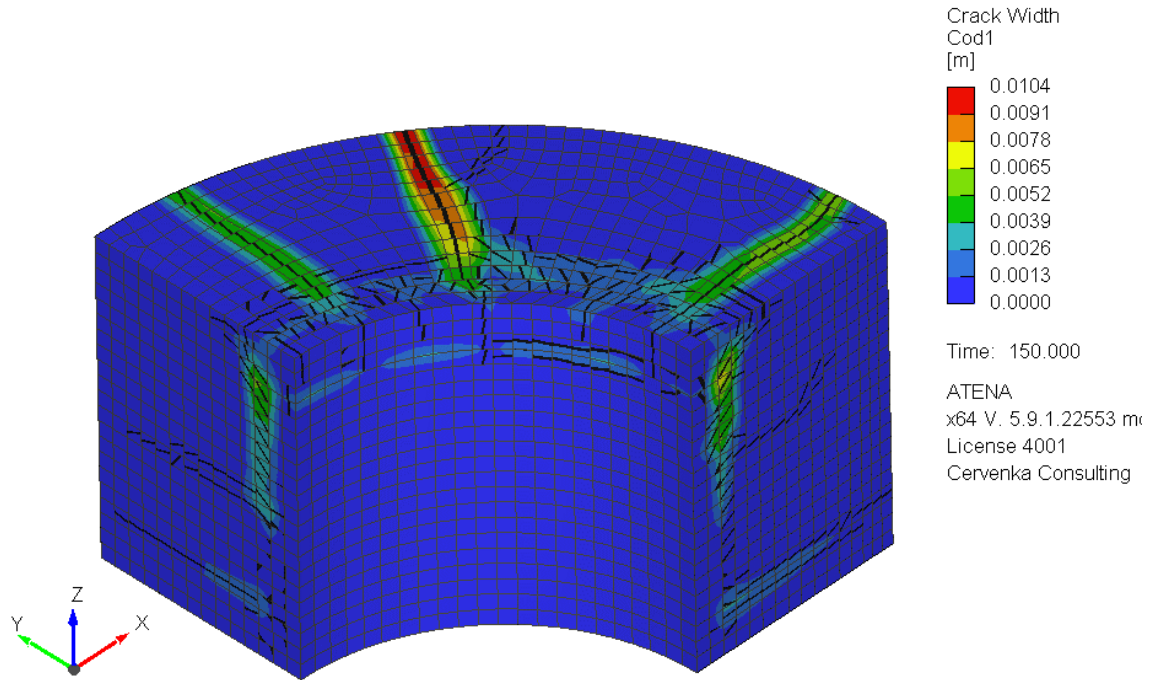
Fig. 8-13 Crack width in structure, concrete compressive strength 70 MPa without reinforcement
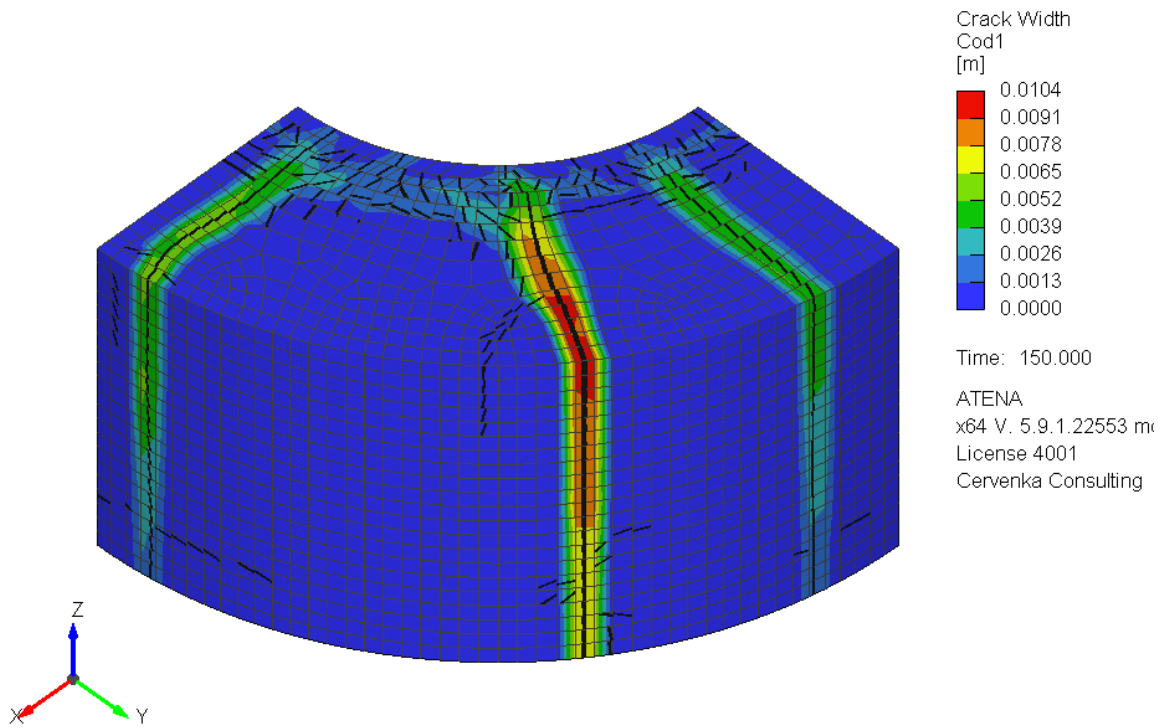
Fig. 8-14 Crack width in structure, concrete compressive strength 70 MPa without reinforcement
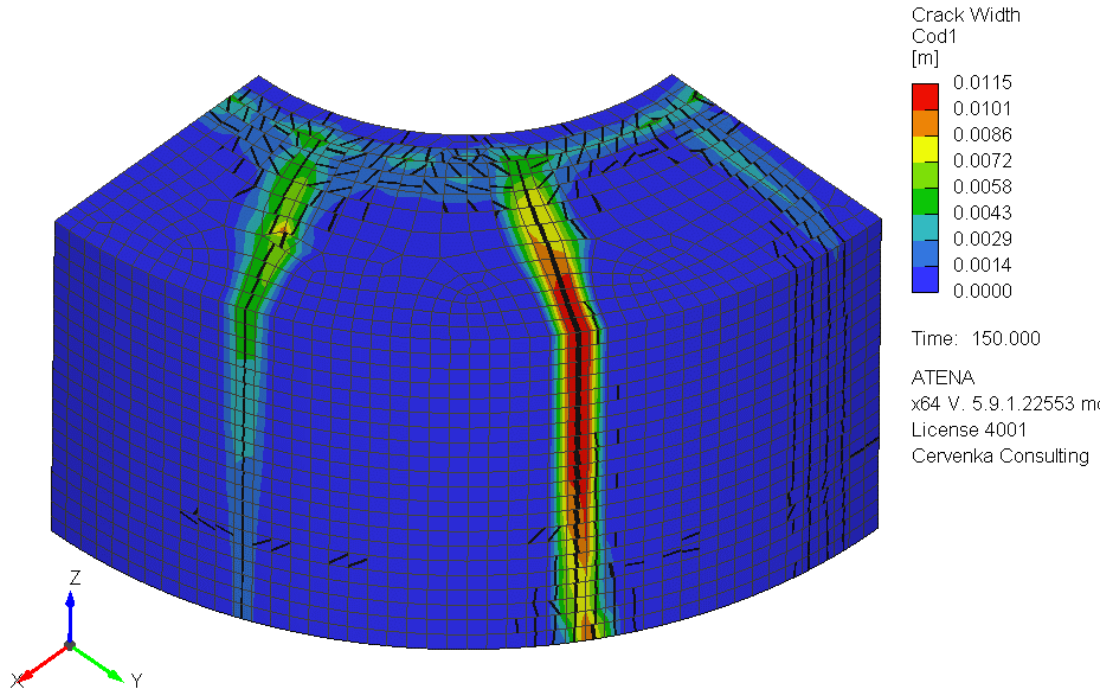
Fig. 8-15 Crack width in structure, concrete compressive strength 70 MPa with reinforcement
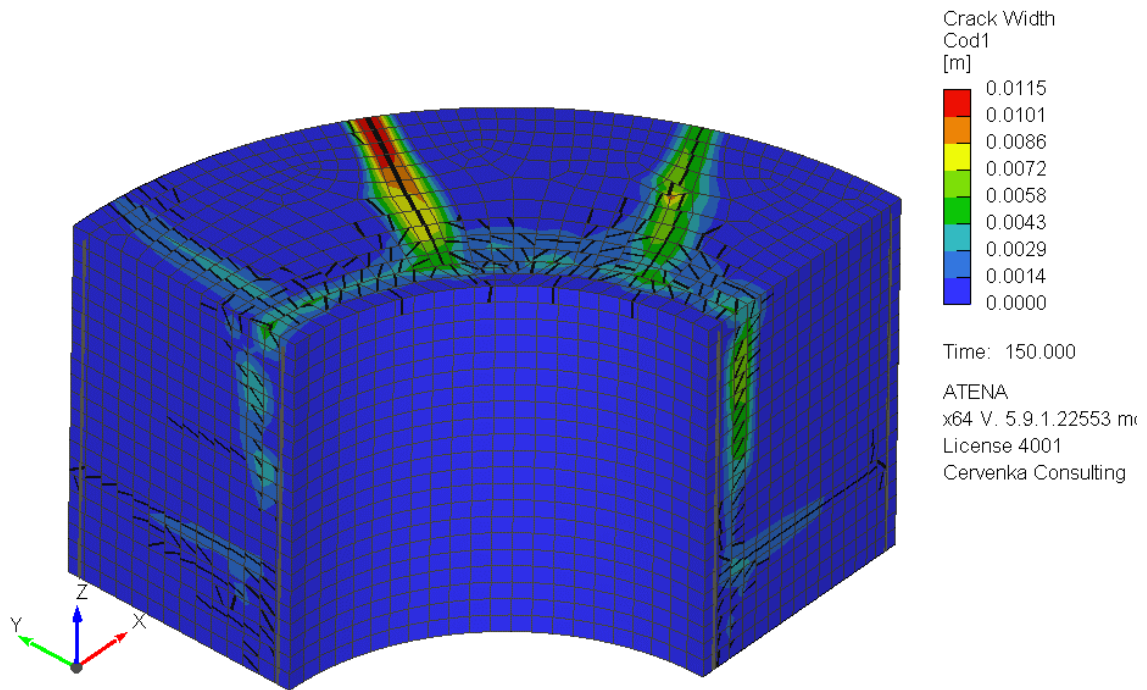
Fig. 8-16 Crack width in structure, concrete compressive strength 70 MPa with reinforcement
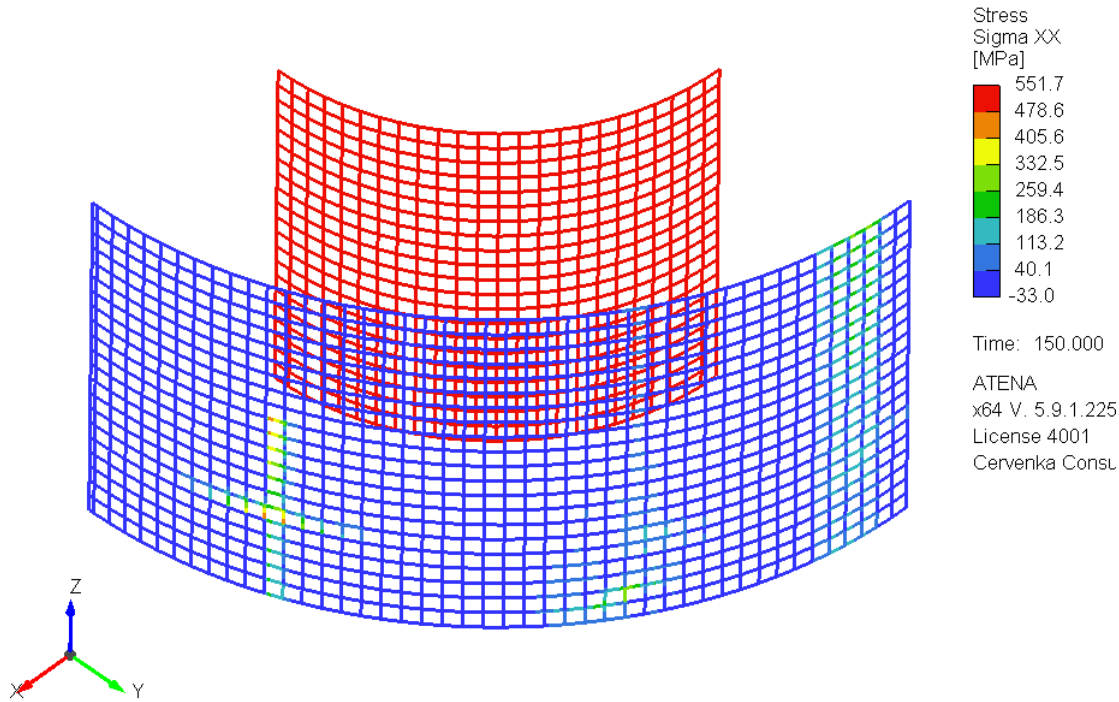
Fig. 8-17 Stress in the reinforcement

Excessive stress levels are reached in the reinforcement mesh on the inner surface of the shielding where the RIVE load is concentrated. Higher stress is also reached on the outer surface where the cracks are developed.

The steel liner on the inner surface of the shielding (which is part of the structures of biological shielding in Czech NPPs) is omitted from this study since it is not always the case for biological shielding structures in general.

Since the radial cracking in the shield is effectively discarding the shielding property of the structure, the possibility of such damage should be taken in account for the design of the future structures. One of the possibilities to avoid the detrimental effects is to create the shielding ring from parts that are separated and are enabled to move with the RIVE effect without causing increased stresses in the structure. The joint between the segments would need to have shear lock that prevents the radiation to pass. Such a possibility is depicted, Fig. 8-18.
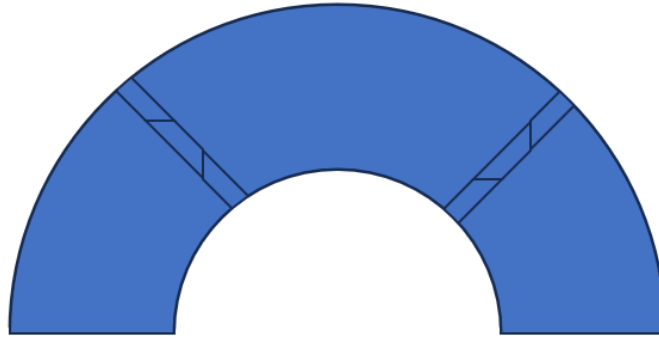
Fig. 8-18 Shear lock within joint between precast segments

9 Summary

Radiation induced effects on minerals, aggregates, cement paste and concrete are presented. Based on the knowledge of radiation effect the fuzzy logic model of irradiated aggregates is proposed. Influence of neutron dose, temperature while irradiated and the mineral composition is included in the model. The proposed model captures trends in aggregate expansion behavior upon irradiation, however, there are limitations to the model that resulted in poor correlations in some cases. Firstly, the model does not take into account the kinetics of expansion of each mineral, specifically the kick-off point of the sigmoid curve as well as the maximum expansion difference between the minerals that definitely influences the propagation of defects. Secondly, the aggregate structure that is given by the aggregate origin (how it is formed in nature) affects defect formation. For example, the sandstone as a sedimentary rock (cementitious) contains more pores than granite or other deep-seated (plutonic) magmatic rocks (compaction). Therefore the interconnection between the minerals contained in the rock should be incorporated into the model as well.

The mesoscale model of irradiated aggregate within the cement paste matrix is simulated, employing the FEM analysis using ATENA software. The aggregate RIVE is the introduced load leading to crack development within the cement paste and aggregate that can be translated to tensile strength reduction. Mesoscale model is validated on experimental data on irradiated concrete performed by Kelly et. al. who studied irradiation effects on concrete and its component while keeping the temperature of sample bellow 100°C. Such conditions are expected in NPP facility as well. The results of mesoscale model correlate well with the experiment which proves efficiency of FEM modeling of concrete in such specific conditions.

Finally the macroscale model shows real potential damage caused by RIVE in the structure. The study reveals the potential of development of radial cracks in the shielding structure which are detrimental regarding the safety purpose of the structure. For the future designs of biological shielding, the RIVE effect should be considered as one of loads in the ageing management. The separation of load-bearing and shielding part of biological shielding would be recommended as well. The shielding part could be sacrificial part of the structure that has limited restraint allowing movement of the structure without increasing stresses. Shear lock between the segments of ring biological shield might be one of solutions of the problem in the future.

10 References

[1]   Hilsdorf H. K., Kropp J., Koch H. The effects of nuclear radiation on the mechanical properties of concrete. Special publication of The American Concrete Institute 55. 1978. pp 223-254.

[2]   Kelly B. T. The effects of reactor radiation on concrete. In 2nd Conference on Prestressed Concrete Pressure Vessels and Their Insulation. London. 1969.

[3]   Elleuch M. F., Dubois F., Rappeneau J. The effects of neutron radiations on special concretes and their components (No. CEA-CONF--1584). CEA Centre d'Etudes Nucleaires de Saclay. 1970.

[4]   Rappeneau J., Lagorio M., Gilbert J., Piron P. Irradiation tests of concretes. Bull. Inf. Sci. Tech. 110, 31–48. 1966.

[5]   Seeberger J., Hilsdorf H. K. Effect of radioactive emission on the strength and structure of concrete. Technical report. Karlsruhe. 1982.

[6]   Field K. G., Remec I., Le Pape Y. Radiation effects in concrete for nuclear power plants – Part I: Quantification of radiation exposure and radiation effects. Nuclear Engineering and Design 282. 2015. pp 126-143.

[7]   Rosseel T.M., et al. Review of the Current State of Knowledge on the Effects of Radiation on Concrete. Journal of Advanced Concrete Technology 14. 2016. pp 368-383.

[8]   Alexander S. Effects of Irradiation on Concrete Final Results. Technical Report HL.63/6438. Atomic Energy Research Establishment, Harwell. 1963.

[9]   Clark R. Radiation Damage to Concrete. Technical Report HW-56195. General Electric. Hanford Laboratories, Richland, WA. 1958.

[10]   Dubrovskii V., Ibragimov S., Korenevskii V., Ladygin A., Pergamenshchik B.,Perevalov V. Hematite concrete for shielding against high neutron fluxes. At. Energ. 28, 258–260. 1970.

[11]   Dubrovskii V., Ibragimov S., Kulakovskii M.Y., Pergamenshchik A.Y.L.B. Radiation damage in ordinary concrete. At. Energ. 23, 310–316 (English translation). 1966a.

[12]   Dubrovskii V., Ibragimov S., Ladgyn A.Y., Pergamenshchik B.K. The effect of neutron irradiation on certain properties of refractory concretes. At. Energ.21, 108–112 (English Translation). 1966b.

[13]   Dubrovskii V., Ibragimov S., Ladygin A., Kulakovskii M., Pergamenshchik B. Radiation stability of serpentine concrete. Sov. At. Energy 25, 1345–1346. 1968.

[14]   Eby R., Ewing R., Birtcher R. The amorphization of complex silicates by ion-beam irradiation. J. Mater. Res. 7, 3080–3102. 1992.

[15]   Weber W., Ewing R., Catlow C., de la Rubia T., Hobbs L., Kinoshita C., Matzke H., Motta A., Nastasi M., Salje E., Vance E., Zinkle S. Radiation effects in crystalline ceramics for the immobilization of high-level nuclear waste and plutonium. J. Mater. Res. 13, 1434–1484. 1998.

[16]   Gray B. The effects of reactor radiation on cement and concrete. In: Benzler,H. (Ed.), Proceedings of an Information Exchange Meeting on 'Results of Concrete Irradiation Programmes'. Commission des Communautés Européennes,Brussels, Belgium. 1971.

[17]   Idei Y., Kamata H., Akutsu Y., Onizawa M., Nakajima N., Sukegawa T., Kakizaki M. Strength of biological shield concrete of JPDR. Technical Report JAERI-M90-205. Japan Atomic Energy Research Institute. 1990.

[18]   Batten A. Effect of Irradiation on the Strength of Concrete. Technical Report AERE-R 3332. Atomic Energy Research Establishment, Harwell. 1960.

[19]   Clinard F., Hobbs L. Radiation effects in non-metals. Modern problems in condensed matter sciences, Physics of Radiation Effects in Crystals. North-Holland Physics Publishing. 1986.

[20]   Vaitová M., Štemberk P., Rosseel T. M. Fuzzy logic model of irradiated aggregates. Neural Network World, 29(1). 2019.

[21]   Cacuci D. G. (Ed.). Handbook of Nuclear Engineering: Vol. 1: Nuclear Engineering Fundamentals; Vol. 2: Reactor Design; Vol. 3: Reactor Analysis; Vol. 4: Reactors of Generations III and IV; Vol. 5: Fuel Cycles, Decommissioning, Waste Disposal and Safeguards (Vol. 1). Springer Science & Business Media. 2010.

[22]   Kontani, O., Ichikawa, Y., Ishizawa, A., Takizawa, M., & Sato, O. Irradiation effects on concrete structures. Infrastructure systems for nuclear energy. 2014. 459-473.

[23] Nordlund K., Sand A. E., Granberg F., Zinkle S. J., Stoller R., Averback R. S., Simeone D. Primary Radiation Damage in Materials. Review of Current Understanding and Proposed New Standard Displacement Damage Model to Incorporate in Cascade Defect Production Efficiency and Mixing Effects. 2015.

[24] Neville A. M. Properties of concrete. 1995.

[25] Denisov A. V., Dubrovski V. B., Solovyov V. N. Radiation resistance of mineral and polymer construction materials. MEI Publish House. Moscow. 2012.

[26] Remec I. Status report on defining a unified parameter for characterization of radiation intended for evaluation of radiation-induced degradation of concrete. ORNL/LTR-2015/542. 2015

[27] Lee S. Y., Daugherty A.M., Broton D.J. Assessing aggregates for radiation-shielding concrete. Concrete International. 2013. pp 31-38.

[28] Wenk, H. R., Bulakh A.. Minerals: their constitution and origin. Cambridge University Press. 2016.

[29] Boffy R., et al. Why neutron guides may end up breaking down? Some results on the macroscopic behaviour of alkali-borosilicate glass support plates under neutron irradiation. Nuclear Instruments and Methods in Physics Research B. 2015. pp 179-187.

[30] Zubov, V., Ivanov, A. Expansion of quartz caused by irradiation with fast neutrons. Sov. Phys. Crystal. 11, 372. 1966.

[31] Zadeh L.A. Fuzzy sets. Information and Control. 8. 1965. pp 338-353

[32] Klir G. J., Clair U. H. S., Yuan B. Fuzzy set theory: Foundations and applications. Prentice Hall. 1997.

[33] Ross T. J. Fuzzy logic with engineering applications. John Wiley & Sons. 2009.

[34] Leal D. S. W. R. Fuzzy logic-based expert systems applied to concrete technology. 2013.

[35] Pokorná N., Štemberk P. Stress-strain Diagram of Hardening and Fiber Concrete Defined by Fuzzy Logic. In: Mechanika 2009 - Proceedings of the 14th International Conference. Kauno technologijos universitetas, Kaunas. 2009. pp 329-333.

[36] Vaitová M., Štemberk P. Numerical Model of Corium-concrete Interaction. In: Mechanika 2014 - Proceedings of the 19th International Conference. Kauno technologijos universitetas, Kaunas. 2014. pp 277-280.

[37]   Piegat A. Fuzzy modeling and control (Vol. 69). 2013. Physica.

[38]   Mamdani E. H. Application of fuzzy algorithms for control of simple dynamic plant. In Proceedings of the institution of electrical engineers (Vol. 121, No. 12, pp. 1585-1588). 1974. IET Digital Library.

[39]   Červenka J., Papanikolaou V. K. Three dimensional combined fracture–plastic material model for concrete. International journal of plasticity, 24(12), 2192-2220. 2008.

[40]   Červenka J., Janda Z., Jendele L., Pukl R., Červenka V. Simulation of Severe Accident Scenarios in Nuclear Containments. Procedia engineering, 210, 425-432. 2017.

[41]   Kurmann D., Janda Z. Seismic Design and Verification of a NPP Structure for the Storage of Radioactive Waste Components in Switzerland. 2013.

[42]   Hůlková G., Červenka J., Janda Z. Analýza odezvy kontejnmentu na extrémní zatížení v programu ATENA. TAČR - TH02020843. 2020.

[43]   Červenka J., Červenka, V. FE Program ATENA for Safety Assessment of NPP Containments. Infrastructure Systems for Nuclear Energy, 397-406. 2014.

[44]   Hordijk D.A. Local Approach to Fatigue of Concrete. Doctor dissertation. Delft. 1991. University of Technology, The Netherlands, ISBN 90/9004519-8.

[45]   Červenka V., Pukl R., Ozbolt J., Eligehausen R. Mesh Sensitivity Effects in Smeared Finite Element Analysis of Concrete Structures. Proc. FRAMCOS 2. 1995. pp 1387-1396.

[46]   Menetrey P., William K.J. Triaxial failure criterion for concrete and its generalization. ACI Structural Journal. 1995. 92(3). pp 311-318.

[47]   Mier J.G.M van. Multiaxial Strain-softening of Concrete, Part I: fracture. Materials and Structures. RILEM Vol. 19. No.111. 1986.

[48]   Červenka J., Jendele L. ATENA Program Documentation Part 6 ATENA Input File Format. Cervenka Consulting sro. 2021.

[49]   Červenka V., Jendele L., Červenka J. ATENA Program Documentation Part 1 Theory. Cervenka Consulting sro. 2021.

[50]   Procházková Z, Červenka J., Janda Z., Pryl D.,Mikolášková J. ATENA Program Documentation Part 4-6 ATENA Science – GiD Tutorial. Cervenka Consulting sro. 2019.

[51]   Červenka V., Červenka J., Janda Z., Pryl D. ATENA Program Documentation Part 8 User's Manual for ATENA GiD Interface. Cervenka Consulting sro. 2022.

[52]   Beneš Š., Mikolášková J., Altman T. ATENA Program Documentation Part 8 User's Manual for ATENA Studio. Cervenka Consulting sro. 2021.

[53]   Pasenau M., et al.. User manual GiD 16. CIMNE, Barcelona. 2022.

[54]   Model Code 2010-Final Draft: Volume 1. fib Fédération internationale du béton, 2012.

[55]   Bentz D. P., Arnold J., Boisclair M. J., Jones S. Z., Rothfeld P., Stutzman P. E., Ardani A. Influence of aggregate characteristics on concrete performance (No. NIST Technical Note 1963). US Department of Commerce. 2017. National Institute of Standards and Technology.

[56]   Giorla A., Vaitová M., Le Pape Y., Štemberk P. Meso-scale modeling of irradiated concrete in test reactor. Nuclear Engineering and Design, 295, 59-73. 2015.

[57]   Le Pape Y., Field K. G., Remec I. Radiation effects in concrete for nuclear power plants, Part II: Perspective from micromechanical modeling. Nuclear Engineering and Design, 282, 144-157. 2015.

[58]   Remec I., Rosseel T. M., Field K. G., Le Pape Y. Characterization of radiation fields in biological shields of nuclear power plants for assessing concrete degradation. In EPJ Web of Conferences (Vol. 106, p. 02002). 2016. EDP Sciences.

[59]   Kujal B, Duspiva J., Jakab J. Analýza vybraných sekvencí nadprojektových havárií bloku VVER-1000 pro JE Temelín. ÚJV Řež. (part of report only).

[60]   Kambayashi D., Sasano H., Sawada S., Suzuki K., Maruyama I. Numerical analysis of a concrete biological shielding wall under neutron irradiation by 3D RBSM. Journal of Advanced Concrete Technology, 18(10), 618-632. 2020.

List of figures and tables